



Delft University of Technology

Report on pile test results at Maasvlakte II

Vibro piles

Duffy, K.

Publication date

2021

Document Version

Final published version

Citation (APA)

Duffy, K. (2021). *Report on pile test results at Maasvlakte II: Vibro piles*. Delft University of Technology.

Important note

To cite this publication, please use the final published version (if applicable).
Please check the document version above.

Copyright

Other than for strictly personal use, it is not permitted to download, forward or distribute the text or part of it, without the consent of the author(s) and/or copyright holder(s), unless the work is under an open content license such as Creative Commons.

Takedown policy

Please contact us and provide details if you believe this document breaches copyrights.
We will remove access to the work immediately and investigate your claim.

*This work is downloaded from Delft University of Technology.
For technical reasons the number of authors shown on this cover page is limited to a maximum of 10.*

Report on pile test results at Maasvlakte II Vibro Piles



Revision 1

Author: Kevin Duffy

Reviewed by: Kenneth Gavin and Dirk de Lange

5th February 2021

Revision Tracker

Date Issued	Revision No.	Author	Notes
03/11/20	0	Kevin Duffy	First submission
05/02/21	1	Kevin Duffy	Recommendations for limiting shaft resistance (Section 7.2) adjusted based on consultation with NPR 7201 committee.

Table of Contents

List of Figures	iii
List of Tables	viii
NPR Registry	ix
1. Introduction.....	13
1.1. Project Background	13
1.2. Test Site Location.....	14
2. Ground Investigation	17
3. Pile Fabrication & Installation	20
3.1. Pile Geometry & Fabrication	21
3.2. Pile Installation.....	22
3.2.1. Installation Data	25
4. Pile Testing	27
4.1. Test Frame.....	27
4.2. Grout Anchors	30
4.3. Strain Measurements	31
4.3.1. Fibre Bragg Grating (FBG).....	32
4.3.2. Brillouin Optical Frequency Domain Analysis (BOFDA)	33
4.3.3. Installation of Fibre Optics	34
4.4. Test Procedure.....	36
5. Measurement Results	39
5.1. Test Results: Pile P01.....	39
5.2. Test Results: Pile P03.....	47
5.3. Test Results: Pile P06.....	56
5.4. Test Results: Pile P11.....	64
6. Interpretation & Analysis.....	72
6.1. Measurement Scatter	72
6.2. Strain to Force Conversion.....	73
6.3. Force/Depth Profiles	77
6.4. Base Mobilisation.....	81
6.5. Shaft Mobilisation.....	84
7. Discussion & Recommendations	88
7.1. Base Capacity.....	89

7.2. Shaft Capacity	90
References	93
Appendix A Site Plan.....	94
Appendix B Site Investigation Data	96
B.1 CPTs	96
B.2 Boreholes.....	101
Appendix C General Photos	107
Appendix D Prediction of Pile Behaviour	111
D.1 Prediction of Failure Load.....	111
D.2 Prediction of Pile Settlement.....	112
Appendix E Detailed Drawings.....	115
E.1 Reinforcement Cage.....	115
E.2 Pile Cap	117
E.3 Transition Piece.....	119
E.4 Reaction Frame	121
Appendix F General Specifications.....	124
F.1 Injection Grout – Grout Anchors	124
F.2 Grout Anchors	127
F.3 Calibration Sheet – Load Cells	128
F.4 Calibration Sheet – LVDTs.....	129

List of Figures

Figure 1.1: Aerial view of the north-eastern end of the pile test site, with Amaliahaven in the background.....	15
Figure 1.2: Site plan of the pile test site. In orange: vibro piles P01, P03, P06, P11; in green: screw injection piles P04, P05, P07, P08; in red: driven precast piles: P02, P09, P11, P12 ...	16
Figure 2.1: Plot of the CPTs along the central axis of each pile.....	18
Figure 2.2: Comparison of CPTs around P11 executed before pile installation (i.e. CPTs E13, E14 and E15; in blue) and executed after installation (i.e. CPTs P1101, P1102, P1103; in red)	19
Figure 2.3: Positions of the CPTs around each test pile	19
Figure 3.1: Sacrificial base plate used for the installation of the vibro piles.....	20
Figure 3.2: Steel reinforcing of the vibro piles lying on site in advance of instrumentation and installation.....	22
Figure 3.3: Installation procedure for the vibro piles	23
Figure 3.4: Pile heads of the four vibro piles immediately after installation. Note the non-centric placement of some of the reinforcement (Photos: Gust van Lysebetten, WTCB).....	24
Figure 3.5: Vibro pile after the installation of the two metre sleeve around the uppermost part of the pile shaft without grout (Photos: Gust van Lysebetten, WTCB).....	24
Figure 4.1: Reaction frame & reference frame	28
Figure 4.2: Overall set up of the testing equipment.....	28
Figure 4.3: Interface between the reaction frame and the pile cap: (a.) underside of the transition piece (b.) top of the pile cap (Photos: Gust Van Lysebetten, WTCB).....	29
Figure 4.4: Schematic of the grout anchor design in both elevation (left) and plan view (right)	30
Figure 4.5: (a.) Installation of the grout anchors around the test pile (b.) Close up of the installation process, highlighting the use of the anchor guide frame in order to install the anchors at the correct position (c.) screw tip of the grout anchors (photo: Gust van Lysebetten, WTCB).....	31
Figure 4.6: Cross-sectional schematic of the SMW-01 FBG cable	32
Figure 4.7: Configuration of the fibre optic sensors in the vibro pile.....	32
Figure 4.8: Schematic of the Solifos BRUsens V9 (Piccolo <i>et al.</i> , 2020)	34
Figure 4.9: The instrumented reinforcement cage in advance of its insertion into the auxiliary tube. Note the two protective metal boxes at the tip of the reinforcement cage.....	35
Figure 4.10: Close-up of the base of the reinforcement cage. Note the loop in the BOFDA cable (blue cable) across the spiral reinforcing. The FBG cable (white) terminates at the end of the reinforcement cage.....	35
Figure 4.11: Egress point for the fibre optics between the pile cap and pile sleeve. Grout was used to fill the annular space between the pile cap and pile sleeve, with a PVC facilitating the safe passage of the fibre optics through the annular space	36
Figure 5.1: Plot of load exerted on pile head against the time elapsed for P01	40
Figure 5.2: Plot of settlement measured at the pile head against the time elapsed for P01. The elastic settlement (and correspondingly the settlement at the pile base) readings shown have been derived from the FBG readings to provide more complete information over time.....	40
Figure 5.3: Plot of strain versus time for selected BOFDA gauges for P01	41
Figure 5.4: Plot of strain versus time for all FBG gauges for P01.....	41

Figure 5.5: Load at pile head readings from each individual load cell for P01	42
Figure 5.6: Settlement at pile head readings from each individual LVDT for P01	42
Figure 5.7: Plot of load versus settlement at pile head for P01	43
Figure 5.8: Creep parameter versus time across selected load steps for P01	43
Figure 5.9: Creep rate versus time across selected load steps for P01	44
Figure 5.10: Development of the total creep settlement at the pile head during selected load steps for P01.....	44
Figure 5.11: Strain versus depth profile for P01 at the end of each load step. Note that the BOFDA measurements are indicated by a continuous line whereas FBG readings are indicated by a discrete point	46
Figure 5.12: Location of the breakage of the pile P03 underneath the pile sleeve	47
Figure 5.13: Close-up photo of the breakage immediately underneath the sleeve of pile P03 (Photo credit: Gust van Lysebetten, WTCB).....	47
Figure 5.14: Plot of load exerted on pile head against the time elapsed for P03.....	49
Figure 5.15: Plot of settlement measured at the pile head against the time elapsed for P03. The elastic settlement (and correspondingly the settlement at the pile base) readings shown have been derived from the FBG readings to provide more complete information over time.....	49
Figure 5.16: Plot of strain versus time for selected BOFDA gauges for P03	50
Figure 5.17: Plot of strain versus time for all FBG gauges for P03.....	50
Figure 5.18: Load at pile head readings from each individual load cell for P03	51
Figure 5.19: Settlement at pile head readings from each individual LVDT for P03	51
Figure 5.20: Plot of load versus settlement at pile head for P03. Note that the structural failure and breakage of the fibres resulted	52
Figure 5.21: Creep parameter versus time across selected load steps for P03	52
Figure 5.22: Creep rate versus time across selected load steps for P03	53
Figure 5.23: Development of the total creep settlement at the pile head during selected load steps for P03.....	53
Figure 5.24: Strain versus depth profile for P03 at the end of each load step. Note that the BOFDA measurements are indicated by a continuous line whereas FBG readings are indicated by a discrete point	55
Figure 5.25: Plot of load exerted on pile head against the time elapsed for P06.....	57
Figure 5.26: Plot of settlement measured at the pile head against the time elapsed for P06. The elastic settlement (and correspondingly the settlement at the pile base) readings shown have been derived from the FBG readings to provide more complete information over time.....	57
Figure 5.27: Plot of strain versus time for selected BOFDA gauges for P06.....	58
Figure 5.28: Plot of strain versus time for all FBG gauges for P06.....	58
Figure 5.29: Load at pile head readings from each individual load cell for P06.....	59
Figure 5.30: Settlement at pile head readings from each individual LVDT for P06	59
Figure 5.31: Plot of load versus settlement at pile head for P06	60
Figure 5.32: Creep parameter versus time across selected load steps for P06	60
Figure 5.33: Creep rate versus time across selected load steps for P06	61
Figure 5.34: Development of the total creep settlement at the pile head during selected load steps for P06.....	61
Figure 5.35: Strain versus depth profile for P06 at the end of each load step. Note that the BOFDA measurements are indicated by a continuous line whereas FBG readings are indicated by a discrete point	63

Figure 5.36: Plot of load exerted on pile head against the time elapsed for P11	65
Figure 5.37: Plot of settlement measured at the pile head against the time elapsed for P11. The elastic settlement (and correspondingly the settlement at the pile base) readings shown have been derived from the FBG readings to provide more complete information over time.....	65
Figure 5.38: Plot of strain versus time for selected BOFDA gauges for P11	66
Figure 5.39: Plot of strain versus time for all FBG gauges for P11	66
Figure 5.40: Load at pile head readings from each individual load cell for P11	67
Figure 5.41: Settlement at pile head readings from each individual LVDT for P11	67
Figure 5.42: Plot of load versus settlement at pile head for P11	68
Figure 5.43: Creep parameter versus time across selected load steps for P11	68
Figure 5.44: Creep rate versus time across selected load steps for P11	69
Figure 5.45: Development of the total creep settlement at the pile head during selected load steps for P11.....	69
Figure 5.46: Strain versus depth profile for P11 at the end of each load step. Note that the BOFDA measurements are indicated by a continuous line whereas FBG readings are indicated by a discrete point	71
Figure 6.1: Photos of the piles after tension tests at the Gaag viaduct in Schipluiden. Noticeable deterioration of concrete towards the pile tip was observed (Geerling and Janse, 1997).....	72
Figure 6.2: Fitted strain-dependent equation to the FBG data for the tangent and secant stiffness moduli of P01. Steps on the unload/reload cycle have been filtered out	74
Figure 6.3: Fitted strain-dependent equation to the FBG data for the tangent and secant stiffness moduli of P03.....	75
Figure 6.4: Fitted strain-dependent equation to the FBG data for the tangent and secant stiffness moduli of P06. Steps on the unload/reload cycles have been filtered out	75
Figure 6.5: Fitted strain-dependent equation to the FBG data for the tangent and secant stiffness moduli of P11. Steps on the unload/reload cycle have been filtered out	76
Figure 6.6: Force-depth profile of P01, taking the forces in the gauges at the end of the load step. Note that the BOFDA measurements are indicated by a continuous line whereas FBG readings are indicated by a discrete point and the force measured by the load cells has also been included as discrete points at NAP +4m. Steps within an unload/reload cycle have been omitted	77
Figure 6.7: Force-depth profile of P03, taking the forces in the gauges at the end of the load step. Note that the BOFDA measurements are indicated by a continuous line whereas FBG readings are indicated by a discrete point and the force measured by the load cells has also been included as discrete points at NAP +4m. Steps within an unload/reload cycle have been omitted	78
Figure 6.8: Force-depth profile of P06, taking the forces in the gauges at the end of the load step. Note that the BOFDA measurements are indicated by a continuous line whereas FBG readings are indicated by a discrete point and the force measured by the load cells has also been included as discrete points at NAP +4m. Steps within an unload/reload cycle have been omitted. The measurement gap in the BOFDA readings at approx. NAP -10.5m is as a result of the coupling sleeve on the reinforcement distorting the readings. This has been corrected for in the FBG measurement	79
Figure 6.9: Force-depth profile of P11, taking the forces in the gauges at the end of the load step. Note that the BOFDA measurements are indicated by a continuous line whereas FBG readings are indicated by a discrete point and the force measured by the load cells has also been	

included as discrete points at NAP +4m. Steps within an unload/reload cycle have been omitted	80
Figure 6.10: Mobilisation of the base capacity for all vibro piles (BOFDA measurements) ..	82
Figure 6.11: Mobilisation of the base capacity for all vibro piles (FBG measurements)	82
Figure 6.12: Mobilisation of the base capacity for all vibro piles (BOFDA measurements; normalised)	83
Figure 6.13: Mobilisation of the base capacity for all vibro piles (FBG measurements; normalised)	83
Figure 6.14: Mobilisation of the shaft capacity in the upper sand layer for all vibro piles (BOFDA measurements)	85
Figure 6.15: Mobilisation of the shaft capacity in the upper sand layer for all vibro piles (FBG measurements)	85
Figure 6.16: Mobilisation of the shaft capacity in the upper sand layer for all vibro piles (BOFDA measurements; normalised)	86
Figure 6.17: Mobilisation of the shaft capacity in the upper sand layer for all vibro piles (FBG measurements; normalised)	86
Figure 7.1: Load vs. settlement response of all vibro piles	88
Figure 7.2: Change in imparted hammer energy with depth for the vibro piles	89
Figure 7.3: (a.) Comparison of the measured (FBG gauges) and the predicted q_s/q_c at a pile base settlement of $0.1D_{eq}$. The layer of intermixed clay/sand has been plotted relative to CPT P01 and the base depth of pile P01 (b.) Comparison of measured and predicted q_s/q_c at peak load from Flynn and McCabe (2015) with the UWA-05 and NEN predictions (where $\delta_f = 33^\circ$ as opposed to 35°)	91
Figure 7.4: Predictions for the pile capacity at peak load compared to the true measurements. The CPT on the piles' central axes was used, with the simplified UWA-05 method and the current NEN 9997-1 with and without limiting resistances included for comparison. A constant α_s was used for the entire profile	92
Figure B.1: Relative positions of the CPTs around each pile	96
Figure B.2: CPTs executed around pile P01	97
Figure B.3: CPTs executed around pile P03	98
Figure B.4: CPTs executed around pile P06	99
Figure B.5: CPTs executed around pile P11, excluding post-installation CPTs	100
Figure C.1: Head of the steel auxiliary tube lying on the test site prior to pile installation ..	107
Figure C.2: IHC S-120 hammer used for the installation of the auxiliary tube	107
Figure C.3: Annular space around the auxiliary pile during pile driving	108
Figure C.4: Lifting of the reinforcement cage for P11 using a mobile crane and the drilling rig crane (left)	108
Figure C.5: Concrete replenishment during the withdrawal of the auxiliary tube	109
Figure C.6: Vibro pile prepared with pile cap, awaiting installation of the reaction frame ..	109
Figure C.7: Close-up of the pile head and pile cap	110
Figure D.1: Predicted load-settlement graph for pile P01 for the aforementioned combinations	112
Figure D.2: Predicted load-settlement graph for pile P03 for the aforementioned combinations	113
Figure D.3: Predicted load-settlement graph for pile P06 for the aforementioned combinations	113

Figure D.4: Predicted load-settlement graph for pile P11 for the aforementioned combinations	114
--	-----

List of Tables

Table 1.1: Parties involved during the pile testing and their respective roles	15
Table 3.1: Vibro pile geometries, installation data & specifications	21
Table 4.1: Depths of the FBG sensors. The depths have been derived from the pile base level obtained from the pile installation records.....	33
Table 5.1: Pile test dates and times	39
Table 5.2: List of load steps and corresponding durations in pile test P01	45
Table 5.3: List of load steps and corresponding durations in pile test P03	54
Table 5.4: List of load steps and corresponding durations in pile test P06	62
Table 5.5: List of load steps and corresponding durations in pile test P11	70
Table 6.1: Estimate of the start depth of the scattered measurements and the depth of the Pleistocene for each pile. Note that in the instance of P03 and P06, the scatter in the BOFDA readings occurs at a shallower depth (at NAP -23.23m and NAP -23.29m respectively)	73
Table 6.2: Slope and intercept of the strain-dependent stiffness equations.....	74
Table 6.3: Pile class factors for the base resistance of each pile retrieved directly from both measurement systems.....	84
Table 6.4: Pile class factors for the shaft resistance in the upper sand layer of each pile retrieved directly from both measurement systems	87
Table D.1: Overview of the alpha factors used for calculation of the pile base and shaft capacities.....	111
Table D.2: Overview of the predicted base and shaft capacities at failure.....	111
Table D.3: Overview of the predicted failure capacities	112

NPR Registry

In line with the stipulations of NPR 7201 for a Class A1 test, the following registry has been completed and presented in this report (originally in Dutch):

Item No.	Description	Location	Additional Comments
A	General		
A1	Location and description of the project, including positions of the CPTs	Section 1, Appendix A and Appendix B	
A2	Description, drawing and photographs of the test site with the location of the test piles	Section 1.2 and Appendix A 1.2	
A3	Name of the client	Table 1.1	
A4	Name of the party who executed the pile test	Table 1.1	
A5	Only for determining national pile class factors: name of the supervisor.	Section 1	
A6	Names of the people responsible for the reporting of the pile tests	Table 1.1	
A7	Date of pile installation and date of testing	Table 3.1	
A8	Description of the test piles with dimensions	Section 3.1	
A9	Cross-sectional diameter of the pile toe and pile shaft	Section 3.1	
A10	Detailed drawings of the pile tip including the depth of the pile toe, pile head and coordinates of all piles with reference to NAP	Table 3.1	<i>Qualitative description and photos given</i>
A11	Description of the load testing system, including rough dimensions, weight of the frame, distance of any grout anchors in relation to the test pile, dimensions and depth with respect to NAP of the grout anchor tip	Section 4.1, Section 4.2, Appendix E and Appendix F	
A12	Description and specifications of the Rapid Load Test apparatus	-	<i>Not applicable</i>
A13	Description of the pulled test piles and measurement of the circumference with plot of circumference against length of the pile. Include calculation of the average pile diameter in the relevant soil layers	-	<i>No piles have been removed following the test programme</i>

A14	Results of the pressure tests from pressure cells on the pulled piles. Calculation of the Young's modulus of the pile material.	-	<i>Not applicable</i>
G	Ground conditions		
G1	Data on the ground conditions surrounding the test piles	Section 2 and Appendix B	
G2	CPT results with reference to the ground investigation report. The ground investigation report is to be an appendix to the load test report. Digital files of all CPTs in GEF format to be included.	Appendix B.1	
G3	Groundwater level during the test, indicating any possible fluctuations	Appendix B	
G4	Indication of any recent improvements to the soil or excavations.	Section 2	
G5	If relevant and known, the nature and extent of contamination.	-	<i>No contamination present</i>
G6	Magnitude of negative skin friction acting on pile	-	<i>Not applicable</i>
G7	Method of calculating the load, displacement and strains in the test piles	Section 4	
G8	Prediction of the maximum resistance of the pile toe in the ground and of the maximum shaft friction in the different soil layers.	Section 6	
G9	Prediction of the load bearing capacity.	Appendix D	
G10	Prediction of the load-settlement path.	Appendix D	
I	Pile installation		
I1	For hammered piles: blow count and imparted energy of the hammer, measurements of the auxiliary tube and the footplate	Section 3.2.1	
I2	For cast-in-place piles: record of the drilling torque and pulldown force with depth.	Section 3.2.1	
I3	Record of the displacement of the pile toe with time and number of revolutions of the auxiliary tube or auger per metre penetration	Section 3.2.1	
I4	Amount of concrete used in the case of cast-in-place piles	Section 3	<i>Only a very approximate estimate has been provided</i>
I5	Duration of pile installation or fabrication	Table 3.1	

I6	Composition of the grout and/or concrete mix	Section 3	
I7	Amount of grout or jetting water used and the range over which these were applied	-	<i>Not applicable</i>
I8	Records of the grout and/or concrete pressure with time	-	<i>Not applicable</i>
I9	Particularities that occurred during pile fabrication and installation	Section 3.2	
M	Instrumentation and measurements – static load test		
M1	Description of the equipment for measuring: <ul style="list-style-type: none"> - Axial force on the pile head - Axial displacement of the pile head - Height reference measurements with respect to a fixed point 	Section 4	
M2	Documents on the calibration of the load cells, the jacks and the sensors.	Appendix F.3 and Appendix F.4	
M3	Photos of the measurement instrumentation after installation on the reinforcement cage	Figure 4.9 and Figure 4.10	
M4	Cross-sectional drawings of the instrumentation within the pile with elevation indicated with respect to NAP	Figure 4.7	
M5	If applicable, the depths of the pile cross-sections in which strain gauges are fitted for measuring the normal force at these sections with elevations given with respect to NAP	Table 4.1	<i>For depths of the FBG sensors see Table 4.1. BOFDA readings taken every 5cm</i>
M6	If applicable, the depths with respect to NAP of the pile cross-sections with respect to which the displacement of the pile head has been determined using telltales or measurement strings.	-	<i>Not applicable</i>
M7	Records of the oil pressures in the jacks and the calculated load based on the oil pressure over time.	-	<i>Measurements not available</i>
M8	Record of the measured load in the load cells with time	Section 5	
M9	Graph in which the load based on oil pressure is plotted against the load measured using the load cell	-	<i>Measurements not available</i>

M10	Measured strains at selected cross-sections along the pile shaft or the relative displacements of the selected cross-sections with respect to the pile head over time	Section 5	
M11	Results of any measurements carried out during the installation of the test piles	Section 3.2.1	
M12	Control measurements carried out during the test, such as levelling with respect to an independent reference point	Section 4.1	<i>Qualitative description given</i>
M13	Any particularities during the test, such as failure of sensors, variations in jack pressures due to faults or other irregularities.	Section 5	
M14	Method of determining the measurement data and the determination of elastic modulus E	Section 6.1	
M15	Method of the static load test, see Article 10.2	Section 4.4	

1. Introduction

This report presents the installation and testing of four vibro piles (also referred to as driven cast-in-situ piles), executed as part of the full-scale axial pile load tests performed at Amaliahaven on Maasvlakte, Rotterdam, in December 2019 and January 2020. The tests were fully funded by the Port of Rotterdam and have a dual purpose: (i.) getting project-specific pile class factors and improved pile design (Class A2 test) and (ii.) updating national pile class factors (Class A1 test) as part of the TKI-funded Improved Axial Capacity of Piles in Sand (InPAD) project.

Three different pile types were tested as part of the overall testing programme for a total of eleven piles. These comprised of three driven precast piles, four screw injection piles and four driven cast-in-situ piles founded in a dense sand layer. Axial load testing was executed on all piles through the use of a reaction frame attached to a series of grout anchors, with the test programme carried out in accordance with the stipulations of NPR 7201 (Netherlands Standardisation Institute, 2017b) and of NEN 9997-1 (Netherlands Standardisation Institute, 2017a), with close collaboration with the national pile test committee. Strains across the full length of each pile have been recorded, in addition to settlement at the pile head and the corresponding pile installation data.

This document succeeds the *Technical note on pile test results performed at the Port of Rotterdam, Maasvlakte Test Site* (Revision 2; issued 13th May 2020) which assesses the test data received immediately after the end of the pile test and provides recommendations with respect to the appropriate capacity prediction method for pile design at Maasvlakte. This document shall present the test data in full and offer recommendations on the vibro piles for acceptance by the national pile test committee. Discussion of the driven precast and the screw injection piles are outside the scope of this report and are discussed in their own individual reports.

In addition, in order to facilitate the publishing of academic papers, a data embargo is in place on the pile test dataset until October 2023 and shall be published under the specific data license and relevant database(s). Special requests may be made to Prof. Ken Gavin (K.G.Gavin@tudelft.nl).

The report is sectioned as follows:

- Introduction
- Ground Investigation
- Pile Fabrication & Installation
- Pile Testing
- Measurement Results
- Interpretation & Analysis
- Discussion & Recommendations

1.1. Project Background

The pile test site is also part of the Improved Axial Capacity of Piles in Sand (InPAD) research project, supported by the Top Consortia for Knowledge and Innovation (TKI). The InPAD

project officially began on October 1st 2019 and will run for four years and is focused on investigating a number of aspects of pile behaviour including, but not limited to:

- i. The impact of friction fatigue on the distribution of α_s values on displacement piles.
- ii. Determination of accurate pile base resistances that include the effect of residual loads and therefore allow consistent α_p factors.
- iii. Whether limiting q_c values are necessary for estimating shaft resistance.
- iv. If limiting values on the pile base resistance are necessary.
- v. Determine the design value of the cone penetration test (CPT) end resistance q_c (i.e. what averaging technique to adopt)?
- vi. What are the impacts of ageing on the capacity of piles?

Two full-scale pile test sites shall be used as part of project: the test site at Maasvlakte described in this report and a test site at Deltares, Delft (scheduled to commence testing end of 2020). In addition, centrifuge testing and advanced statistical analyses shall be carried out to further investigate these research questions. The project is supported by the following partners:

- Deltares
- Fugro
- Gemeente Rotterdam
- NVAF
- Port of Rotterdam
- Rijkswaterstaat
- TU Delft

1.2. Test Site Location

The pile test site itself forms part of a larger deep-sea quay wall construction around Amaliahaven on Maasvlakte 2 in the port of Rotterdam. The Maasvlakte 2 itself consists of approximately 2000 hectares of recently reclaimed land with land reclamation completed in 2013. The land has been under persistent development ever since and already hosts a significant number of port-related developments with extensive road and rail connections.

The Amaliahaven quayside, currently partially developed, is to consist of approximately three kilometres of quay wall for some of the world's largest container ships along with a three-kilometre crane track and other associated quayside constructions. This will be realised using an anchored combi-wall with approximately 2600 foundation piles consisting of primarily screw injection piles. It was identified that there was scope to reduce the cost of the construction through the execution of pile load tests, whilst providing valuable insight into the behaviour of piles in deep dense sands.

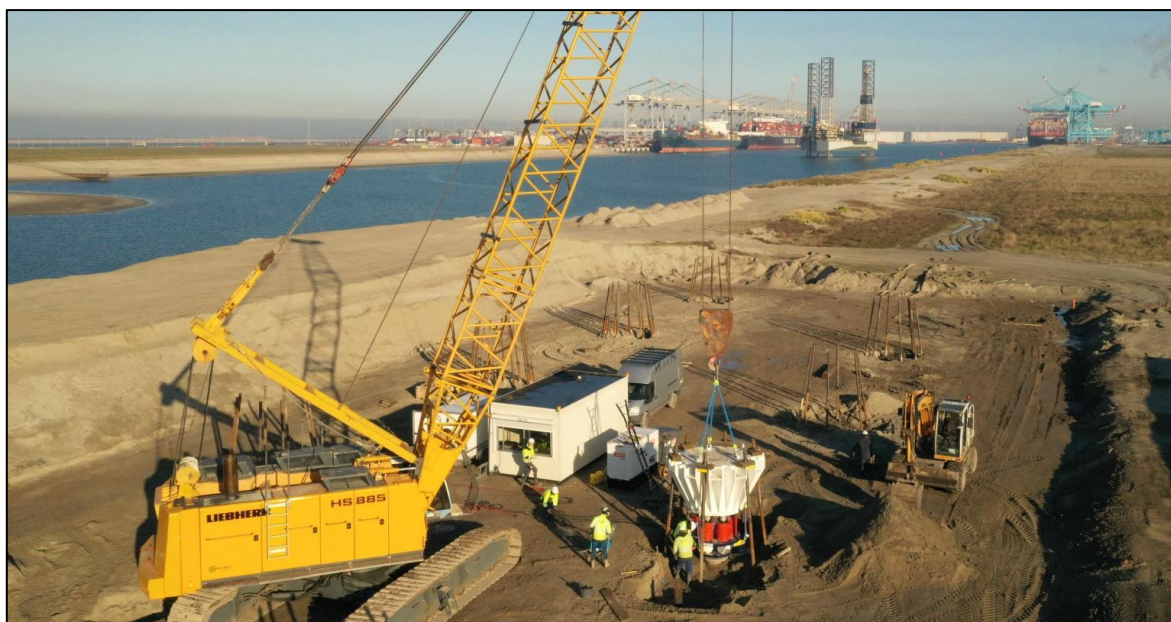


Figure 1.1: Aerial view of the north-eastern end of the pile test site, with Amaliahaven in the background

The test site was a greenfield site adjacent to the proposed quayside (Figure 1.1). Twelve test locations (four of each pile type) were originally planned for the site and were laid out in two rows of six piles with at least 16.5m between each pile (see Figure 1.2; for the full site plan see Appendix A). Four vibro piles were tested: P01, P03, P06 and P11 and was carried out amongst the tests on the two other pile types.

The roles and responsibilities of all parties involved directly with the construction and execution of the pile test programme are included in the Table 1.1. The representatives of the national pile test committee for the pile test at Maasvlakte were Jan van Dalen, Bert Everts and Ad Vriend.

Table 1.1: Parties involved during the pile testing and their respective roles

Party	Role(s)
De Klerk	General contractor
Deltares	Specification and interpretation of pile tests
High 5 Solutions	Subcontractor – Anchor installation
MariTeam	Consultant; Designers of Amaliahaven Quay Wall Project;
MOS Grondmechanica	Subcontractor – Ground investigation
Port of Rotterdam	Client & project management
Terracon	Subcontractor – Pile installation
TU Delft	Specification and interpretation of pile tests
WTCB	Measuring and instrumentation

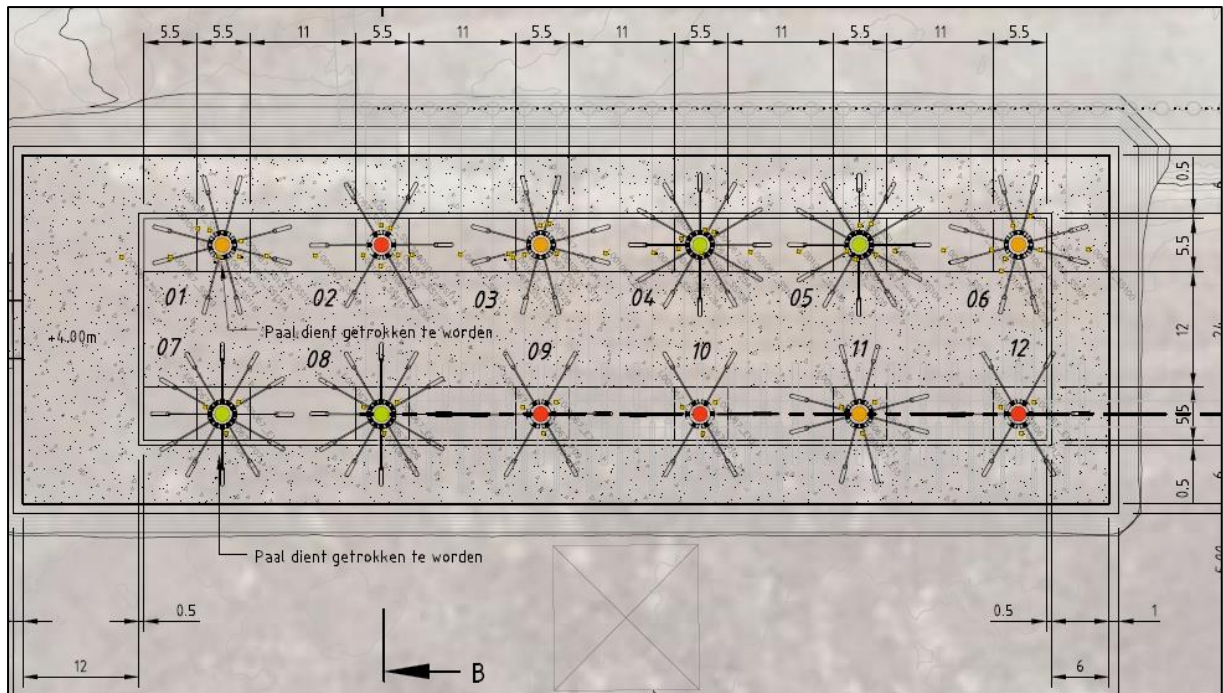


Figure 1.2: Site plan of the pile test site. In orange: vibro piles P01, P03, P06, P11; in green: screw injection piles P04, P05, P07, P08; in red: driven precast piles: P02, P09, P11, P12

2. Ground Investigation

An extensive ground investigation consisting of approximately 500 CPTs and 40 sampling boreholes was carried out in 2018 and 2019 as part of the overall Amaliahaven harbour development, the details of which are given in *1802965 Aanvullend grondonderzoek APMT* provided by MOS Grondmechanica. A ground investigation programme specific to the pile test site was also carried out and consisted of three to four CPTs approximately two metres from the central axis of each test pile, in addition to one CPT on each of these central axes, eponymously named after their respective piles. Three CPTs (i.e. CPTs 1101, 1102, 1103) were also executed after pile installation around P11 and are compared to the pre-installation CPTs in Figure 2.2.

All of the CPTs at the pile test site including their positions relative to their respective piles itself are provided in Appendix B.1, with Figure 2.1 showing an overview of the CPTs on the central axis of each vibro pile.

As part of the overall Amaliahaven investigation programme, one borehole was carried out directly on the site (BB20, see Appendix B.2) to NAP -25.57m located eight metres to the east of driven precast pile P09. Two more boreholes were also executed in the immediate vicinity of the pile test site (BB10 and BB11 to NAP -45.09m and NAP -45.08m respectively). A variety of laboratory tests have been performed on samples from these boreholes and on samples from across the Amaliahaven harbour, namely index parameter tests, oedometer, triaxial and particle size distribution tests. Sample photographs that have been taken are available in the site investigation report provided by MOS Grondmechanica. None of the soil samples taken from the ground investigation are still existing in storage. Seismic refraction has also been carried out using a line of geophones between P01 and P06.

The groundwater table is at approximately NAP +1m. This is based on a visual interpretation during the drilling of sampling boreholes in the winter season. No detailed groundwater monitoring programme has been executed in the vicinity of the pile test site.

Based on this data, the subsurface at the site can be described as follows:

- **NAP +4m to NAP -15m:** moderately dense to dense sand, with pockets of clay and very silty sand. Primarily dredged deposits up to the former seabed level at approximately NAP -8m.
- **NAP -15m to NAP -23m:** Interlaminated and/or mixture of sand and clayey silty sand of the Naaldwijk deposit.
- **NAP -23m to NAP -24m:** 1m bed of stiff clay of the Wijchen layer
- **NAP -24m to NAP -38m:** dense to extremely dense sand of the Kreftenheye formation. This layer also contains occasional clayey sand to sandy clay lenses at approximately NAP -28 m, around the vicinity of which pockets of clay can be found.
- **> NAP -38m:** Loose to moderately dense clayey sand from the Waalre formation.

It should be noted that a one metre deep excavation was also carried out across the entirety of the test site, bringing the elevation of the top surface from NAP +5m to NAP +4m. CPTs at the test site have been executed have been carried out before and after this excavation and thus,

the start depth of the CPTs can range from NAP +4m to NAP +5m. All piles are at least ten metres from any embankments created from the excavation.

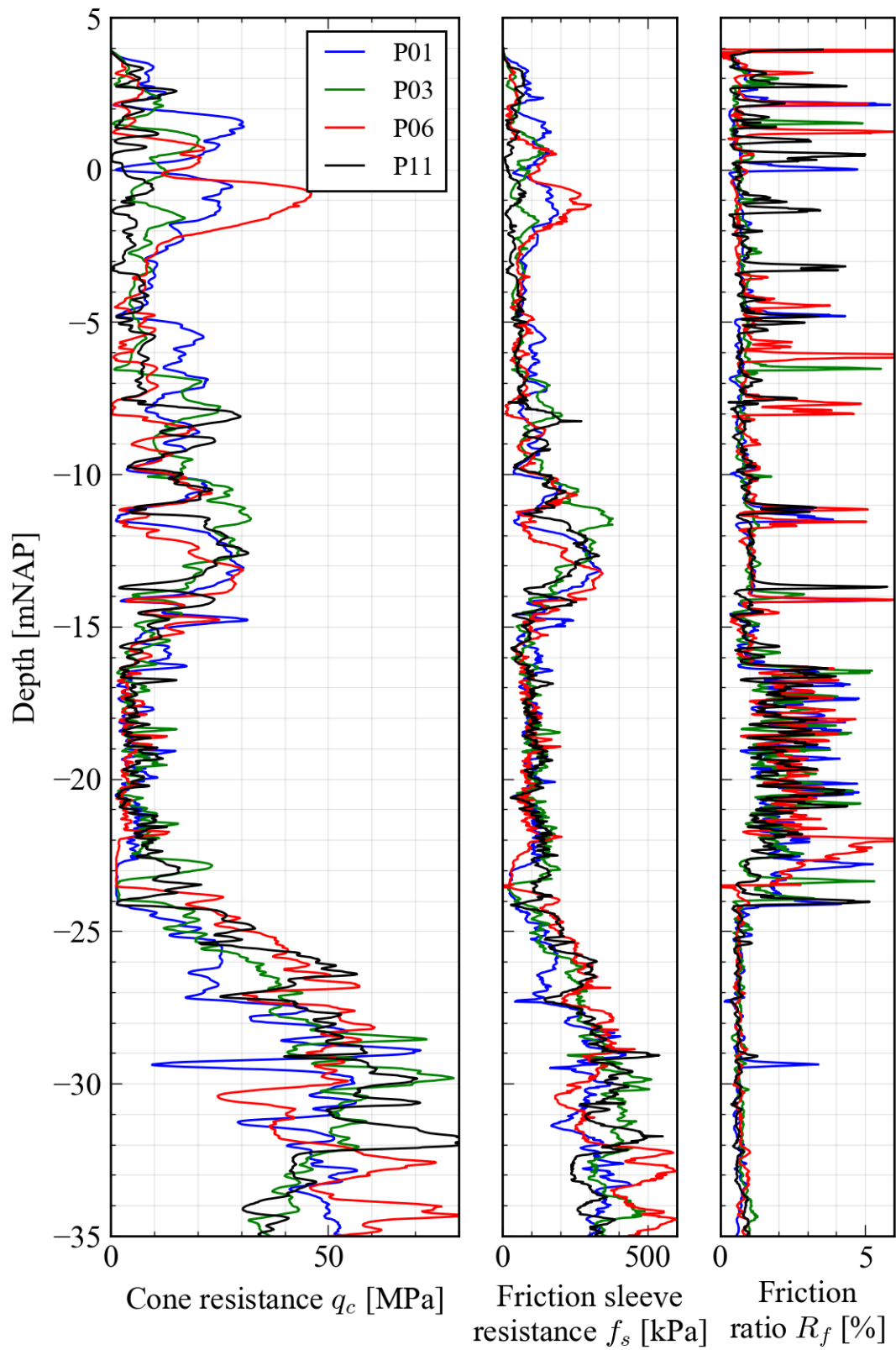


Figure 2.1: Plot of the CPTs along the central axis of each pile

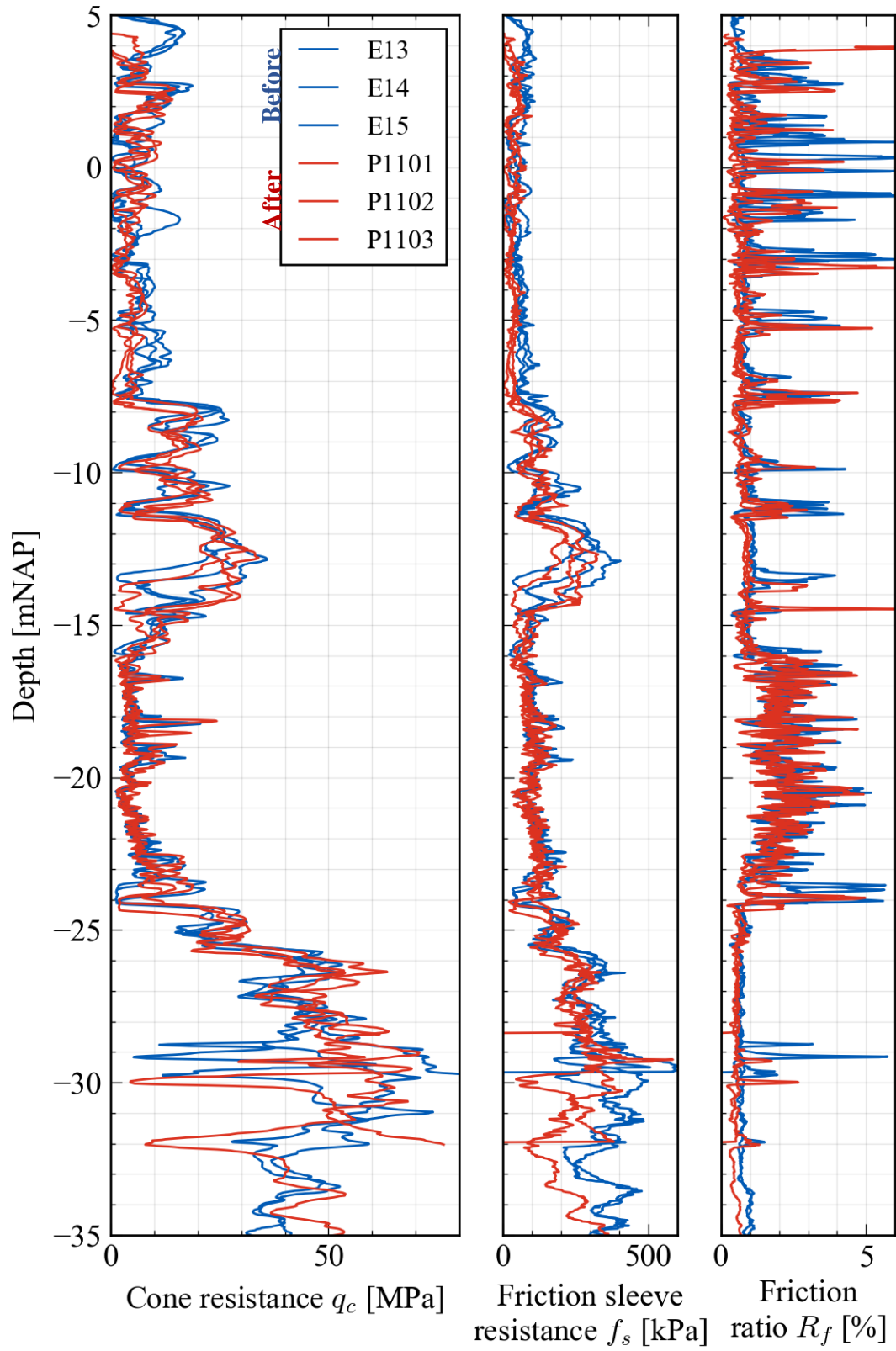


Figure 2.2: Comparison of CPTs around P11 executed before pile installation (i.e. CPTs E13, E14 and E15; in blue) and executed after installation (i.e. CPTs P1101, P1102, P1103; in red)

3. Pile Fabrication & Installation

This section shall elaborate on the design of the piles, in addition to their fabrication and installation. Four vibro piles were installed and tested, named P01, P03, P06 and P11. The geometries of these piles along with other relevant information are listed in Table 3.1.

The installation of the driven cast-in-situ piles (vibro piles) has been facilitated by a reusable steel auxiliary tube, with an identical sacrificial base plate used across all four piles. For all piles a similar base plate has been used. In order to limit the ultimate test load, piles with a scaled-down diameter have been used, whilst the absolute distance (or offset) between the outer diameter of the base plate and the inner diameter of the auxiliary tube is similar to what is typically used in practice. Consequently, the ratio between these two diameters contravenes the requirements of NEN 9997-1 and the results can be interpreted as conservative. Furthermore, the size of the reinforcement cage chosen is significantly larger than that used in traditional practice in order to load the piles up to geotechnical failure, as required by a Class A1 test.

The target pile toe level (also referred to as the pile tip or the elevation of the base plate) was identical for all four vibro piles, with all piles reaching this target depth. P01 features a significantly lower $q_{c,avg}$ (see Table 3.1) using both the Koppejan and De Boorder averaging techniques compared to the three other piles due to the presence of pockets of clay or clayey sand in the CPTs executed within two metres of the pile's central axis. These laminations are also present in the vicinity of other piles across the test site, however these pockets either fade out across this two-metre zone or are not present altogether and thus do not exert a dominating influence on the obtained $q_{c,avg}$.



Figure 3.1: Sacrificial base plate used for the installation of the vibro piles

Table 3.1: Vibro pile geometries, installation data & specifications

	P01	P03	P06	P11
Pile length [m]	32.54	32.49	32.50	32.50
Pile head level [mNAP]	4.00	4.00	4.00	4.00
Pile toe level [mNAP]	-28.54	-28.49	-28.50	-28.50
Target pile toe level	-28.50			
Pleistocene sand depth [mNAP]	-24.05	-23.95	-23.50	-24.10
Auxiliary tube, Inner diameter [m]	0.330			
Auxiliary tube, outer diameter [m]	0.380			
Base plate outer diameter [m]	0.480			
$q_{c,avg, Koppejan}$ [MPa]*	16.68	41.09	30.31	39.82
$q_{c,avg, De Boorder}$ [MPa]*	40.94	52.43	51.02	50.54
Installation date [DD/MM/YY]	14/11/19-15/11/19	15/11/19	18/11/19	18/11/19
Installation duration (hammering) [mins]	28	22	39	22
Installation duration (extraction) [mins]	40	21	19	17
Testing date [DD/MM/YY]	13/01/20-14/01/20	19/12/19	07/01/20-08/01/20	09/01/20-10/01/20
No. days between installation and testing	59	34	50	52

3.1. Pile Geometry & Fabrication

All four vibro piles were provided by and installed by Terracon Funderingstechniek B.V. Installation was first facilitated by the hammering of a steel auxiliary tube (Appendix C), 380mm in outer diameter and 330mm in inner diameter. A sacrificial base plate was attached to the bottom of this, with a 480mm outer diameter and a base thickness of 25mm. This base plate was geometrically compatible with the bottom of the auxiliary tube so the base plate could be attached to the bottom of the auxiliary tube without the use of any epoxy or joints, with the exception of a rubber strip placed along the inner diameter of the base plate in order to minimise water ingress into the borehole at the auxiliary tube—base plate interface.

The pile body was composed of C35/45 XC2 S3 grade concrete with a maximum aggregate size of 8mm. A smaller-than-normal maximum aggregate size was used due to the larger steel reinforcing used. This steel reinforcing consisted of four GEWI® TR670/800 bars (diameter 50mm), with spiral reinforcing encircling the four bars at a diameter of 250mm (Figure 3.2; for detailed drawing see Appendix E.1). Prior to installation, this reinforcement cage was instrumented with fibre optics, outlined in Section 4.3.

* $q_{c,avg}$ has been calculated based on the average of all CPTs within two metres of the piles' central axes



Figure 3.2: Steel reinforcing of the vibro piles lying on site in advance of instrumentation and installation

3.2. Pile Installation

The installation of all piles was carried out with a Woltman HDPR 900 drilling rig provided and operated by the subcontractor Terracon, with an IHC S-120 hydraulic hammer used to hammer the auxiliary tube into place. Once the target depth was reached, the inside of the auxiliary tube was dipped to check if water infiltrated the auxiliary tube—base plate interface. If no water was present, the installation process proceeded with the placement of the reinforcement cage and concrete, with none of the piles requiring reinstallation due to water ingress (or otherwise). Notwithstanding, it was observed for at least one vibro pile (P11) that a 5-10cm layer of wet concrete was present at the bottom of the auxiliary tube immediately after its installation. This is most likely as a result of fresh concrete from the previous installation sticking to the tube and falling to the bottom during the following installation.

The reinforcement cage was placed within the empty hammered-in-place auxiliary tube using two cranes (Figure C.4) in order to avoid damage to the fibre optic instrumentation affixed to the reinforcement. Once placed within the auxiliary tube, the reinforcement cage was left resting directly on the base plate and was not suspended in any form. Immediately after the placement of the reinforcement cage, concrete was poured into the auxiliary tube and the tube was retracted using a reverse hammering action supplied by the same IHC S-120 hammer, with the concrete in the auxiliary tube being replenished at regular intervals. No pre-lining of the reinforcement with highly liquid concrete was applied (in Dutch: *vertinnen*) and no additional downward hammer blows were applied to compact the concrete after its pouring. A schematic of the installation process can also be seen in Figure 3.3.

For the entirety of the installation process (i.e. both the insertion and removal of the auxiliary tube), regular measurements were made of a variety of drilling parameters using the on-board rig computer and associated software provided by Tomer Systems B.V., with the data shown

in Section 3.2.1. The frequency of the reverse hammering action used to extract the auxiliary tube was not recorded. Furthermore, roughly 4.5m^3 of concrete was used for each pile, based on a visual interpretation of the amount of concrete poured out of the concrete skips and into the pile, however this number should only be used for indicative purposes.

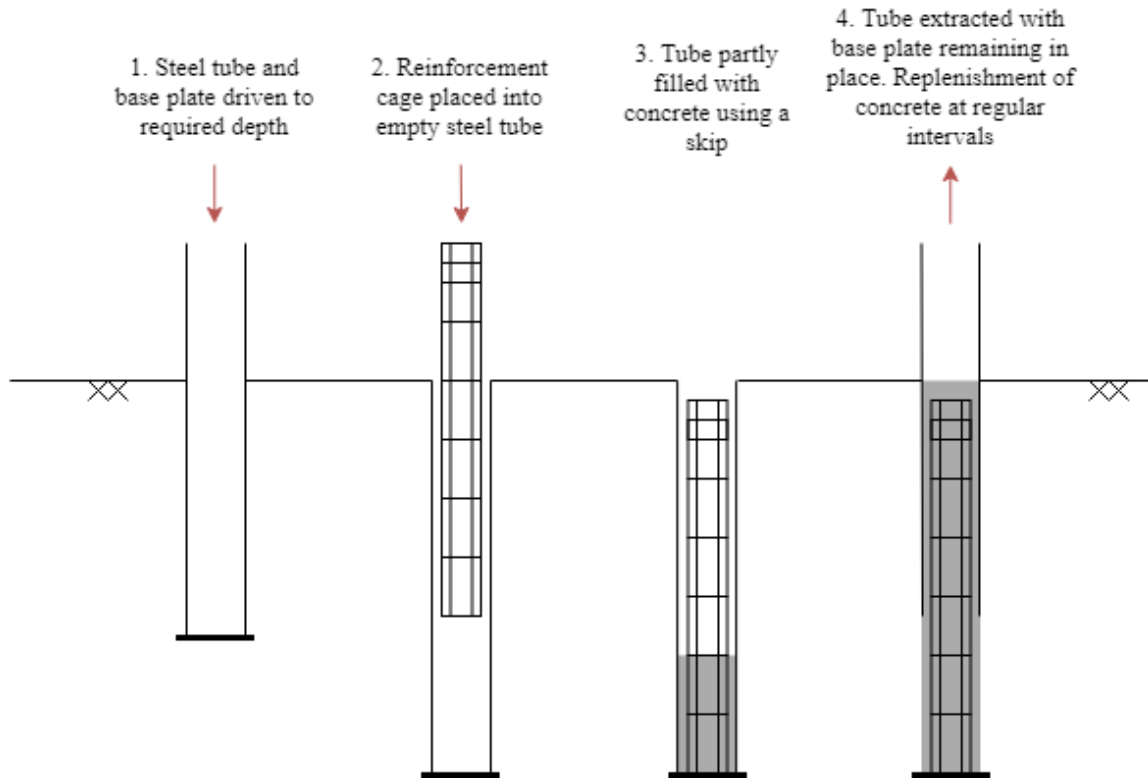


Figure 3.3: Installation procedure for the vibro piles

During inspection of the pile heads, it was found that the reinforcement was not centrally positioned at the pile head (Figure 3.4), most likely as a result of the reinforcement resting directly on the base plate. To provide further support to the pile head under the loading of the test frame, a steel sleeve with a length of two metres was placed around the upper part of each pile, with a hole drilled through the wall of the sleeve to allow the passage of the fibre optics (Figure 3.5). The pile cap was then placed over this steel sleeve, described in more detail in Section 4.1.

In terms of specific on-site observations of the installation process, it should be noted that the first vibro pile to be installed, P01, was first installed to NAP -2m and left in place overnight in order to stabilise the drilling rig overnight; allowing the immediate installation of the pile the following morning. The measurements of the first part of installation have not been recorded. Furthermore, problems with the drilling rig measurement system were experienced during the installation of P06, resulting in a lack of measurements between NAP -16.16m and NAP -24.27m.

For videos or further pictures of the pile installation, please contact k.duffy@tudelft.nl.



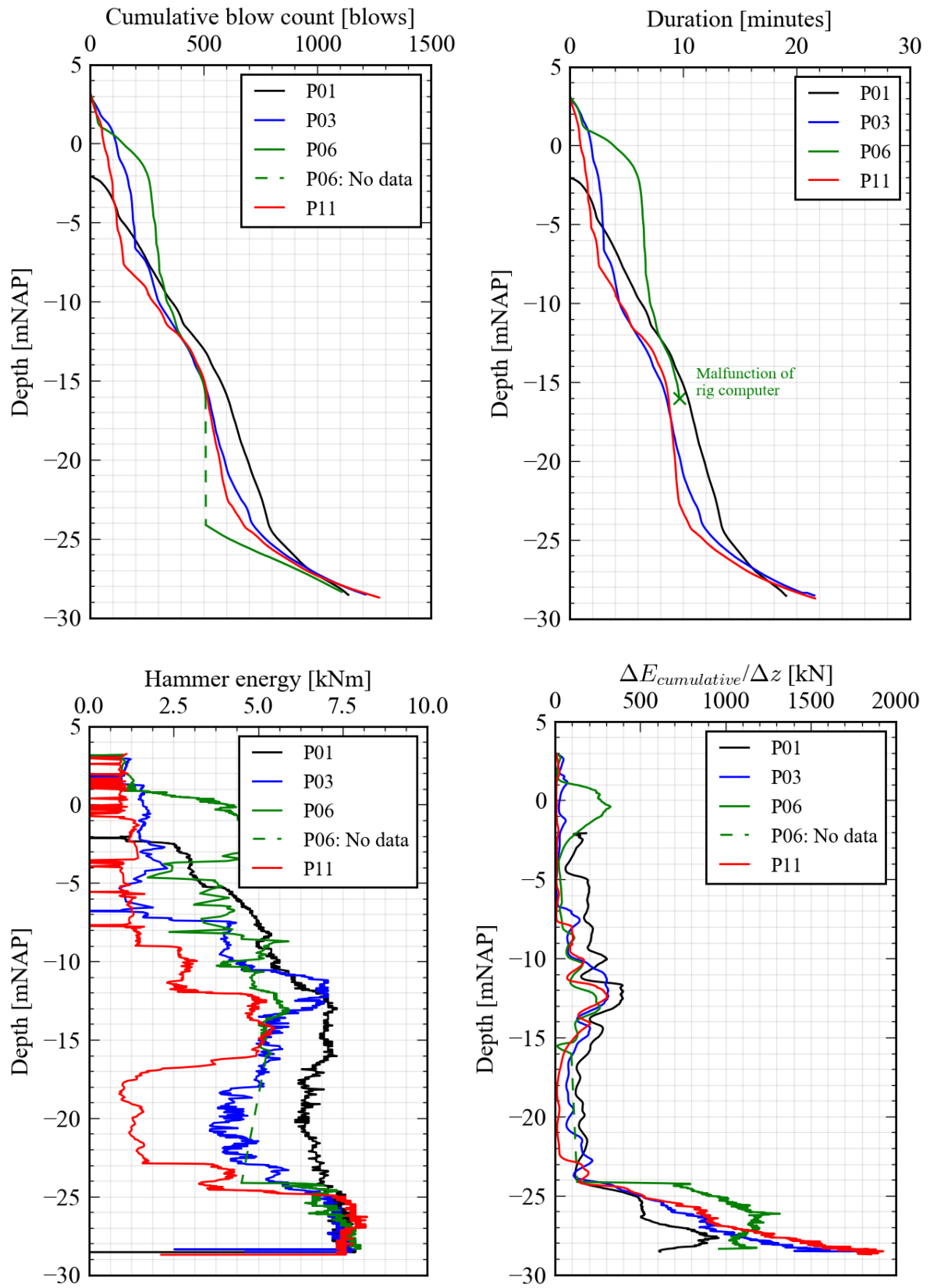
Figure 3.4: Pile heads of the four vibro piles immediately after installation. Note the non-centric placement of some of the reinforcement (Photos: Gust van Lysebetten, WTCB)



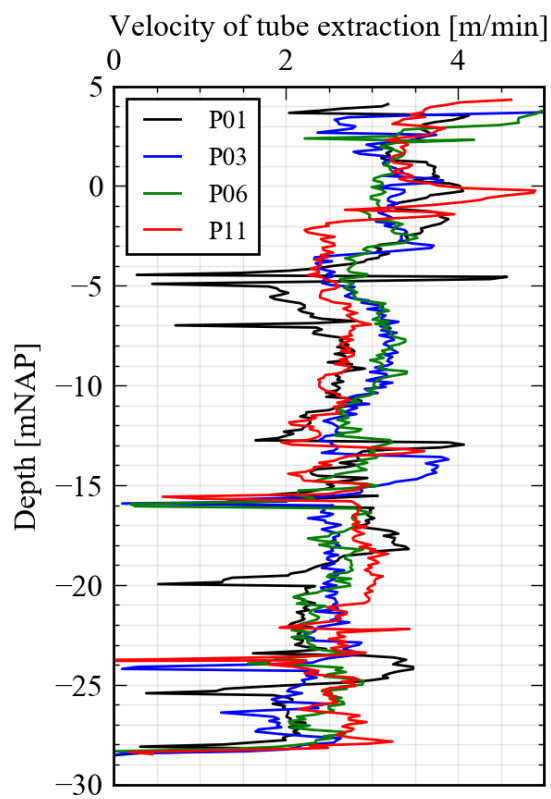
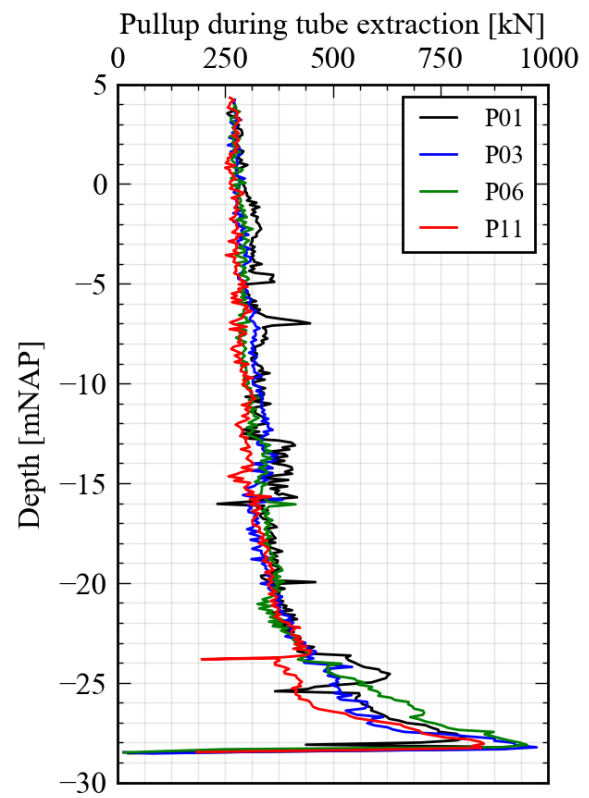
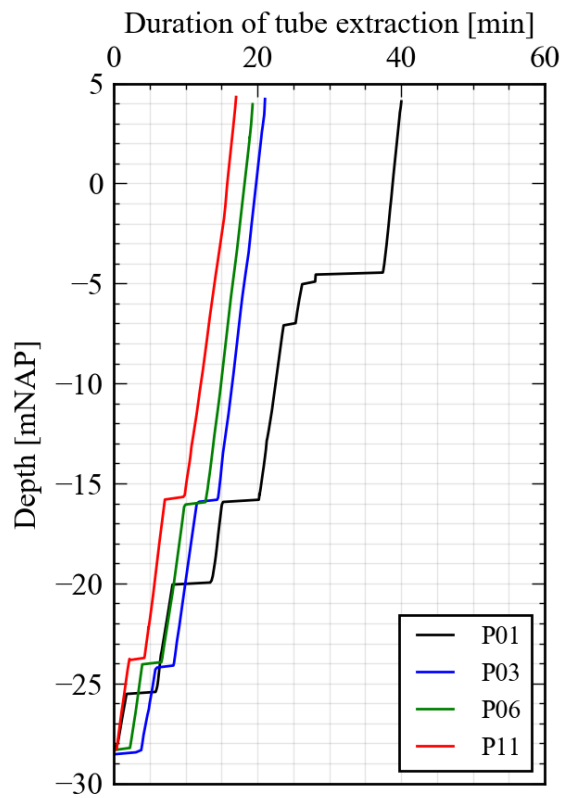
Figure 3.5: Vibro pile after the installation of the two metre sleeve around the uppermost part of the pile shaft without grout (Photos: Gust van Lysebetten, WTCB)

3.2.1. Installation Data

Hammering



Extraction



4. Pile Testing

This chapter shall introduce the equipment used in during the pile test, including the reaction frame and the associated grout anchors used to develop the reaction force atop of the pile. Thereafter, the measurement systems shall be discussed.

4.1. Test Frame

The test frame in its entirety consists of a reaction frame (colloquially known as the spider's head or *de spinnenkop* in Dutch) tied in by eight grout anchors (i.e. in the case of the vibro piles), six hydraulic jacks, six load cells, a transition piece and a pile cap.

Each jack had a capacity of approximately 5000kN in order to attain the capacity of the other pile types used at the test site, with the jacks controlled automatically by a programmable logic controller (PLC) at the hydraulic unit (capacity of 700 bars). The oil pressure from this hydraulic unit was continuously recorded throughout the test in order to verify and act as backup to the load cell readings, however, no records of the results have been kept. On top of each jacks were six calibrated load cells (i.e. dynamometers) with an accuracy of ± 1 kN. The configuration of these load cells and jacks was ensured using a transition piece (see Appendix E.3), which transferred the load from the jacks through the pile cap and to the pile.

The settlement of the pile head was measured using four displacement transducers (linear variable differential transformers (LVDTs), accuracy of ± 0.01 mm), placed at four diametrically opposing ends of the pile. This settlement was measured relative to a reference frame, whose supports were installed in the ground at a distance ranging from 3.6m to 3.8m from the pile's central axis (see Figure 4.1). Cross-checking of the pile head settlement and the inclinations and elevations of the reference frame and the grout anchors was carried out using a total station and surveying prisms (see Figure 4.1 and Figure 4.2).

The calibration sheets of the load cells and LVDTs can be found in Appendix F.3 and Appendix F.4 respectively.

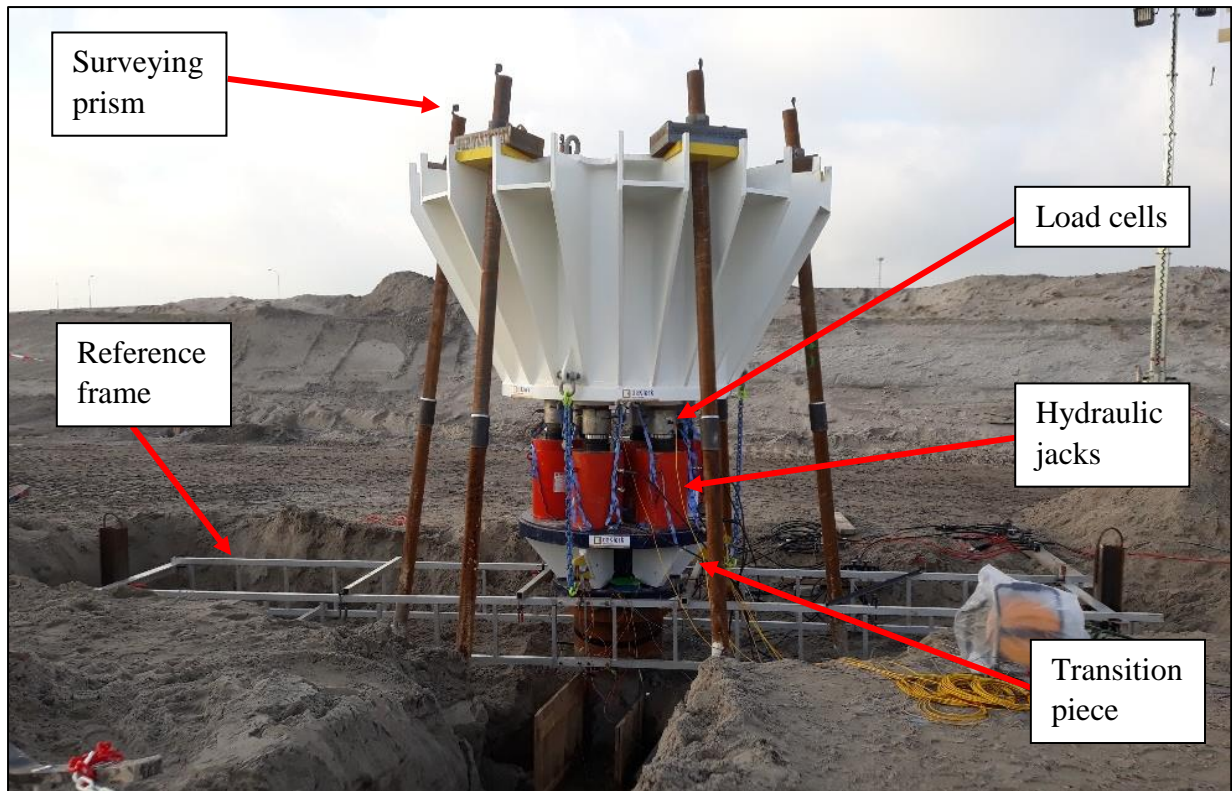


Figure 4.1: Reaction frame & reference frame

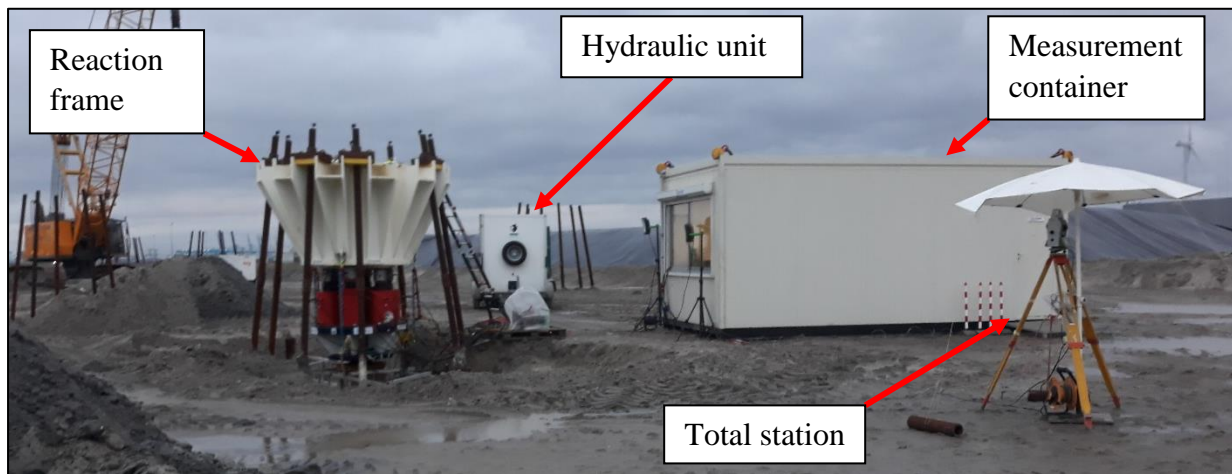


Figure 4.2: Overall set up of the testing equipment

The pile caps on the vibro piles were designed in such a way to ensure fully centric loading on the piles. To achieve this, a steel ring was welded onto the top of each pile cap (Figure 4.3a), within which a round insert underneath the reaction frame's transition piece could be placed (Figure 4.3b). The pile cap was fitted onto the pile sleeve (described in Section 3.2) with the space between the sleeve, the pile cap and the vibro pile itself filled with a steel fibre reinforced mortar (BASF MasterEmaco T 1400 FR) to ensure the full development of the pile cap—pile head interface and to fill the annular space between the sleeve and the concrete pile itself. A detailed drawing of the pile cap is shown in Appendix E.2.

The total weight of the reaction frame including the load cells, jacks, transition piece and pile cap is 22.7 tonnes and has been included in the measured load on top of the pile. Zero-

measurements of the pile head settlement and the fibre optics have been made with the full weight of the reaction frame on the pile.



Figure 4.3: Interface between the reaction frame and the pile cap: (a.) underside of the transition piece (b.) top of the pile cap (Photos: Gust Van Lysebetten, WTCB)

4.2. Grout Anchors

The reaction force for pile testing was obtained using a ring of eight symmetrically placed grout anchors affixed to the reaction frame, each at an angle of 8° from vertical with a grout body length of 7.5m and a total anchor length of 38m. The design of these anchors was realised by MariTeam. The layout of the anchors ensured that the grout body of each anchor was at least five metres from the pile shaft (see Figure 4.4) and a finite element analysis was also performed in order to show that the anchors would have minimal influence on the capacity of the piles.

Installation of the grout anchors was carried out by High 5 Solutions using self-boring ground-displacement screw injection anchors conforming to CUR166 (CUR, 2008). This procedure is carried out using sonic drilling whereby the anchor segments simultaneously rotate and vibrate at a high frequency. Each segment of the threaded grout anchor was connected using a coupling sleeve, with the angle of the grout anchors during the installation process being assured by a drilling template, as shown in Figure 4.5b.

During the installation process, water is pumped through a hollow section within the grout anchor itself until the starting depth for the grout body is reached from which point grout is pumped through the anchor until the end depth was reached. The grout used was provided by Beamix and is of type GM 42, CEM III with a strength class $> 25 \text{ N/mm}^2$ (for the specification sheet see Appendix F.1). Following this, the inside of the rod was rinsed with water.

Further specifications on the grout anchors are given in Appendix F.1 and Appendix F.2. No anchor testing was carried out in advance of pile testing of the vibro piles, unlike the screw injection piles on the same site.

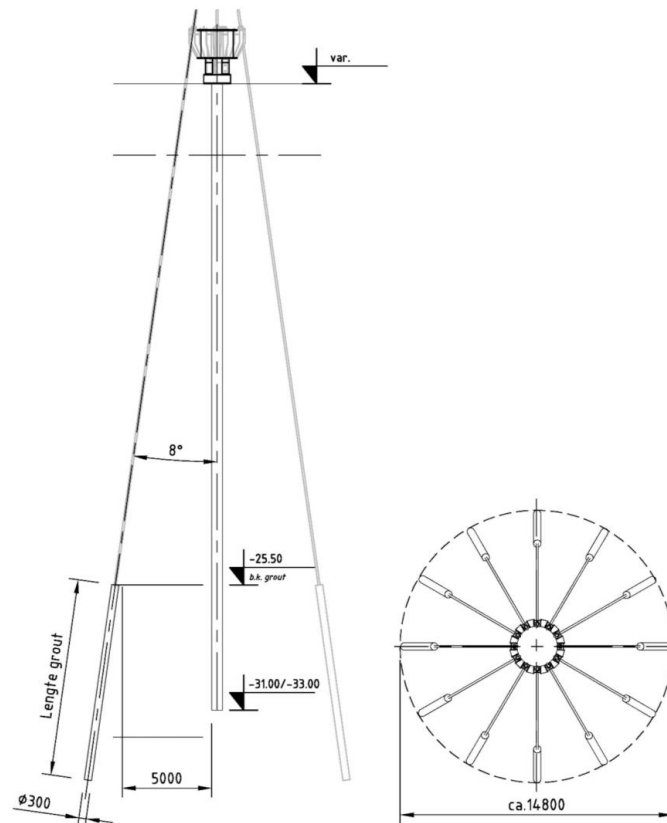


Figure 4.4: Schematic of the grout anchor design in both elevation (left) and plan view (right)



Figure 4.5: (a.) Installation of the grout anchors around the test pile (b.) Close up of the installation process, highlighting the use of the anchor guide frame in order to install the anchors at the correct position (c.) screw tip of the grout anchors (photo: Gust van Lysebetten, WTCB)

4.3. Strain Measurements

All vibro piles were instrumented across their length using two fibre optic measurement systems: FBG (Fibre Bragg Grating) and BOFDA (Brillouin Optical Frequency Domain Analysis). A brief introduction to each sensing technique is given as follows:

4.3.1. Fibre Bragg Grating (FBG)

FBG fibres provide strain measurements at discrete intervals along the pile shaft through the use gratings incised into the optical fibre, each approximately 1cm in length. are incised into the optical fibre. These gratings (hereunder referred to as a sensor or a gauge) reflect light of a certain wavelength depending on the strain and temperature measured within the range of the sensor. In a process known as multiplexing, multiple sensors can be placed along the length of the fibre optic cable.

The FBG data logger used in the pile test was the Micron Optics SM125 and the fibre type used was the FBGS SMW-01, a glass fibre reinforced polymer (GFRP) fibre shown in Figure 4.6. This system provided strain readings every ten seconds from gratings placed along the full length of the pile (for depths of the sensors, see Table 4.1). Each vibro pile consisted of two FBG fibres at opposing corners of the steel reinforcing along its entire length, affixed using a combination of epoxy glue and cable ties (Figure 4.7 and Figure 4.10).

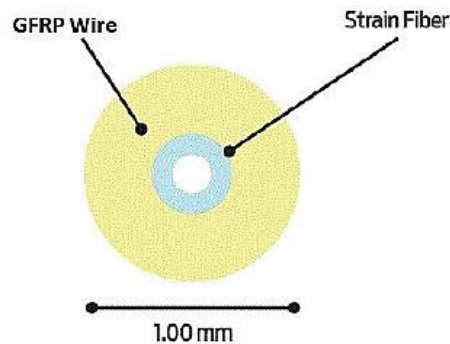


Figure 4.6: Cross-sectional schematic of the SMW-01 FBG cable

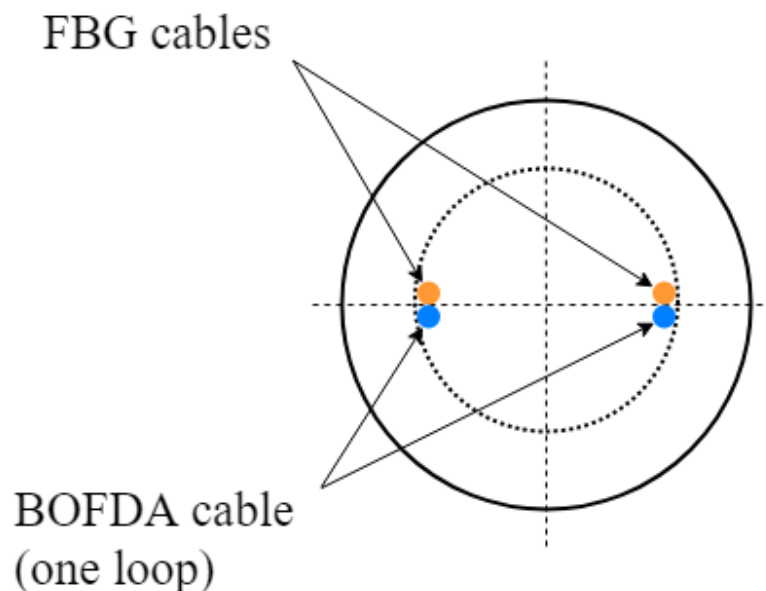


Figure 4.7: Configuration of the fibre optic sensors in the vibro pile

Table 4.1: Depths of the FBG sensors. The depths have been derived from the pile base level obtained from the pile installation records

	P01		P03		P06		P11	
	Elevation [mNAP]	ΔL [m]	Elevation [mNAP]	ΔL [m]	Elevation [mNAP]	ΔL [m]	Elevation [mNAP]	ΔL [m]
FBG 1	0.72		0.77		0.76		0.76	
FBG 2	-1.28	2.00	-1.23	2.00	-1.24	2.00	-1.24	2.00
FBG 3	-4.28	3.00	-4.23	3.00	-4.24	3.00	-4.24	3.00
FBG 4	-7.28	3.00	-7.23	3.00	-7.24	3.00	-7.24	3.00
FBG 5	-10.28	3.00	-10.23	3.00	-10.24	3.00	-10.24	3.00
FBG 6	-13.28	3.00	-13.23	3.00	-13.24	3.00	-13.24	3.00
FBG 7	-16.28	3.00	-16.23	3.00	-16.24	3.00	-16.24	3.00
FBG 8	-19.28	3.00	-19.23	3.00	-19.24	3.00	-19.24	3.00
FBG 9	-22.28	3.00	-22.23	3.00	-22.24	3.00	-22.24	3.00
FBG 10	-23.28	1.00	-23.23	1.00	-23.24	1.00	-23.24	1.00
FBG 11	-24.28	1.00	-24.23	1.00	-24.24	1.00	-24.24	1.00
FBG 12	-24.78	0.50	-24.73	0.50	-24.74	0.50	-24.74	0.50
FBG 13	-25.28	0.50	-25.23	0.50	-25.24	0.50	-25.24	0.50
FBG 14	-25.78	0.50	-25.73	0.50	-25.74	0.50	-25.74	0.50
FBG 15	-26.28	0.50	-26.23	0.50	-26.24	0.50	-26.24	0.50
FBG 16	-26.78	0.50	-26.73	0.50	-26.74	0.50	-26.74	0.50
FBG 17	-27.28	0.50	-27.23	0.50	-27.24	0.50	-27.24	0.50
FBG 18	-27.78	0.50	-27.73	0.50	-27.74	0.50	-27.74	0.50
FBG 19	-28.28	0.50	-28.23	0.50	-28.24	0.50	-28.24	0.50

4.3.2. Brillouin Optical Frequency Domain Analysis (BOFDA)

The BOFDA measurement system provides a quasi-continuous measurement of strain along the pile shaft, with measurements being made every four minutes throughout the pile test. Furthermore, the optical fibre does not require special manufacturing techniques such as the gratings of the FBG system, however, the system requires that the fibre optic cable is placed in a looped configuration where the BOFDA cable runs down to the bottom of the pile, and loops back up to the top of the pile.

With this configuration, the data logger sends a probe light down one end of the loop, and a pump light down the other end. The incidence of these light waves causes a backscattering of light which consists of three different spectral components: Raman, Brillouin and Rayleigh. Brillouin-based data loggers can measure the frequency of this backscattered light wave, which is concurrently dependent on the mechanical strain and temperature across the sensor.

The BOFDA data logger used at Maasvlakte was the fibrisTerre 2505 and the sensing cable used was the Solifos BRUsens DSS V9 (see Figure 4.8), with a measurement frequency of four minutes. This fibre is encased in a metal tube in order to increase the robustness of the cable, along with a polyamide outer sheath. Each vibro pile consisted of one BOFDA loop, with either end of the loop affixed to two diagonally opposing reinforcing bars, affixed using a combination of epoxy glue and cable ties (Figure 4.7 and Figure 4.10). The loop at the bottom

of the pile was facilitated by the spiral reinforcing, around which the loop could pass from one side of the reinforcement cage to the other (Figure 4.10).

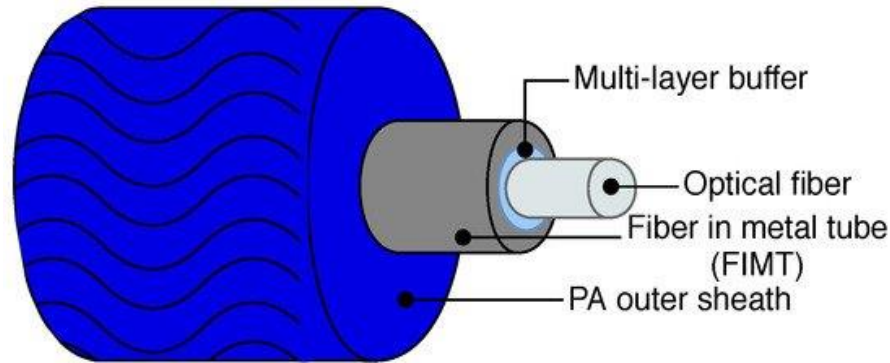


Figure 4.8: Schematic of the Solifos BRUsens V9 (Piccolo *et al.*, 2020)

4.3.3. Installation of Fibre Optics

The ends of both the BOFDA and FBG cables were stored in two metal boxes at the top of the reinforcement cage to avoid any damage that may arise during the insertion of the reinforcement cage and concrete pouring (Figure 4.9). During the lifting of the reinforcement cage, care was taken to ensure no striking of the reinforcement cage against other objects (such as the head of the auxiliary tube) and the use of two cranes (for further details on the lifting procedure, see Section 3.2) mitigated the amount of bending in the reinforcement cage, and consequently, the fibre optics. Following the installation of the reinforcement cage and the placement of the concrete, a sleeve was placed around the pile head (Figure 3.5) along with the pile cap, between which the fibres were able to exit the pile (Figure 4.11).

During the testing phase, all cables were connected to outdoor patch cables to ensure the integrity of the cables on the construction site. All cables (of the same measurement type) were spliced together using fusion splicing before connection with their respective data loggers. No temperature correction was applied to the strain readings as it is assumed that the temperature has remained relatively constant over the course of the pile test and nor have there been any measurement of the residual loads (or lack thereof). All fibres were tested in advance of the pile load test and were verified to be in full working order.



Figure 4.9: The instrumented reinforcement cage in advance of its insertion into the auxiliary tube. Note the two protective metal boxes at the tip of the reinforcement cage.



Figure 4.10: Close-up of the base of the reinforcement cage. Note the loop in the BOFDA cable (blue cable) across the spiral reinforcing. The FBG cable (white) terminates at the end of the reinforcement cage



Figure 4.11: Egress point for the fibre optics between the pile cap and pile sleeve. Grout was used to fill the annular space between the pile cap and pile sleeve, with a PVC facilitating the safe passage of the fibre optics through the annular space

4.4. Test Procedure

The pile testing was carried out in accordance with NPR 7201 (Netherlands Standardisation Institute, 2017b) albeit with the omission of the unload/reload cycles following each load step. During each pile test, at least one representative from each of MariTeam, Port of Rotterdam, TU Delft/Deltares and WTCB was present in order to coordinate and supervise the pile test.

At the start of each test, a reference measurement was made with the weight of the reaction frame on top of the pile (referred to as “refSLT”). Thereafter, the pile was loaded to 5% of the predicted pile capacity, calculated according to current NEN 9997-1 recommendations without limiting factors (see Appendix D for calculation details). This load step allowed for the proper functioning of the load cells, hydraulic jacks, displacement transducers and other apparatus to be verified. During each load step, the load was kept as constant as possible using the PLC-driven hydraulic unit and during changes in the load size, the load was adjusted gradually in order to monitor the inclination of the reaction frame and the pile head. In the event of an increasing inclination of the reaction frame or the pile head, this was compensated for by adjusting the load within each individual jack or series of jacks. During each step (i.e. where the load was kept constant), the creep parameter (*kruipmaat*; as per NPR 7201) was assessed according to the following formula:

$$k = \frac{s_{0,t_2} - s_{0,t_1}}{\log_{10} \left(\frac{t_2}{t_1} \right)}$$

where: s_{0,t_1} , s_{0,t_2} = settlement (in millimetres) of the pile head at times t_1 and t_2 respectively; t_1 = time at the beginning of the period being assessed (in seconds); t_2 = time at the end of the period being assessed (in seconds).

From the 5% load, the load was increased by step sizes of 12.5% of the predicted pile capacity. In the event of pile unloading and reloading, the load was reduced back to 5% of the predicted pile capacity and reloaded from there. At higher loads and/or where the creep parameter exceeds 1mm over the previous thirty minute period, the step size was halved (i.e. a step size of 6.25%). Consequently, each load test had a minimum of eight load steps.

It should be noted that the first load test in the overall test programme, driven precast pile P02, incorporated unload/reload cycles to 5% of the predicted pile capacity at the end of each load step. A mutual agreement between the pile test supervisors and the NPR following the first load test resulted in these unload/reload cycles being removed from all succeeding tests and so for all vibro piles, no regular cyclical loading after each load step was carried out.

Notwithstanding, unload/reload cycles were incorporated in some of the pile tests if the pile did not fail at the test frame's maximum permissible load in order to reduce some of the pile shaft friction and to transfer more of the load to the Pleistocene sand layer. Unload/reload cycles were also incorporated to alleviate any excessive tilting of the test frame, if necessary, or if issues had arisen with the hydraulic unit. No anchor testing was carried out (unlike at the locations of other pile types in the overall test programme) and therefore, the piles experienced no cyclical loading in advance of their testing.

At the 5% load (both at the start of the test and at unload/reload stages), the load was held for approximately five minutes. Load steps up until 50% of the pile capacity were sustained for at least thirty minutes, with load steps greater than 50% being held for at least one hour. If the amount of creep in the last thirty minutes of the load step had not stabilised or continued to increase significantly, then it was decided by the test supervisors to extend the duration of the load step.

The pile test was ended if one of the following stopping criteria was met:

- The hydraulic unit or the hydraulic jacks can no longer increase the load on top of the pile.
- The reaction frame can no longer sustain enough contact with the pile due to excessive settlement of the pile head or if the yield strength of the anchors was reached.

Pile failure was determined if the settlement of the pile base (calculated by subtracting the elastic shortening s_{el} of the pile from the settlement at the pile top s_0) exceeded 10% of the equivalent pile diameter D_{eq} . The elastic shortening of the pile was determined by integrating the strain readings across the pile length for both the BOFDA and FBG measurement systems*. The mean s_{el} from both measurement systems was then taken.

Later in the test programme, the pile test termination first consisted of the closing of the hydraulic jacks (a step named "close hydr.", e.g. Figure 5.1), whereby the pile continued to

* Due to the scattered readings at the bottom of the pile (see Section **Error! Reference source not found.**), the average strain over the non-scattered area has been taken and has been multiplied by the full pile length. The scattered measurements have not been included due to the uncertainty with regards to the representativeness of the fibre optic readings in this area (e.g. potential slippage between the fibre and the reinforcing) and the chosen method provides a conservative estimate of the base settlement (with respect to the corresponding α_p at $s_b = 0.1D_{eq}$).

experience settlement and thus the pressure in the jacks reduced (i.e. the length of the jacks decreased) so that the reaction frame could follow the settling pile. The pile-reaction frame system would therefore reach an equilibrium once the pressure in the jacks (i.e. the load on the pile head) was reduced to a certain amount.

Furthermore, three of the four pile tests were divided across two days due to time constraints. For the second vibro test P06 (the first pile test intentionally carried out across two days), the pile was loaded to 50% of its predicted capacity on the first day and then unloaded to 5% of its predicted capacity and kept at that load overnight before the load test programme resumed the following day. Conversely for the vibro piles thereafter (P01 and P11), the hydraulic jacks were closed overnight once the load reached 50% of the piles' predicted capacities, resulting in a gradual overnight decrease of the load on the piles of around 1000kN from the 50% load.

5. Measurement Results

This chapter shall give a factual description of each test, providing the results of the reference strain and temperature measurements, in addition to the measurements made during each pile test. Interpretation and analysis of the data has been discussed in Section 6. The data processing, analysis and visualisation has been primarily carried out using the Python programming language, including the apriori prediction of pile capacity and the CPT averaging methods. Microsoft Excel has also been used for specific tasks.

Note that compressive strain and downward settlement of the pile are indicated as positive quantities.

Table 5.1: Pile test dates and times

Pile	Test Date(s)	Test Duration
P01*	13/01/20-14/01/20	33 hours, 0 minutes
P03	19/12/19	15 hours, 16 minutes
P06†	07/01/20-09/01/20	30 hours, 15 minutes
P11*	09/01/20-10/01/20	33 hours, 21 minutes

5.1. Test Results: Pile P01

Testing of pile P01 was carried out over two days. The first day, the pile was loaded to step 4 at 3800kN with the valves to the hydraulic jacks being closed overnight, resulting in a gradual reduction in the load on top of the pile to 3300kN upon the resumption of testing the following morning. From this point, the pile was loaded incrementally to step 8, with an unload/reload cycle incorporated with the aim of reducing some of the shaft friction and mobilise further base resistance.

The breakage of one FBG line occurred just at the start of step 8; the reason for which is unclear. Furthermore, extremely scattered strain measurements are evident from NAP -23.80m onwards, possibly as a result of concrete segregation (Section 6.1).

Results of the test are provided as follows:

- Figure 5.1: Plot of load exerted on pile head against the time elapsed for P0
- Figure 5.2: Plot of settlement measured at the pile head against the time elapsed for P01
- Figure 5.3: Plot of strain versus time for selected BOFDA gauges for P01
- Figure 5.4: Plot of strain versus time for all FBG gauges for P01
- Figure 5.5: Load at pile head readings from each individual load cell for P01
- Figure 5.6: Settlement at pile head readings from each individual LVDT for P01
- Figure 5.7: Plot of load versus settlement at pile head for P01
- Figure 5.8: Creep parameter versus time across selected load steps for P01
- Figure 5.9: Creep rate versus time across selected load steps for P01
- Figure 5.10: Development of the total creep settlement at the pile head during selected

*Test was divided across two days, with the hydraulic jacks closed overnight at load step 4

†Test was divided across two days, with the pile unloaded to 5% load and sustained at that load overnight

load steps for P01

- Figure 5.11: Strain versus depth profile for P01 at the end of each load step

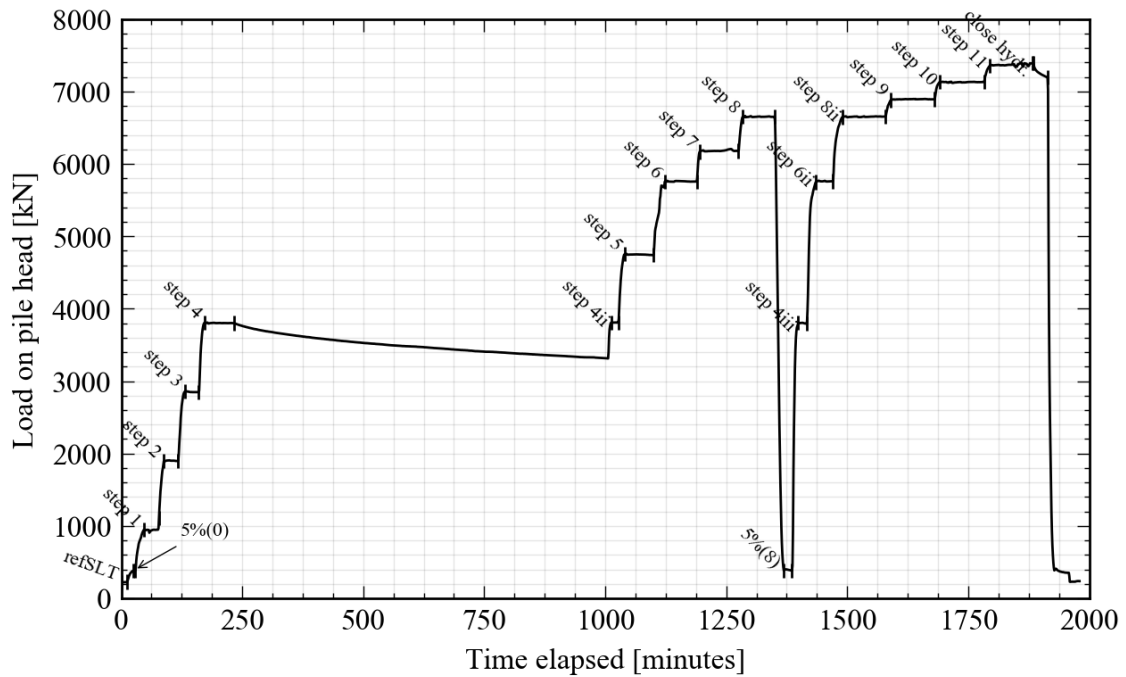


Figure 5.1: Plot of load exerted on pile head against the time elapsed for P01

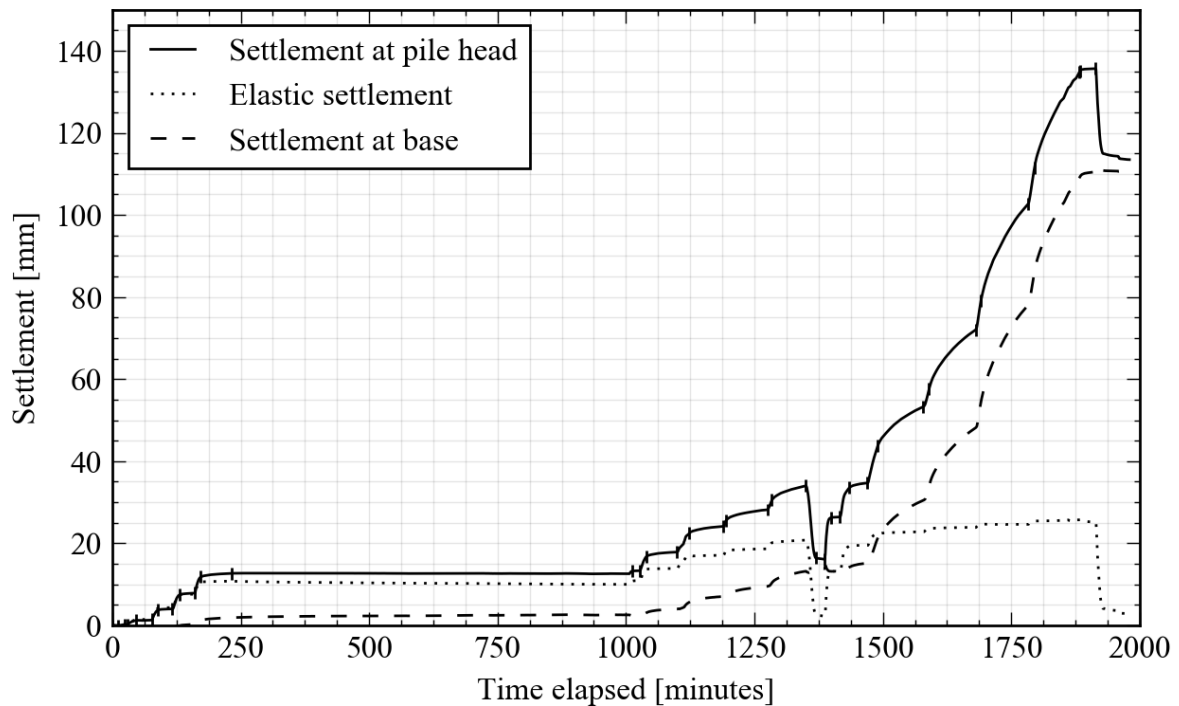


Figure 5.2: Plot of settlement measured at the pile head against the time elapsed for P01. The elastic settlement (and correspondingly the settlement at the pile base) readings shown have been derived from the FBG readings to provide more complete information over time

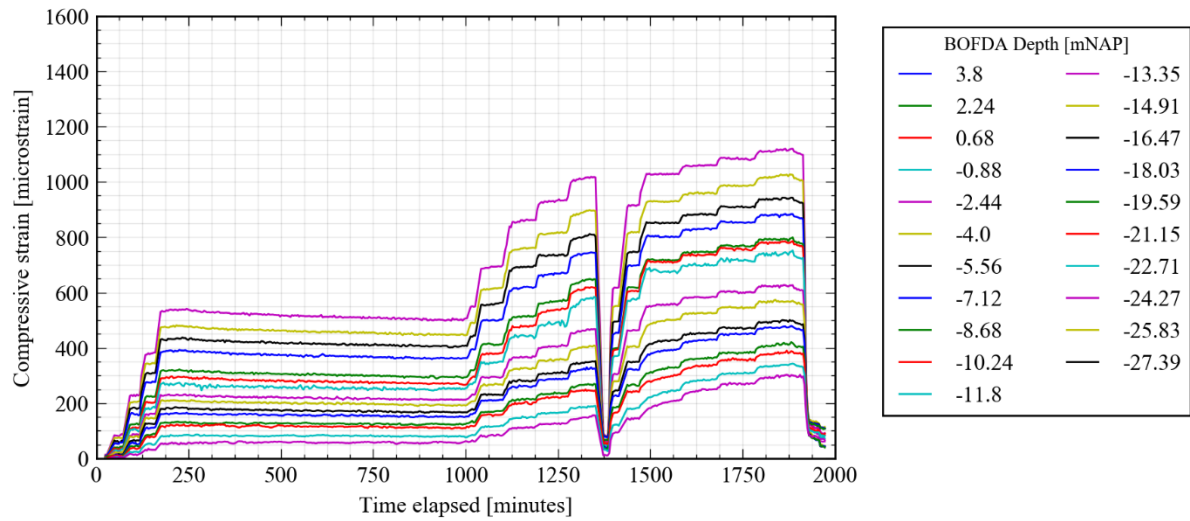


Figure 5.3: Plot of strain versus time for selected BOFDA gauges for P01

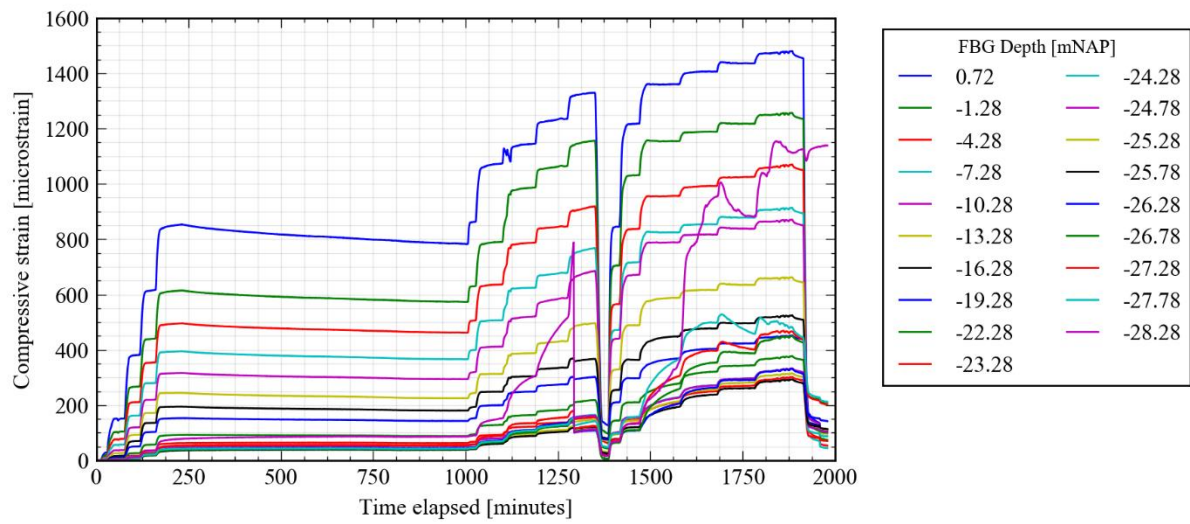


Figure 5.4: Plot of strain versus time for all FBG gauges for P01

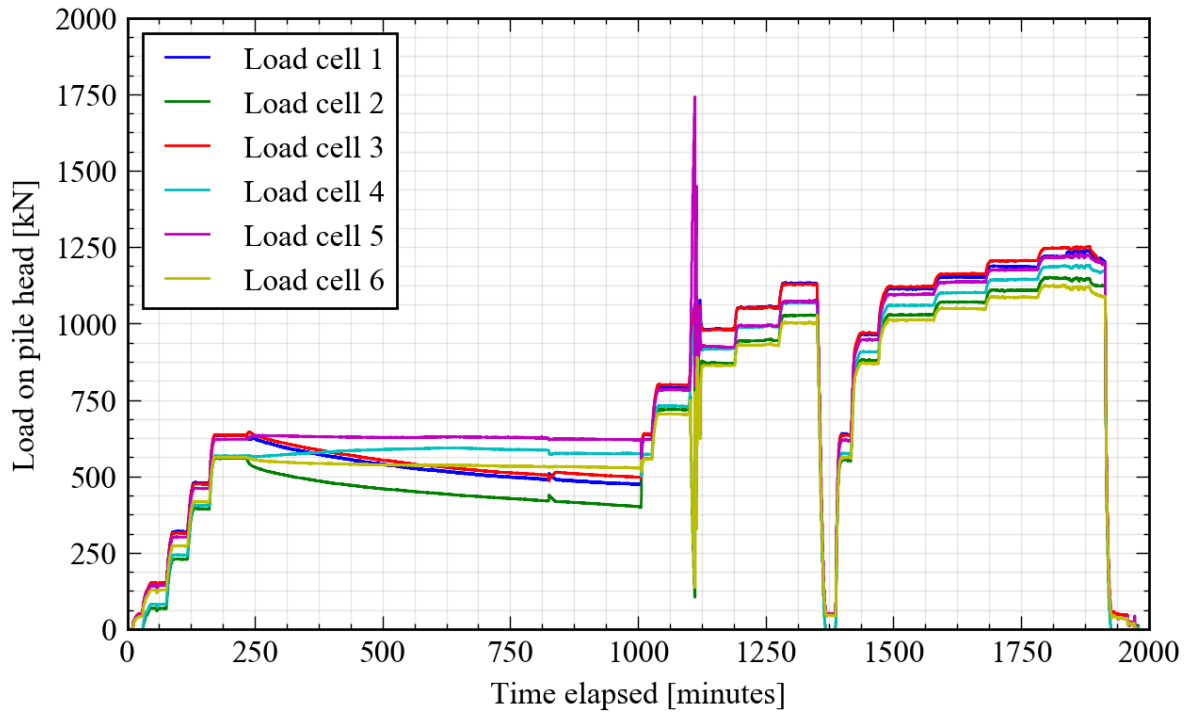


Figure 5.5: Load at pile head readings from each individual load cell for P01

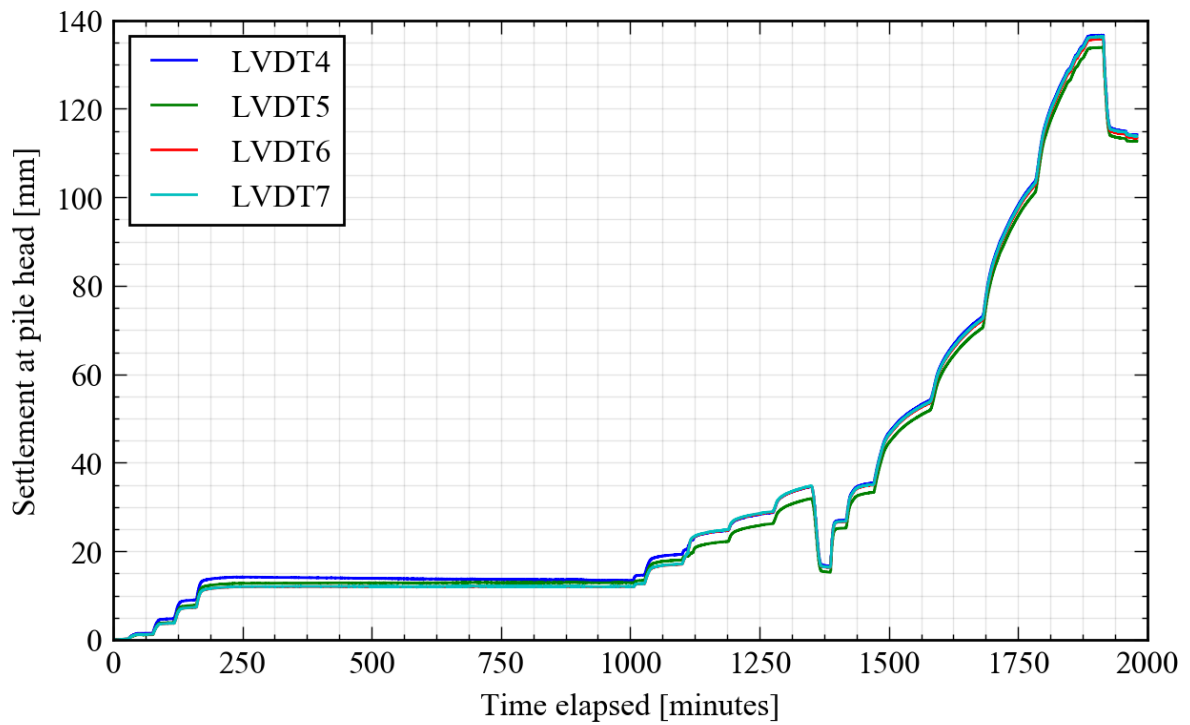


Figure 5.6: Settlement at pile head readings from each individual LVDT for P01

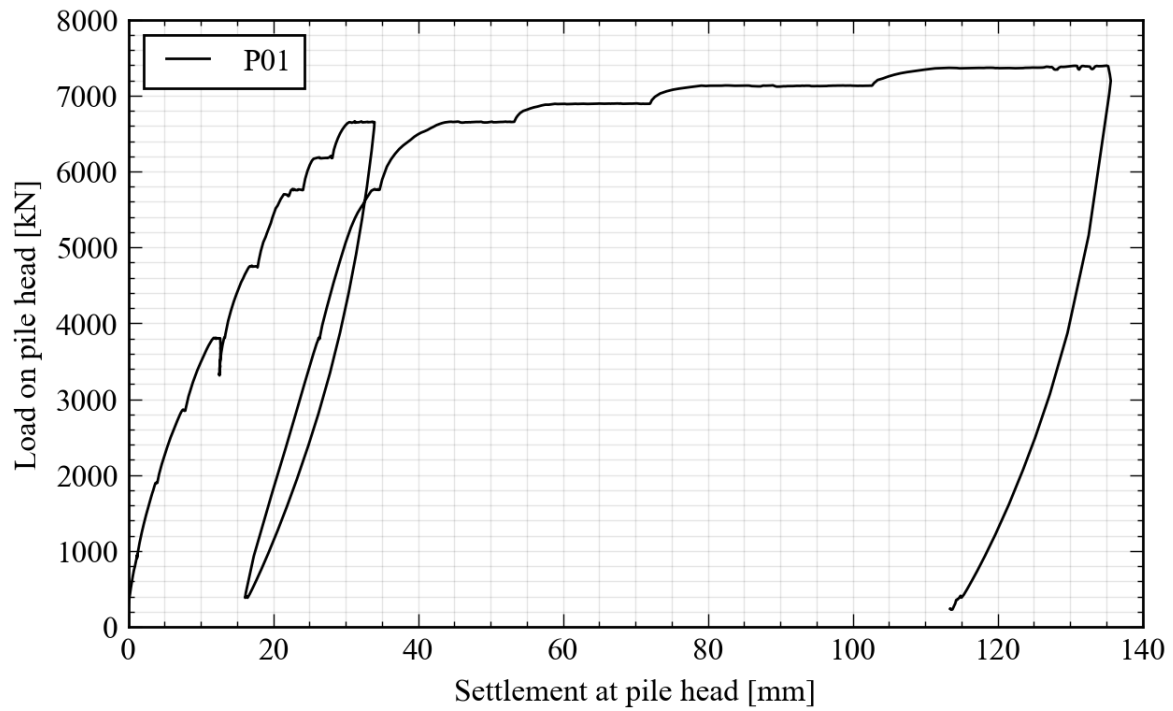


Figure 5.7: Plot of load versus settlement at pile head for P01

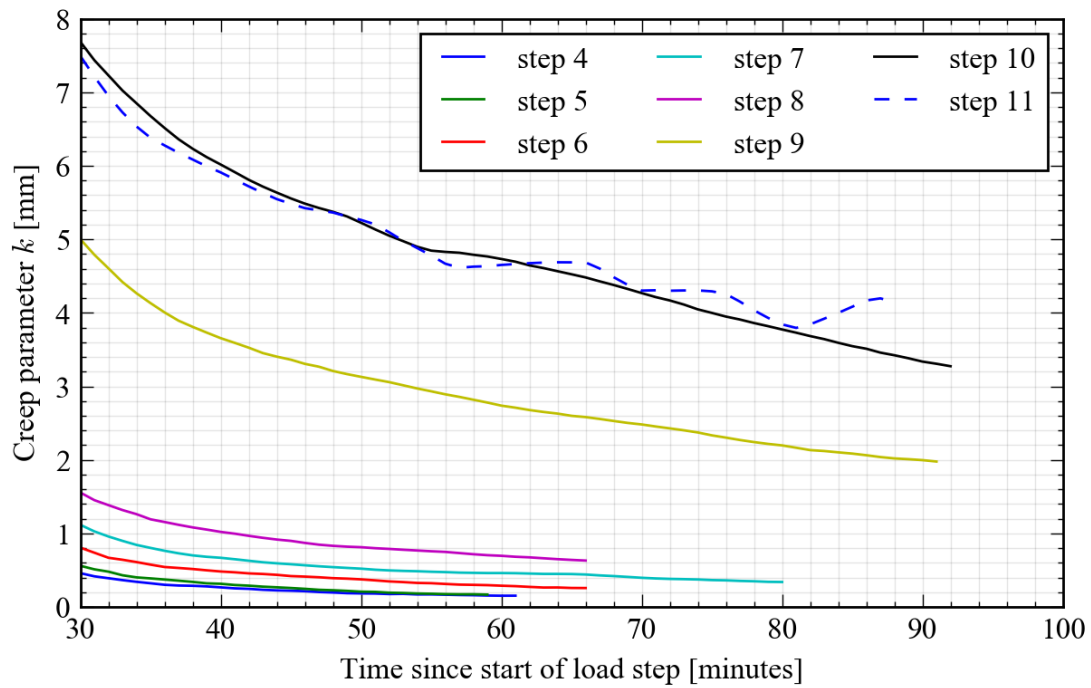


Figure 5.8: Creep parameter versus time across selected load steps for P01

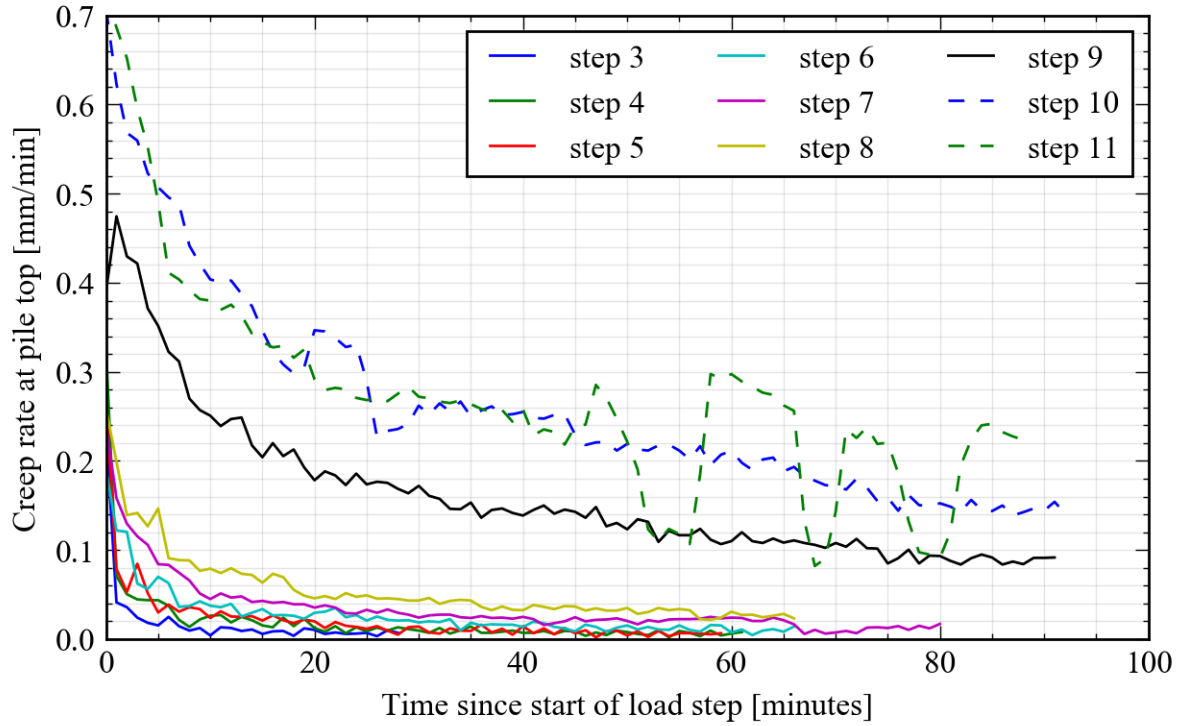


Figure 5.9: Creep rate versus time across selected load steps for P01

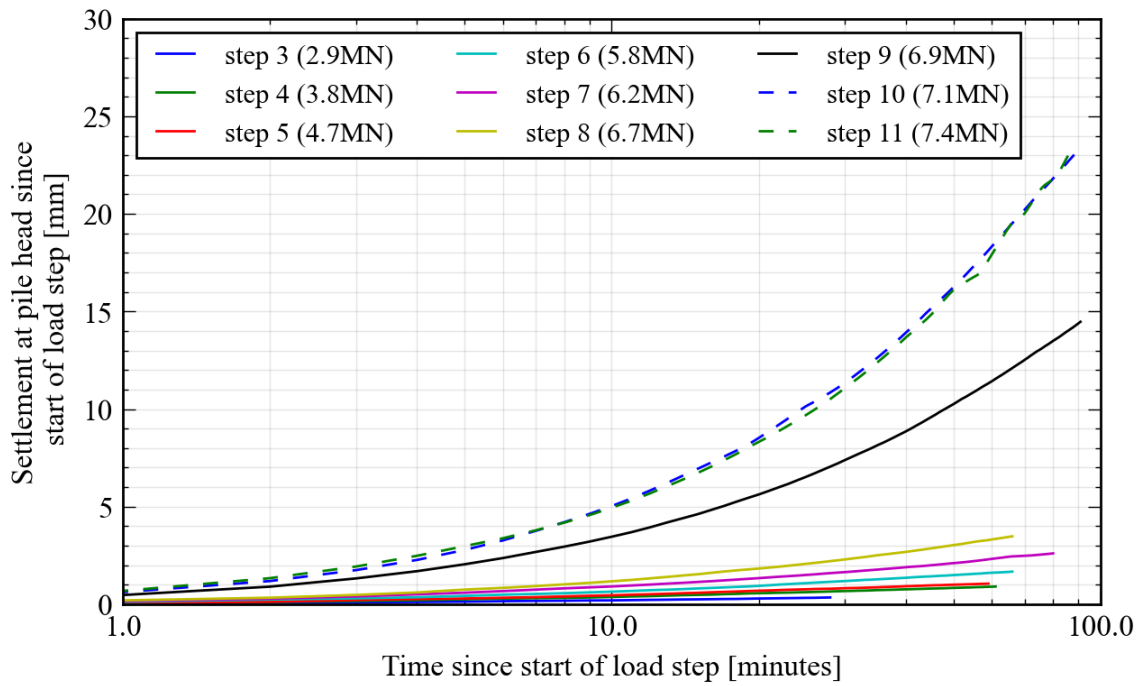


Figure 5.10: Development of the total creep settlement at the pile head during selected load steps for P01

Table 5.2: List of load steps and corresponding durations in pile test P01

Load Step	Start Time [DD/MM/YYYY hh:mm]	End Time [DD/MM/YYYY hh:mm]	Duration [hh:mm]	Average Load [kN]
refSLT	13/01/2020 13:30	13/01/2020 14:44	01:14	223.04
5%(0)	13/01/2020 14:56	13/01/2020 15:01	00:05	381.83
step 1	13/01/2020 15:19	13/01/2020 15:50	00:31	947.97
step 2	13/01/2020 16:00	13/01/2020 16:29	00:29	1899.84
step 3	13/01/2020 16:44	13/01/2020 17:12	00:28	2850.97
step 4	13/01/2020 17:24	13/01/2020 18:25	01:01	3802.00
step 4ii	14/01/2020 07:25	14/01/2020 07:39	00:14	3809.55
step 5	14/01/2020 07:52	14/01/2020 08:51	00:59	4747.26
step 6	14/01/2020 09:15	14/01/2020 10:21	01:06	5758.45
step 7	14/01/2020 10:27	14/01/2020 11:47	01:20	6182.23
step 8	14/01/2020 11:56	14/01/2020 13:02	01:06	6650.83
5%(8)	14/01/2020 13:21	14/01/2020 13:38	00:17	391.77
step 4iii	14/01/2020 13:51	14/01/2020 14:08	00:17	3801.02
step 6ii	14/01/2020 14:27	14/01/2020 15:02	00:35	5759.74
step 8ii	14/01/2020 15:22	14/01/2020 16:51	01:29	6651.54
step 9	14/01/2020 17:02	14/01/2020 18:33	01:31	6892.45
step 10	14/01/2020 18:43	14/01/2020 20:15	01:32	7128.65
step 11	14/01/2020 20:27	14/01/2020 21:56	01:29	7368.42
close hydr.	14/01/2020 21:56	14/01/2020 22:26	00:30	7257.91

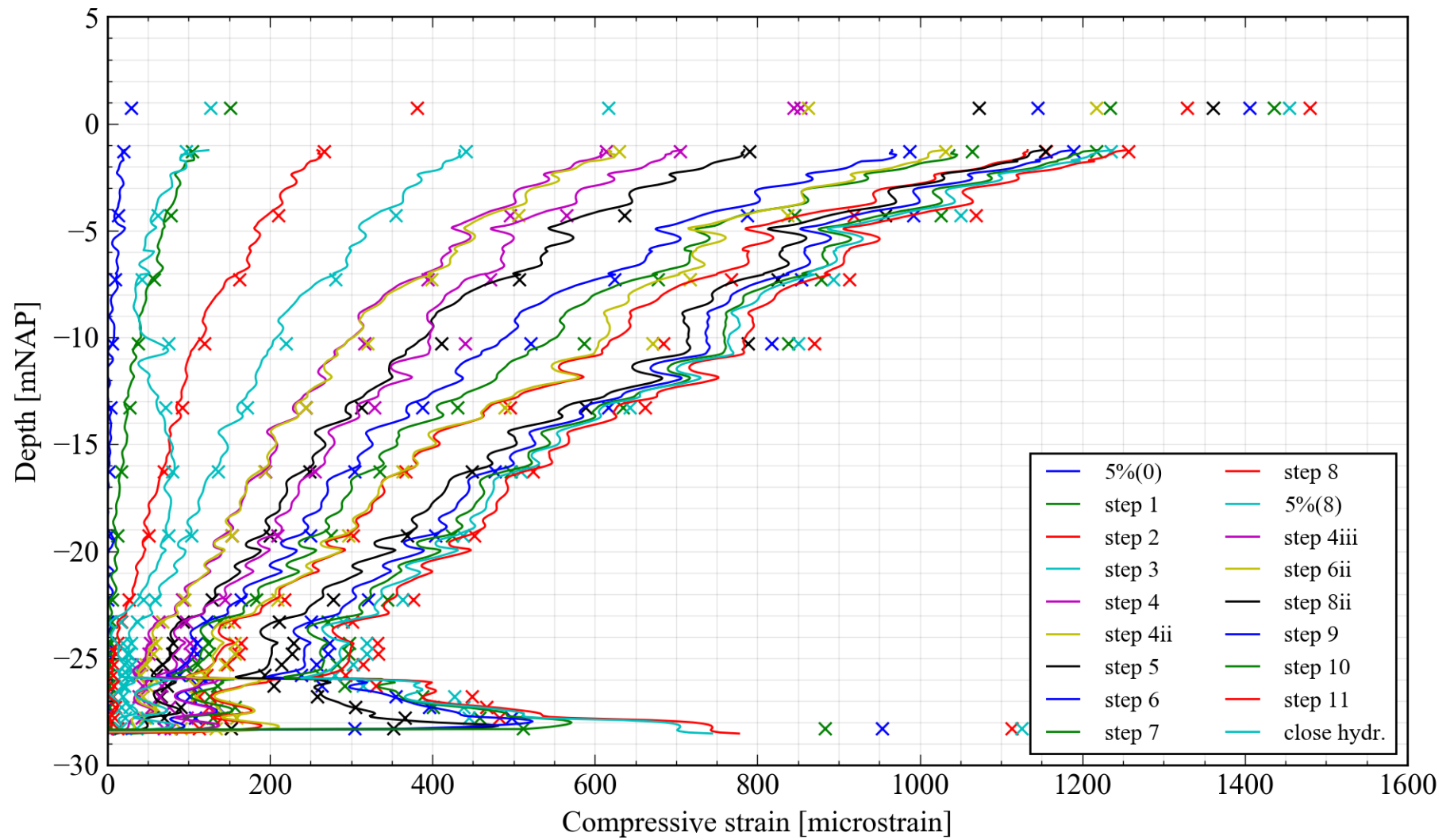


Figure 5.11: Strain versus depth profile for P01 at the end of each load step. Note that the BOFDA measurements are indicated by a continuous line whereas FBG readings are indicated by a discrete point

5.2. Test Results: Pile P03

P03 was tested on the 19th December and contained no unload/reload cycles or any overnight closing of the jacks. The end of the test was signalled by the breakage of the pile at the bottom of the steel sleeve surrounding the pile head (see Figure 5.12 and Figure 5.13) just at the start of step 11. This resulted in the breakage of all strain fibres and a sudden drop in the elevation of the pile head. Concurrently, this led to the hydraulic jacks and load cells keeling out of position, causing a knock-on effect on future load measurements, however, this has been corrected for in the data processing.

Extremely scattered strain measurements are evident from NAP -24.73m onwards, possibly as a result of concrete segregation (Section 6.1).

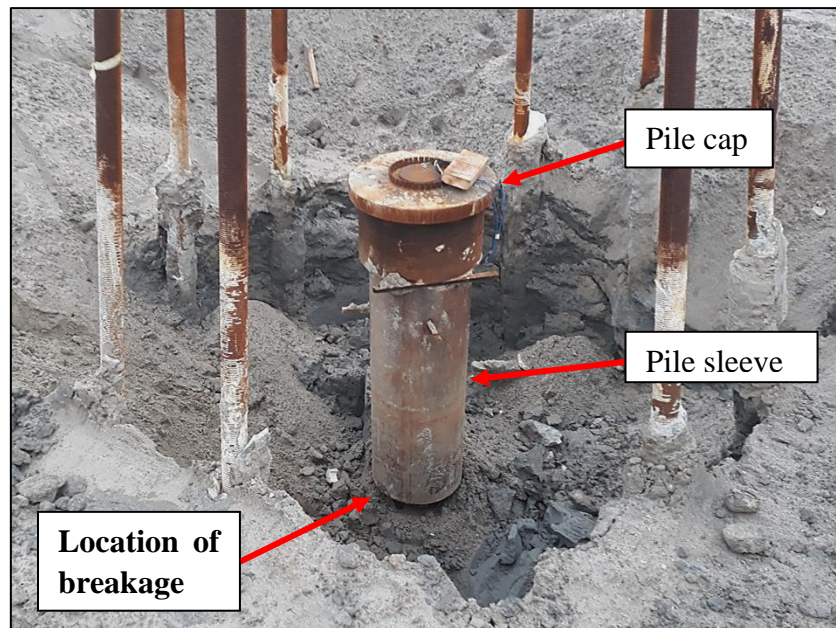


Figure 5.12: Location of the breakage of the pile P03 underneath the pile sleeve



Figure 5.13: Close-up photo of the breakage immediately underneath the sleeve of pile P03 (Photo credit: Gust van Lysebetten, WTCB)

Results of the test are provided as follows:

- Figure 5.14: Plot of load exerted on pile head against the time elapsed for P03
- Figure 5.15: Plot of settlement measured at the pile head against the time elapsed for P03
- Figure 5.16: Plot of strain versus time for selected BOFDA gauges for P03
- Figure 5.17: Plot of strain versus time for all FBG gauges for P03
- Figure 5.18: Load at pile head readings from each individual load cell for P03
- Figure 5.19: Settlement at pile head readings from each individual LVDT for P03
- Figure 5.20: Plot of load versus settlement at pile head for P03
- Figure 5.21: Creep parameter versus time across selected load steps for P03
- Figure 5.22: Creep rate versus time across selected load steps for P03
- Figure 5.23: Development of the total creep settlement at the pile head during selected load steps for P03
- Figure 5.24: Strain versus depth profile for P03 at the end of each load step

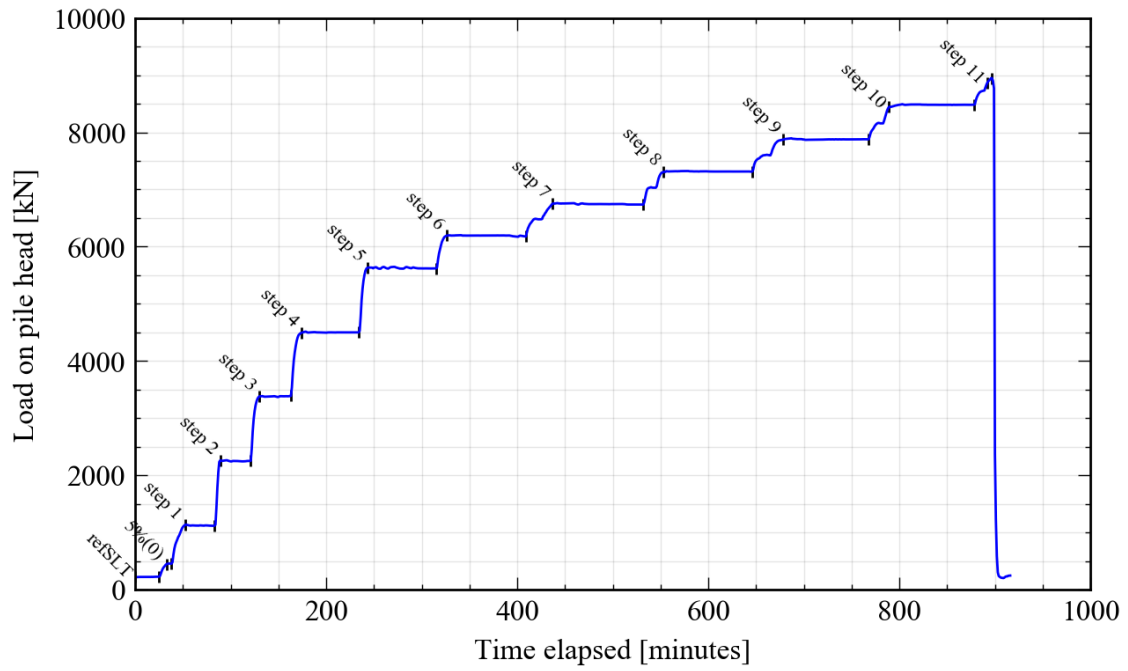


Figure 5.14: Plot of load exerted on pile head against the time elapsed for P03

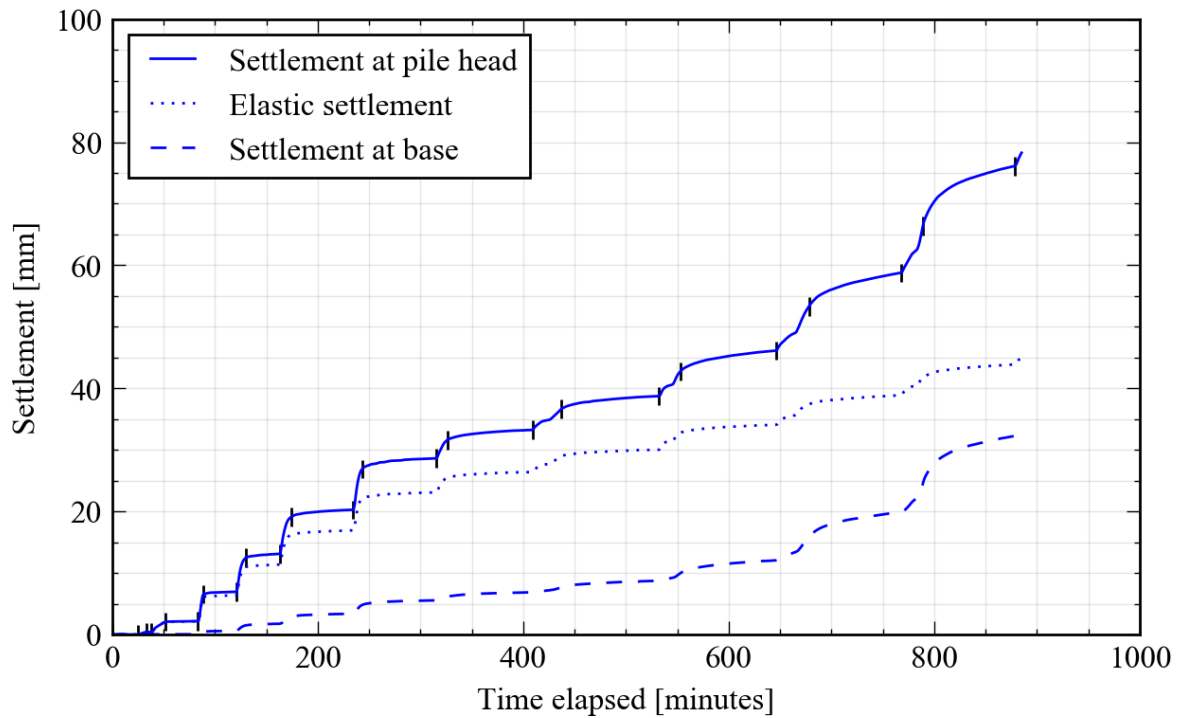


Figure 5.15: Plot of settlement measured at the pile head against the time elapsed for P03. The elastic settlement (and correspondingly the settlement at the pile base) readings shown have been derived from the FBG readings to provide more complete information over time

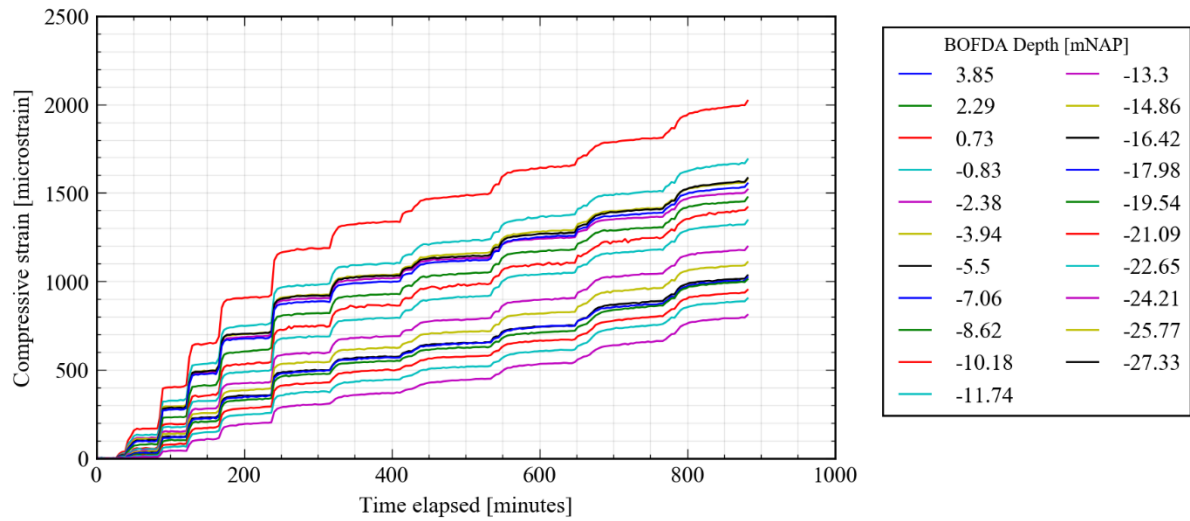


Figure 5.16: Plot of strain versus time for selected BOFDA gauges for P03

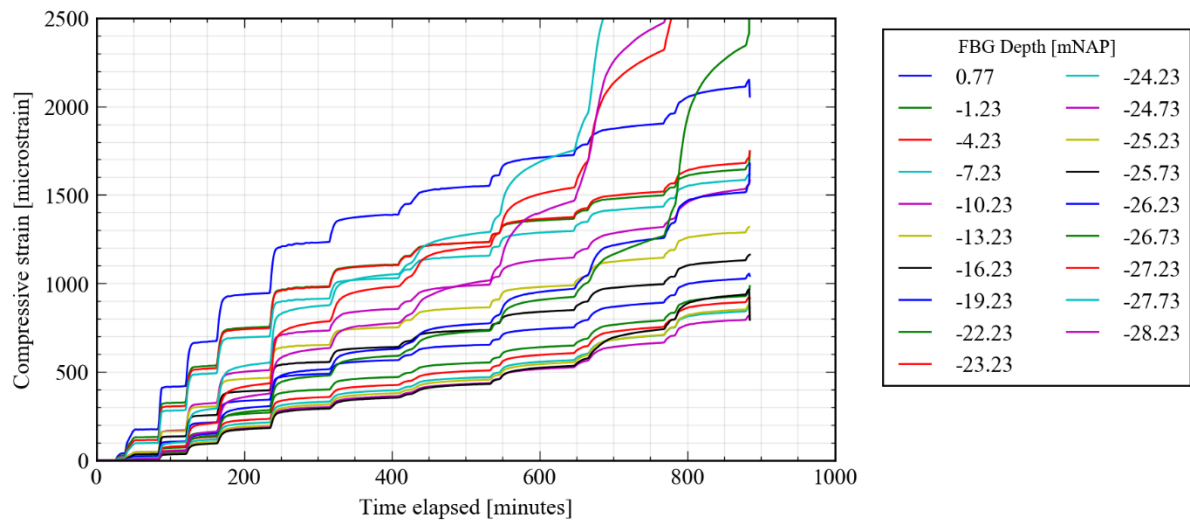


Figure 5.17: Plot of strain versus time for all FBG gauges for P03

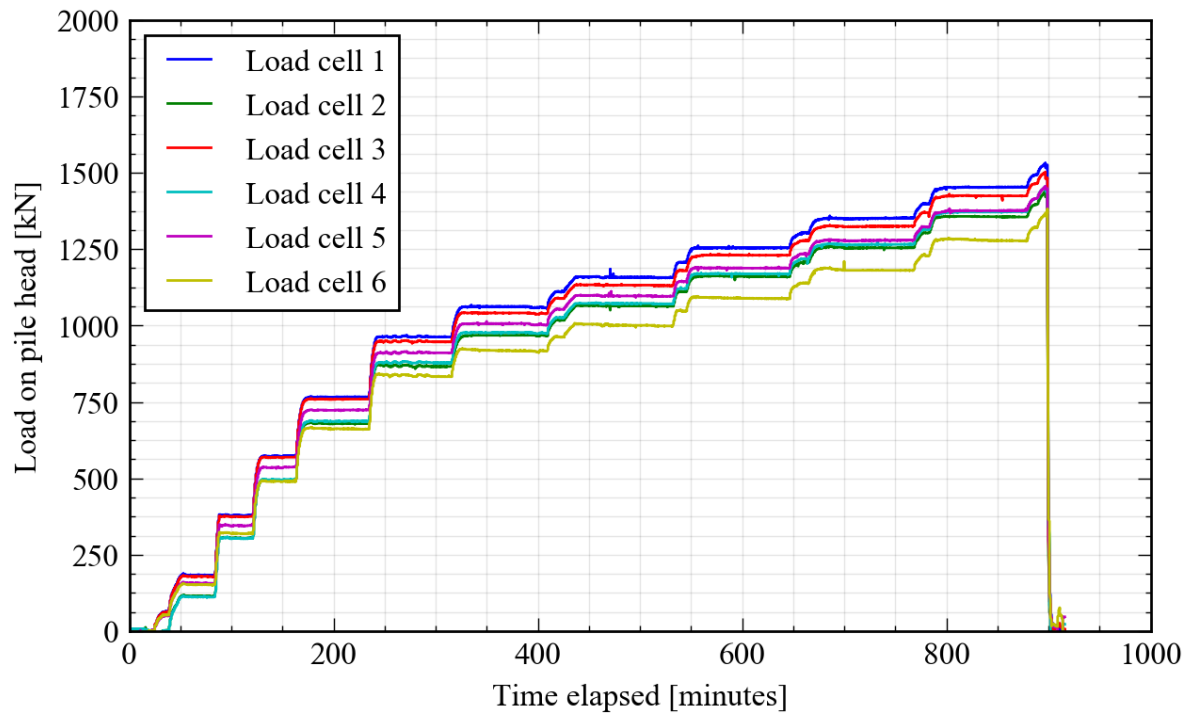


Figure 5.18: Load at pile head readings from each individual load cell for P03

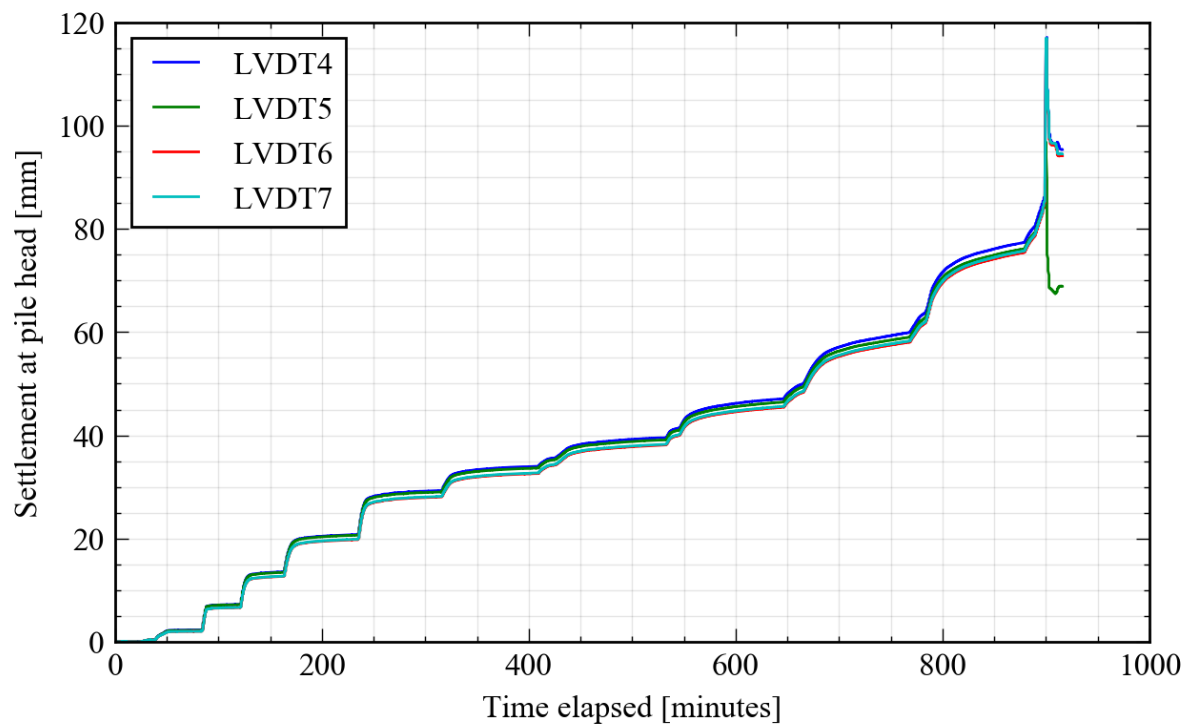


Figure 5.19: Settlement at pile head readings from each individual LVDT for P03

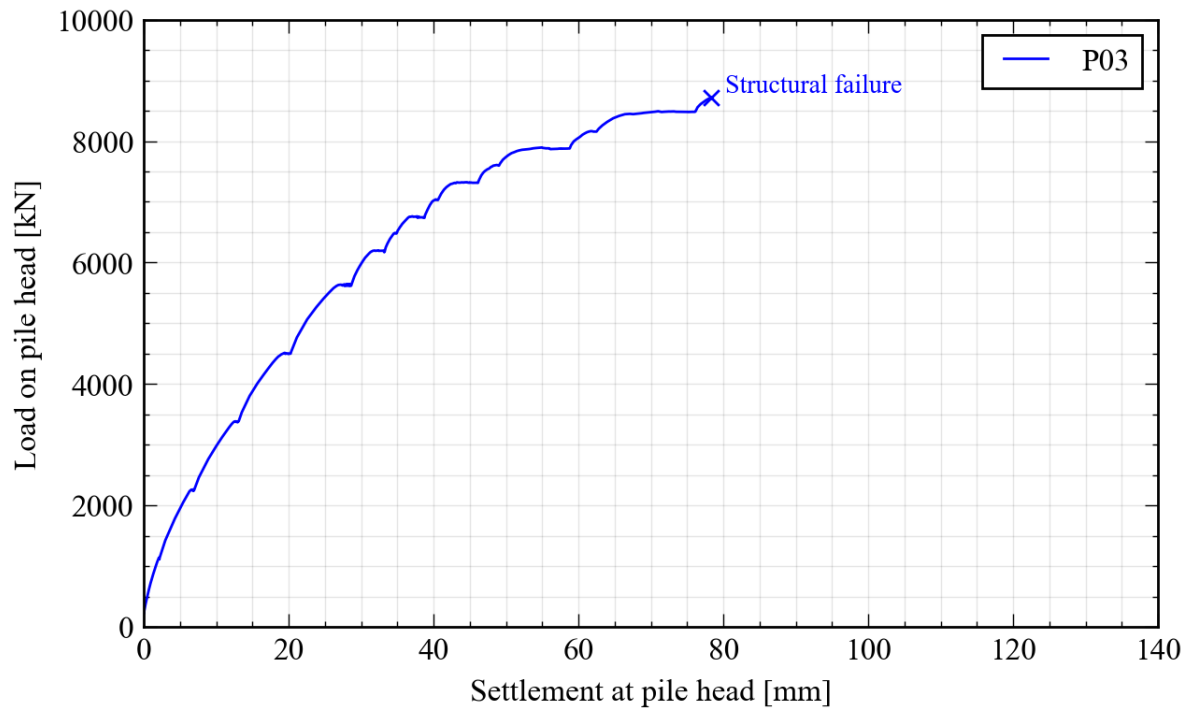


Figure 5.20: Plot of load versus settlement at pile head for P03. Note that the structural failure and breakage of the fibres resulted

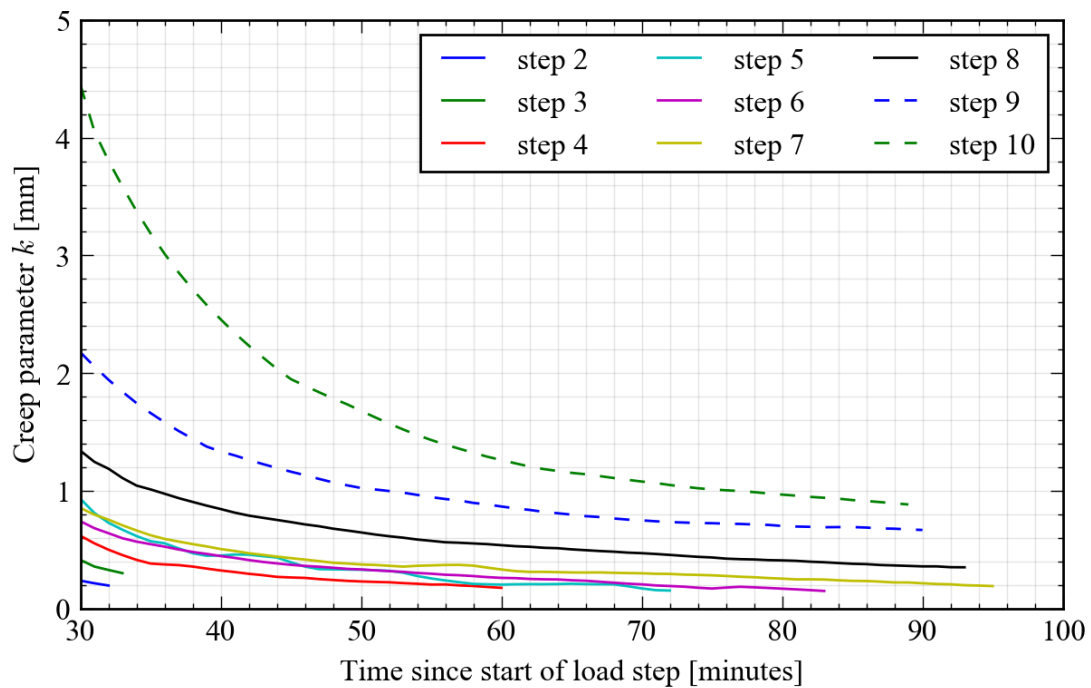


Figure 5.21: Creep parameter versus time across selected load steps for P03

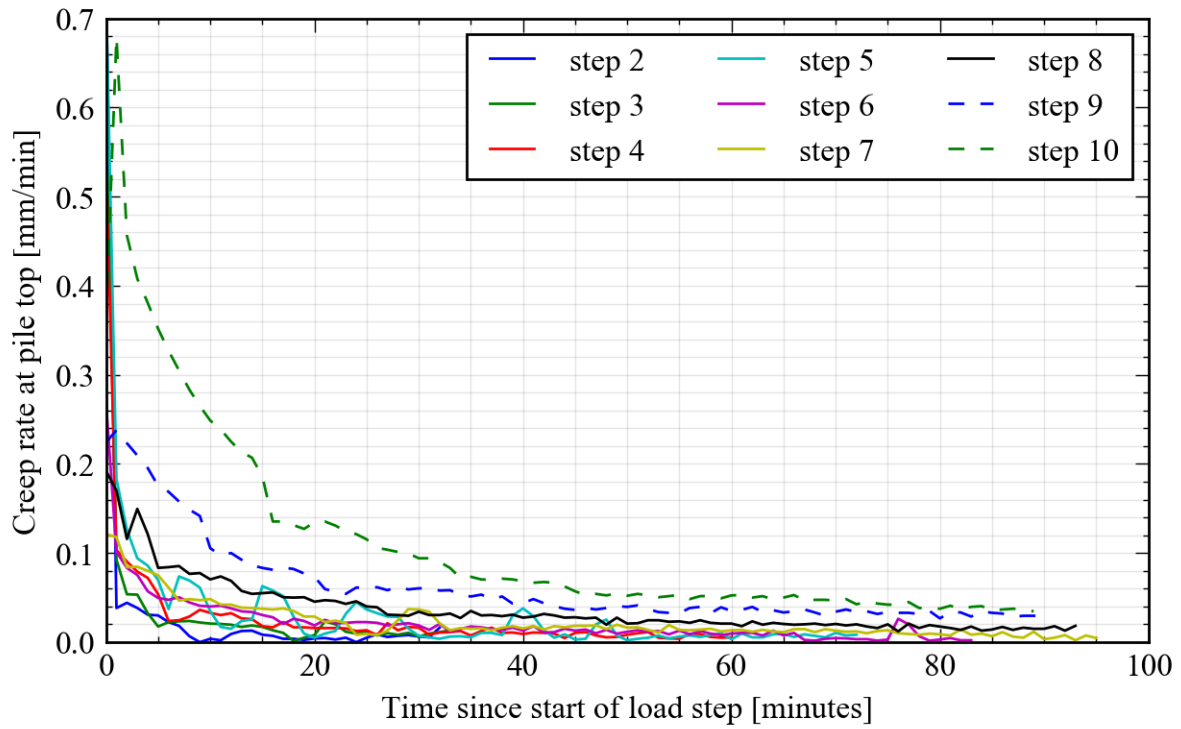


Figure 5.22: Creep rate versus time across selected load steps for P03

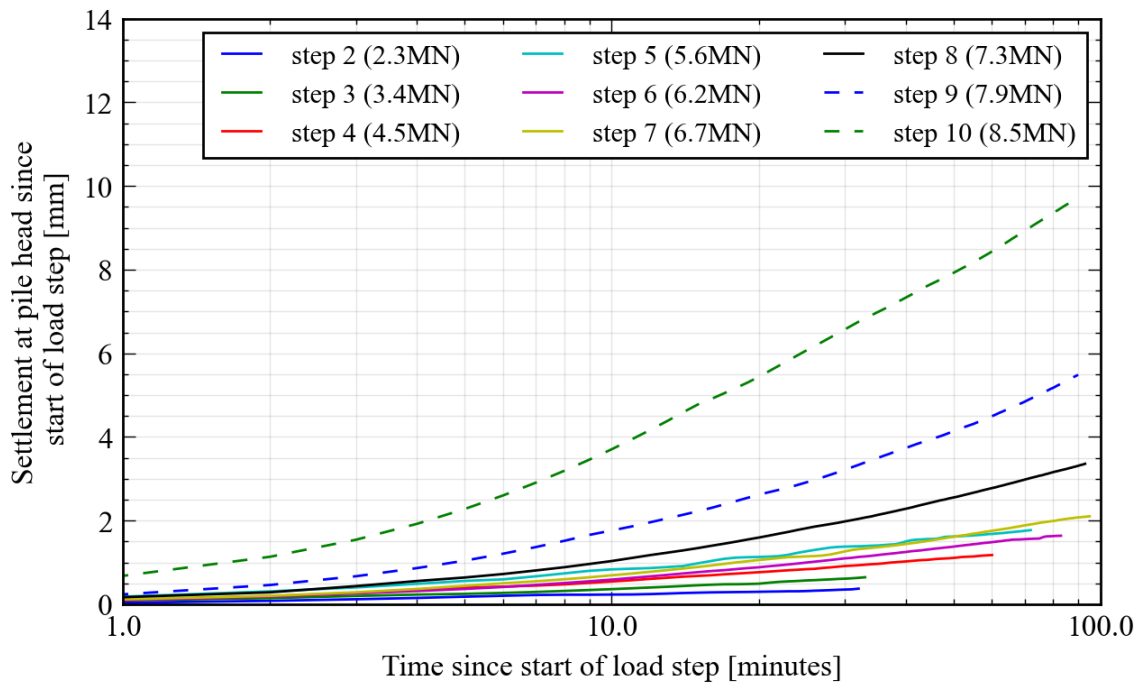


Figure 5.23: Development of the total creep settlement at the pile head during selected load steps for P03

Table 5.3: List of load steps and corresponding durations in pile test P03

Load Step	Start Time [DD/MM/YYYY hh:mm]	End Time [DD/MM/YYYY hh:mm]	Duration [hh:mm]	Average Load [kN]
refSLT	19/12/2019 07:51	19/12/2019 08:16	00:25	221.49
5%(0)	19/12/2019 08:24	19/12/2019 08:29	00:05	452.59
step 1	19/12/2019 08:43	19/12/2019 09:14	00:31	1121.53
step 2	19/12/2019 09:20	19/12/2019 09:52	00:32	2250.23
step 3	19/12/2019 10:01	19/12/2019 10:34	00:33	3380.15
step 4	19/12/2019 10:45	19/12/2019 11:45	01:00	4500.03
step 5	19/12/2019 11:54	19/12/2019 13:06	01:12	5626.90
step 6	19/12/2019 13:17	19/12/2019 14:40	01:23	6192.42
step 7	19/12/2019 15:08	19/12/2019 16:43	01:35	6746.43
step 8	19/12/2019 17:04	19/12/2019 18:37	01:33	7316.15
step 9	19/12/2019 19:09	19/12/2019 20:39	01:30	7877.59
step 10	19/12/2019 21:00	19/12/2019 22:29	01:29	8480.62

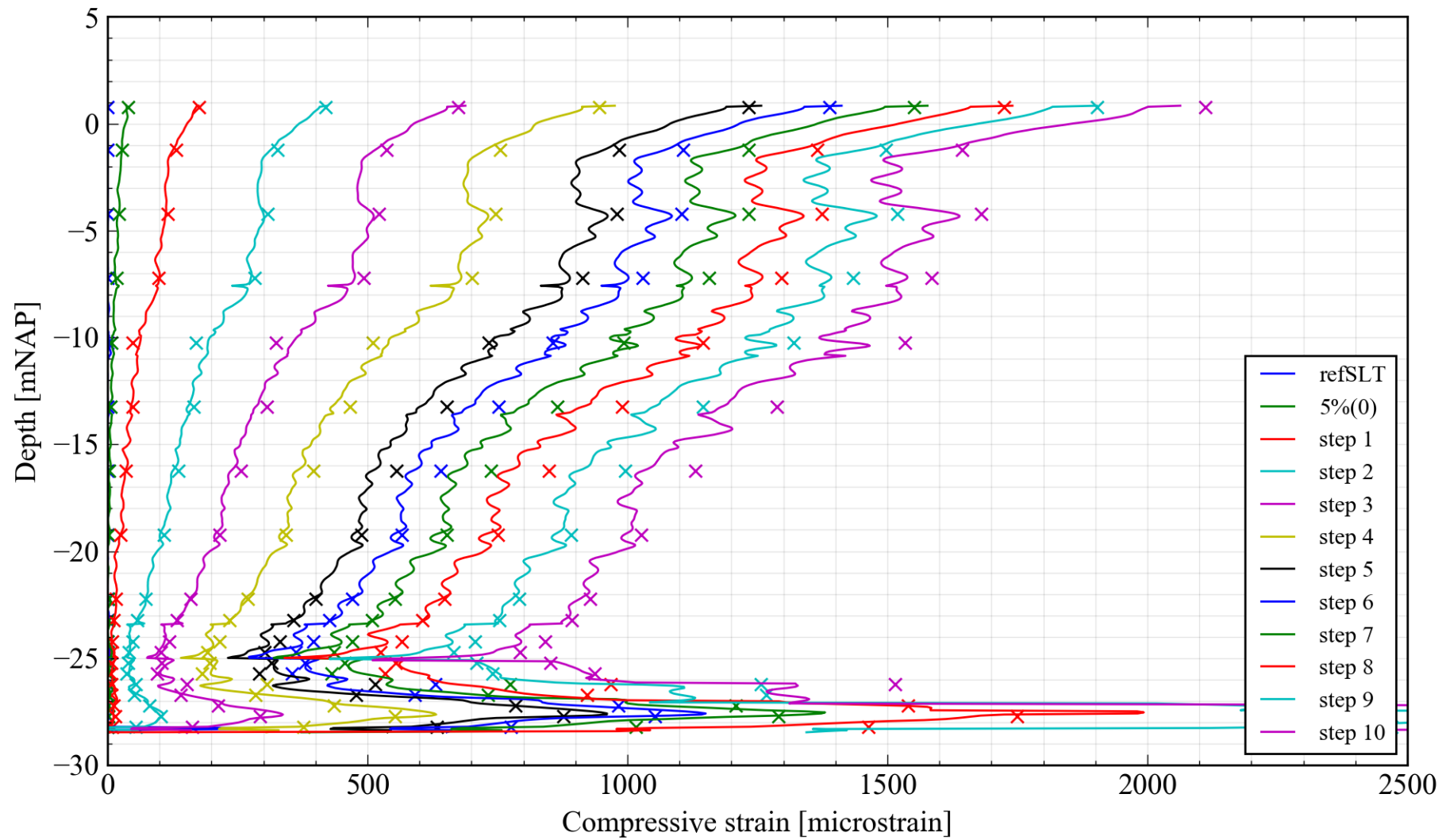


Figure 5.24: Strain versus depth profile for P03 at the end of each load step. Note that the BOFDA measurements are indicated by a continuous line whereas FBG readings are indicated by a discrete point

5.3. Test Results: Pile P06

Pile P06 was the first test to be intentionally divided over two working days, with 50% of the predicted pile capacity reached on the evening of the 7th of January, with the pile being unloaded to the 5% load overnight. The pile was then incrementally loaded up to load step 8, after which an unload/reload cycle was implemented to develop more base resistance.

Extremely scattered strain measurements are evident from NAP -24.24 onwards, possibly as a result of concrete segregation (Section 6.1).

Results of the test are provided as follows:

- Figure 5.25: Plot of load exerted on pile head against the time elapsed for P06
- Figure 5.26: Plot of settlement measured at the pile head against the time elapsed for P06
- Figure 5.27: Plot of strain versus time for selected BOFDA gauges for P06
- Figure 5.28: Plot of strain versus time for all FBG gauges for P06
- Figure 5.29: Load at pile head readings from each individual load cell for P06
- Figure 5.30: Settlement at pile head readings from each individual LVDT for P06
- Figure 5.31: Plot of load versus settlement at pile head for P06
- Figure 5.32: Creep parameter versus time across selected load steps for P06
- Figure 5.33: Creep rate versus time across selected load steps for P06
- Figure 5.34: Development of the total creep settlement at the pile head during selected load steps for P06
- Figure 5.35: Strain versus depth profile for P06 at the end of each load step

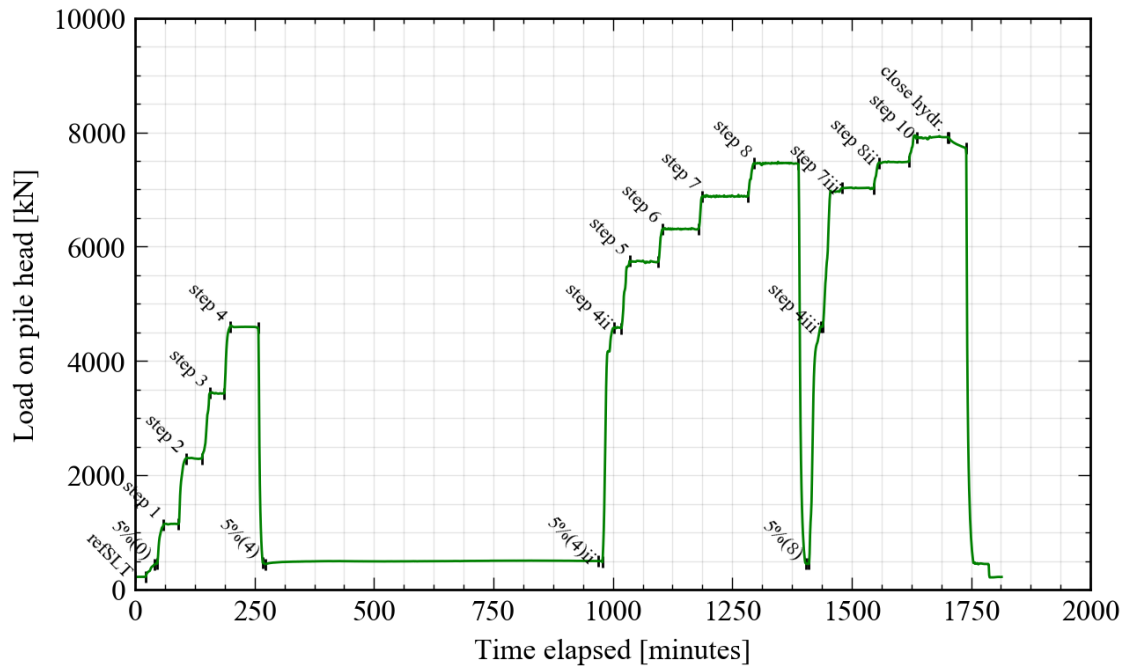


Figure 5.25: Plot of load exerted on pile head against the time elapsed for P06

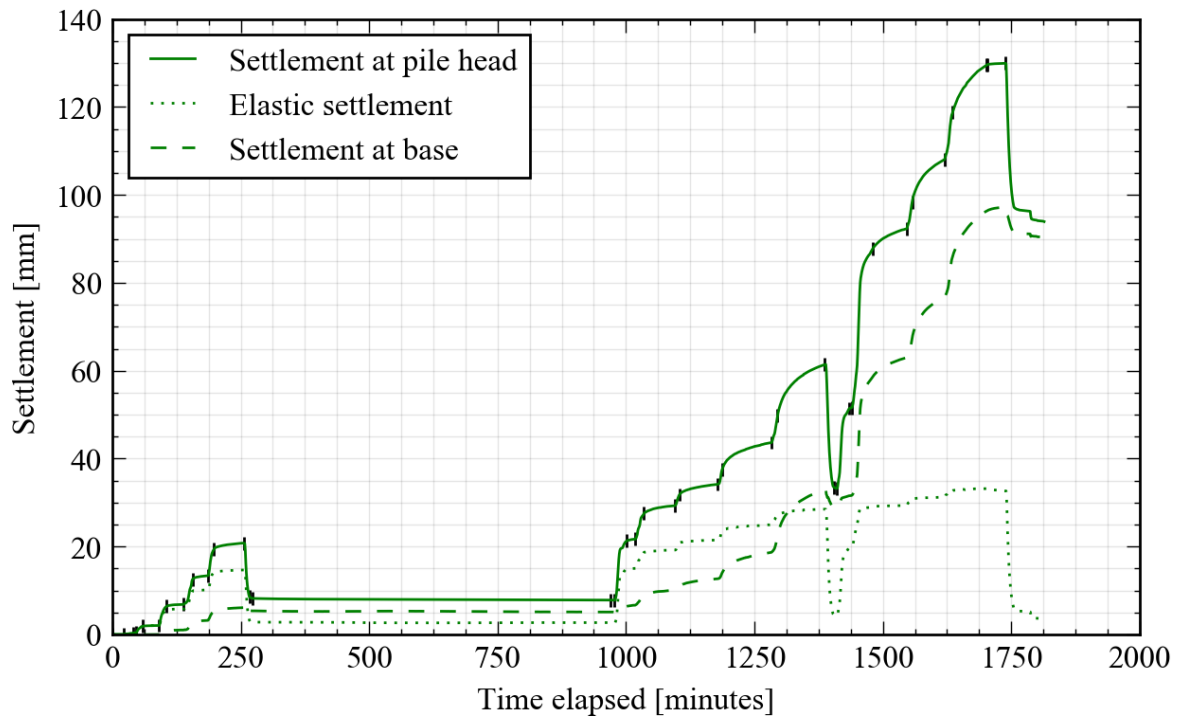


Figure 5.26: Plot of settlement measured at the pile head against the time elapsed for P06. The elastic settlement (and correspondingly the settlement at the pile base) readings shown have been derived from the FBG readings to provide more complete information over time

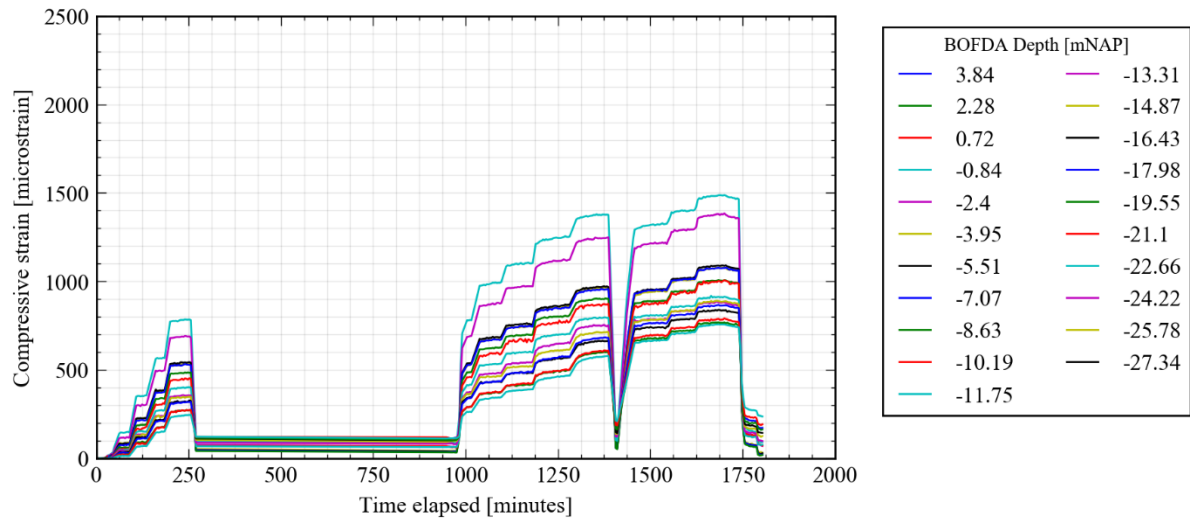


Figure 5.27: Plot of strain versus time for selected BOFDA gauges for P06

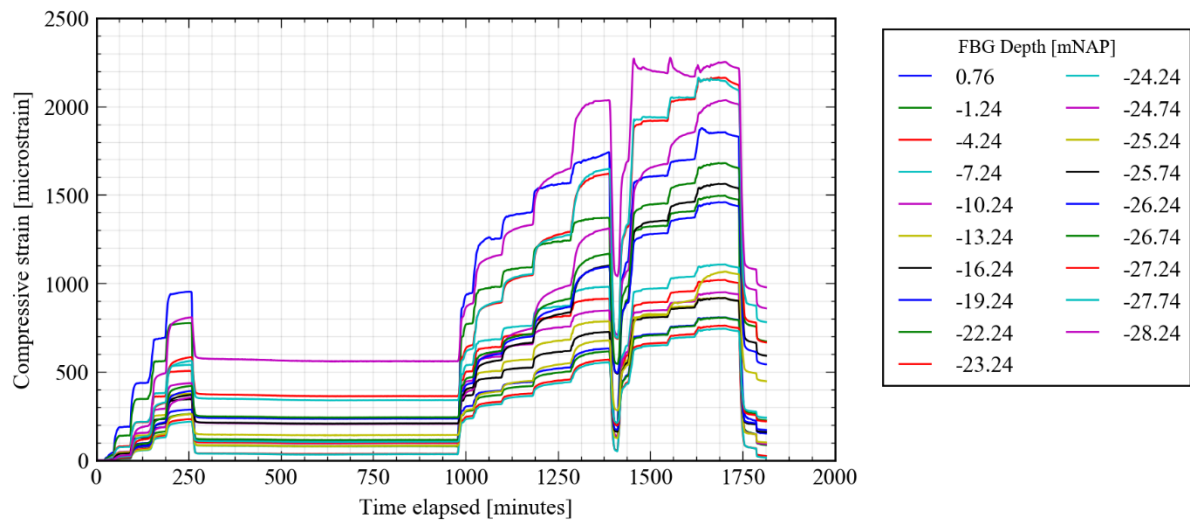


Figure 5.28: Plot of strain versus time for all FBG gauges for P06

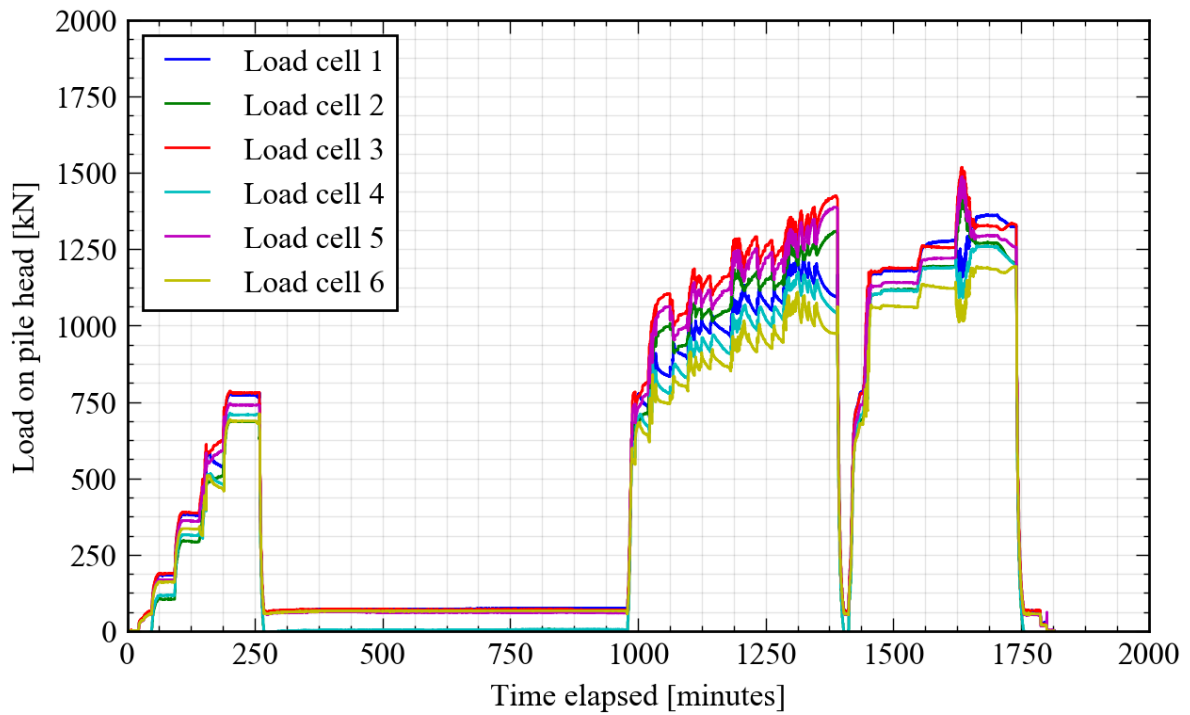


Figure 5.29: Load at pile head readings from each individual load cell for P06

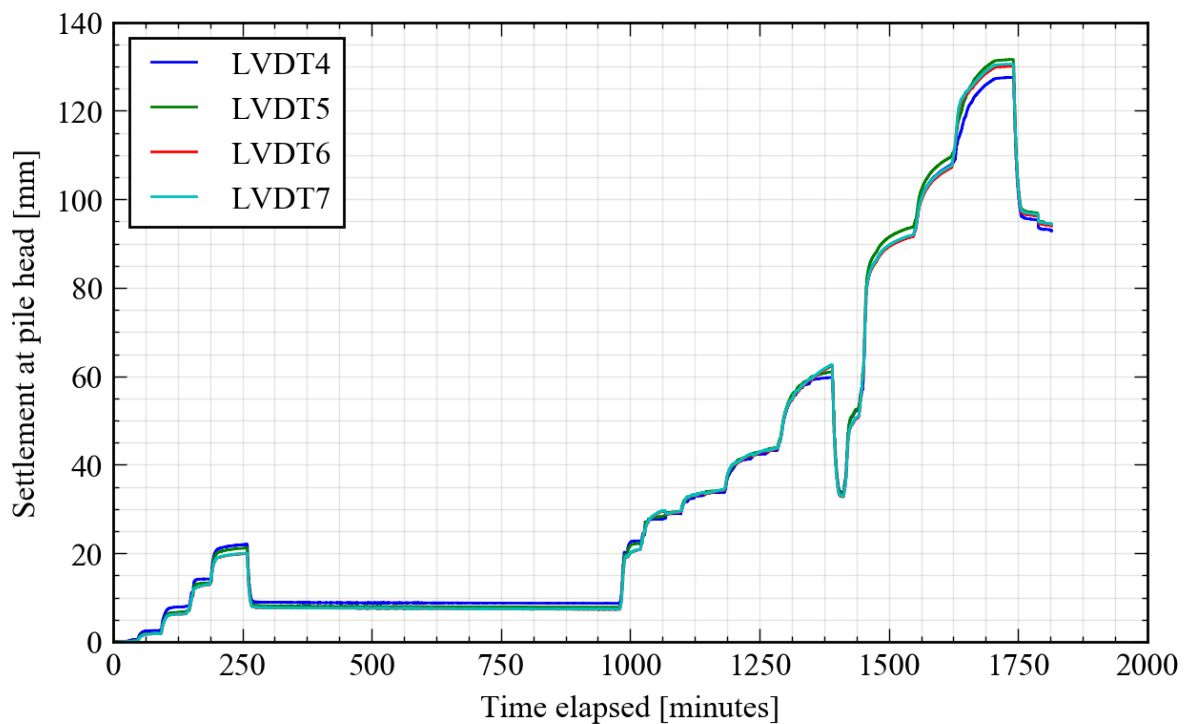


Figure 5.30: Settlement at pile head readings from each individual LVDT for P06

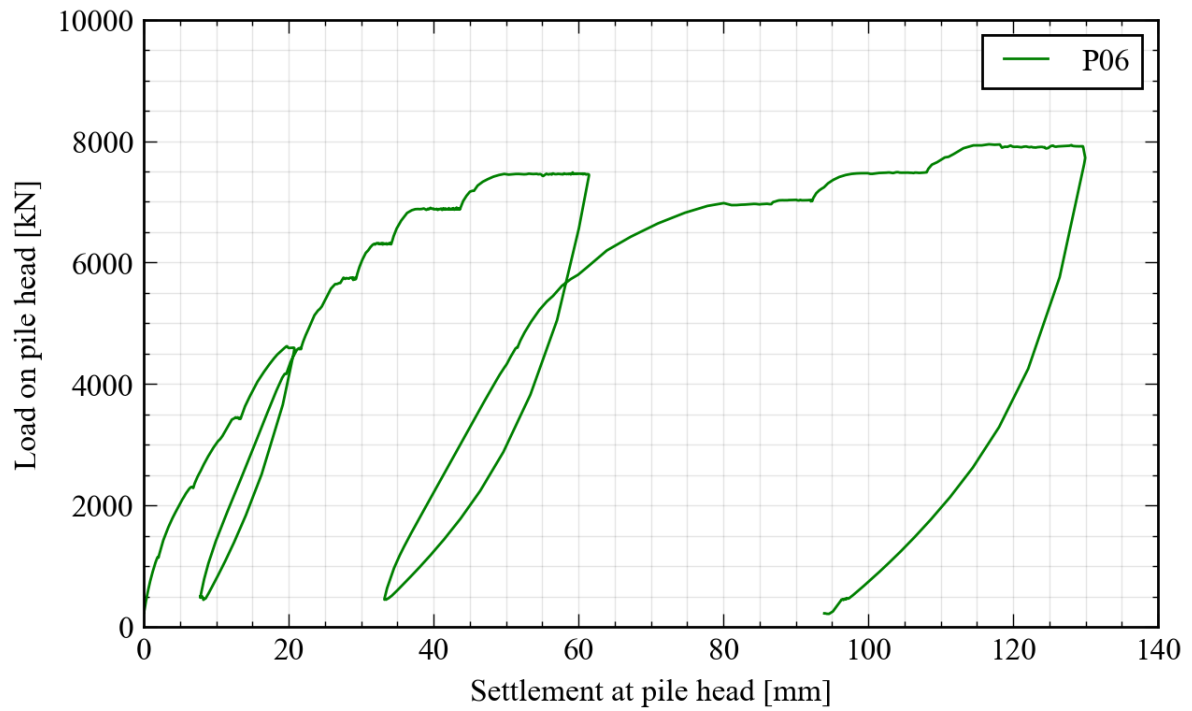


Figure 5.31: Plot of load versus settlement at pile head for P06

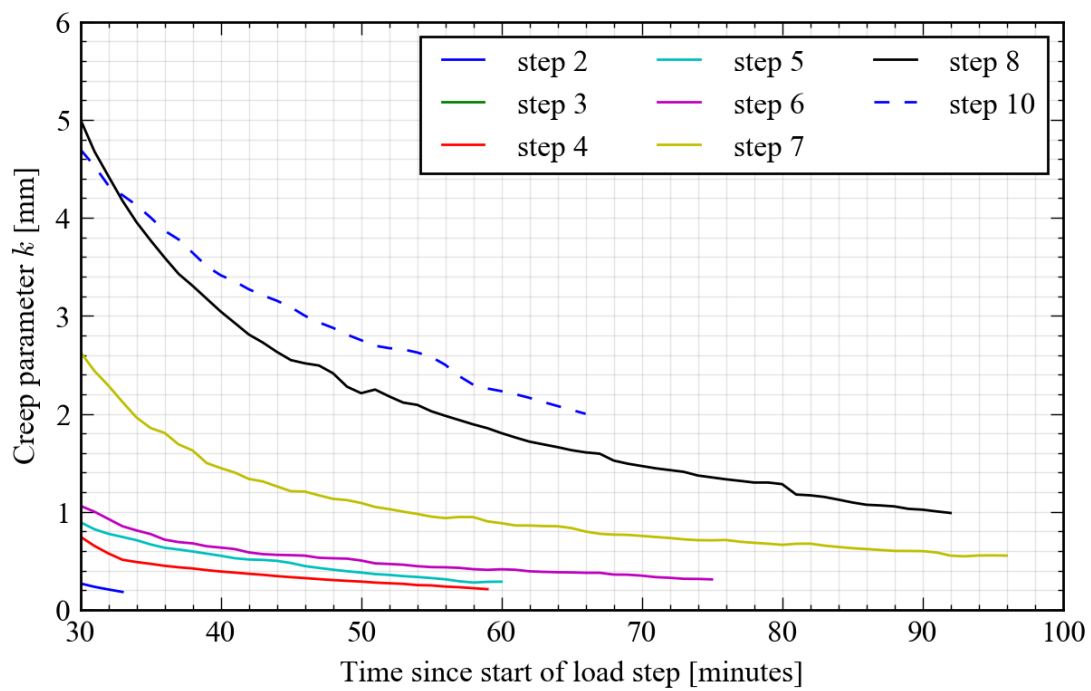


Figure 5.32: Creep parameter versus time across selected load steps for P06

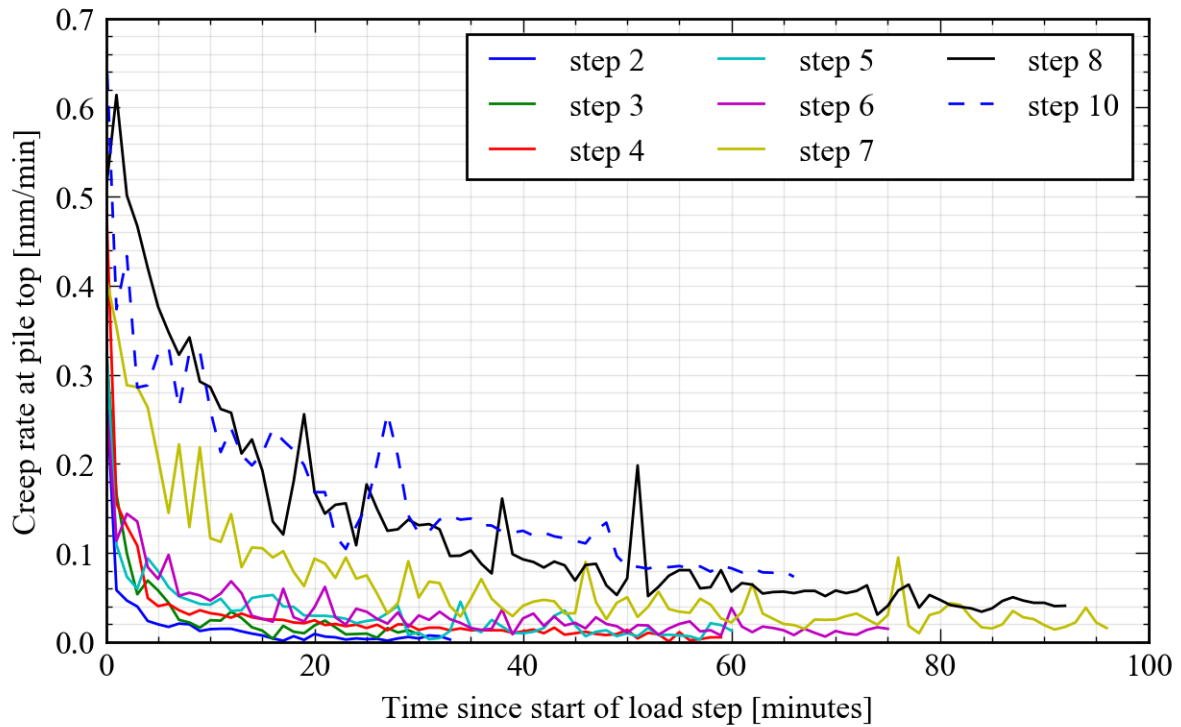


Figure 5.33: Creep rate versus time across selected load steps for P06

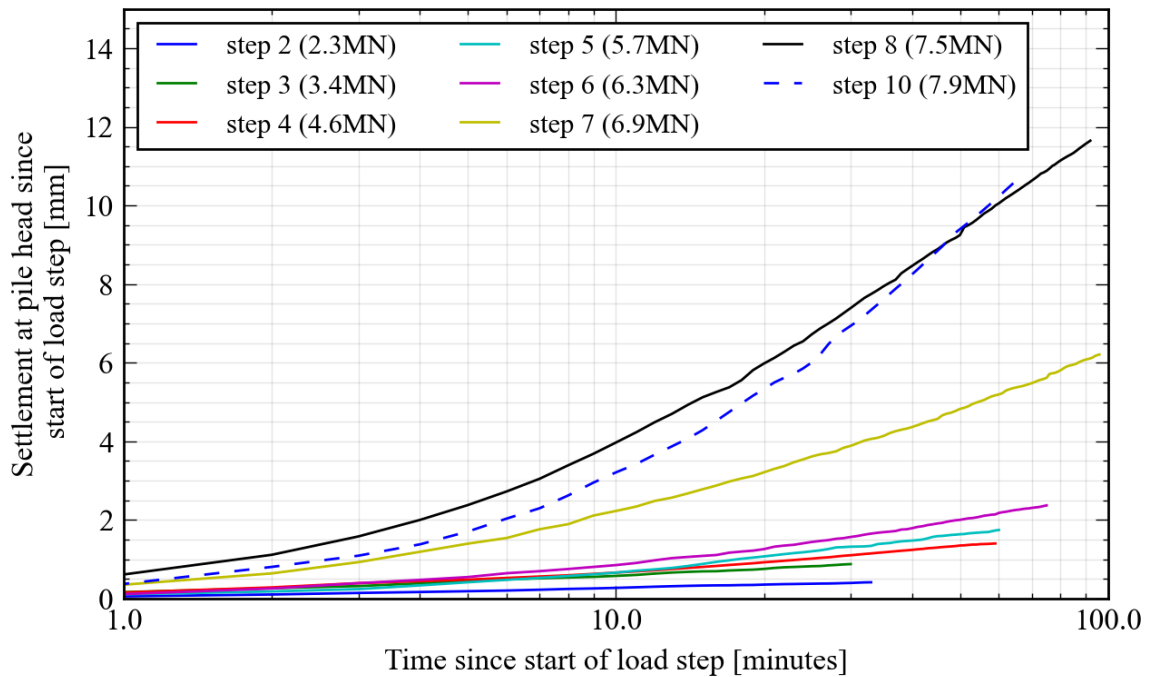


Figure 5.34: Development of the total creep settlement at the pile head during selected load steps for P06

Table 5.4: List of load steps and corresponding durations in pile test P06

Load Step	Start Time [DD/MM/YYYY hh:mm]	End Time [DD/MM/YYYY hh:mm]	Duration [hh:mm]	Average Load [kN]
refSLT	07/01/2020 15:25	07/01/2020 15:48	00:23	222.96
5%(0)	07/01/2020 16:07	07/01/2020 16:12	00:05	450.12
step 1	07/01/2020 16:25	07/01/2020 16:57	00:32	1147.44
step 2	07/01/2020 17:12	07/01/2020 17:45	00:33	2295.49
step 3	07/01/2020 18:02	07/01/2020 18:32	00:30	3435.37
step 4	07/01/2020 18:44	07/01/2020 19:43	00:59	4596.38
5%(4)	07/01/2020 19:53	07/01/2020 19:59	00:06	455.52
5%(4)ii	08/01/2020 07:35	08/01/2020 07:44	00:09	496.07
step 4ii	08/01/2020 08:08	08/01/2020 08:24	00:16	4581.42
step 5	08/01/2020 08:41	08/01/2020 09:41	01:00	5737.79
step 6	08/01/2020 09:50	08/01/2020 11:05	01:15	6308.92
step 7	08/01/2020 11:13	08/01/2020 12:49	01:36	6881.34
step 8	08/01/2020 13:01	08/01/2020 14:33	01:32	7457.96
5%(8)	08/01/2020 14:51	08/01/2020 14:56	00:05	450.57
step 4iii	08/01/2020 15:21	08/01/2020 15:25	00:04	4600.11
step 7iii	08/01/2020 16:06	08/01/2020 17:12	01:06	7025.94
step 8ii	08/01/2020 17:23	08/01/2020 18:26	01:03	7478.68
step 10	08/01/2020 18:42	08/01/2020 19:49	01:07	7911.09
close hydr.	08/01/2020 19:49	08/01/2020 20:25	00:36	7795.88

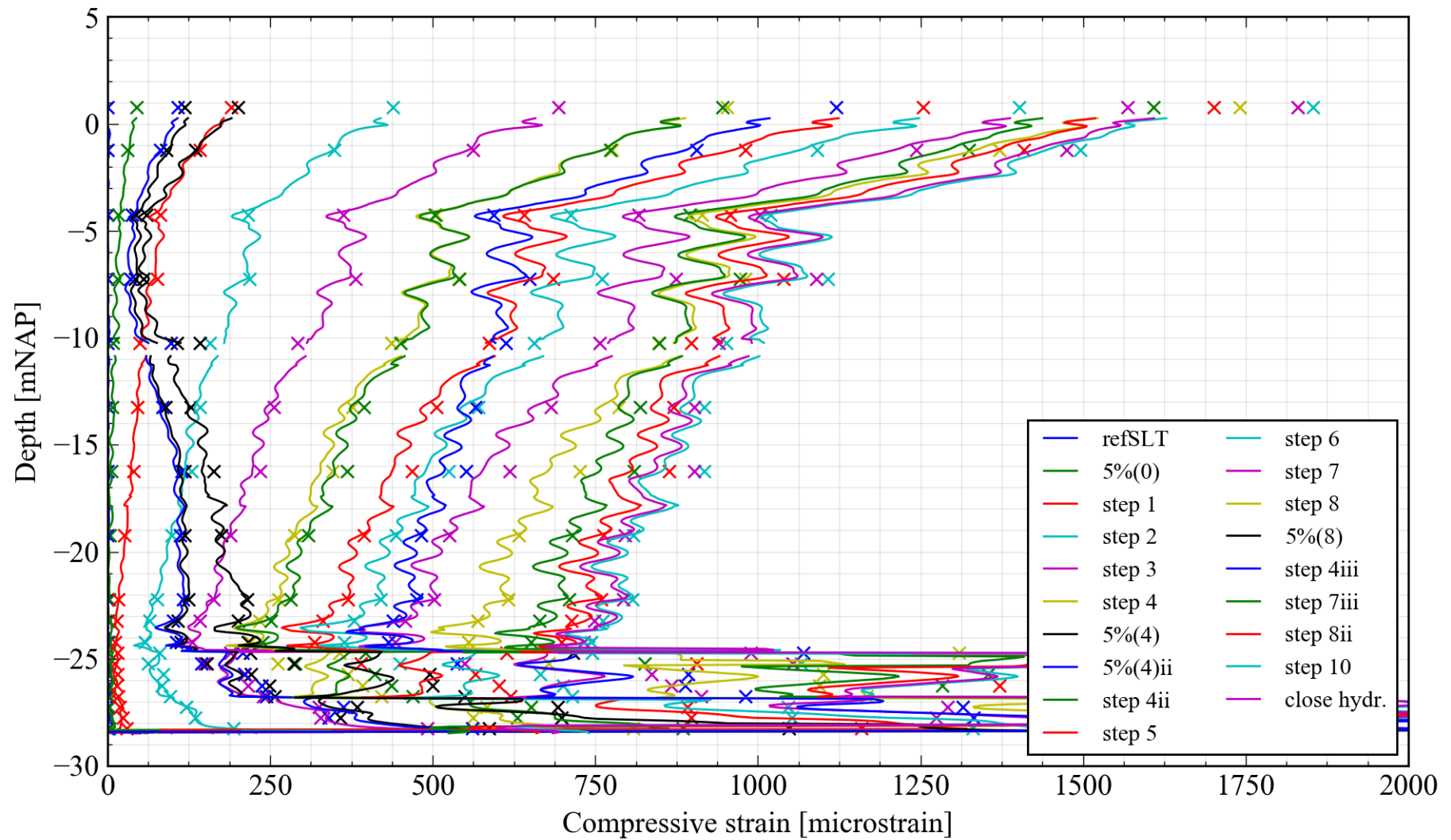


Figure 5.35: Strain versus depth profile for P06 at the end of each load step. Note that the BOFDA measurements are indicated by a continuous line whereas FBG readings are indicated by a discrete point

5.4. Test Results: Pile P11

The test on pile P11 was divided across two days and commenced testing on the 10th January. The pile was loaded incrementally to step 4 at 4600kN, after which the hydraulic jacks were closed overnight bringing a gradual reduction in the load on top of the pile to 4000kN. Like preceding tests, an unload/reload cycle was executed after 100% of the predicted pile capacity was reached in order to develop more base resistance. The pile was then loaded to step 10 at 8340kN during which the failure criteria were met.

The breakage of one FBG line occurred at the beginning of step 7 and the breakage of both BOFDA lines occurred after the completion of step 7ii – the reasons for both being unclear. Extremely scattered strain measurements are also evident from NAP -23.50m onwards, possibly as a result of concrete segregation (Section 6.1).

Results of the test are provided as follows:

- Figure 5.36: Plot of load exerted on pile head against the time elapsed for P11
- Figure 5.37: Plot of settlement measured at the pile head against the time elapsed for P11
- Figure 5.38: Plot of strain versus time for selected BOFDA gauges for P11
- Figure 5.39: Plot of strain versus time for all FBG gauges for P11
- Figure 5.40: Load at pile head readings from each individual load cell for P11
- Figure 5.41: Settlement at pile head readings from each individual LVDT for P11
- Figure 5.42: Plot of load versus settlement at pile head for P11
- Figure 5.43: Creep parameter versus time across selected load steps for P11
- Figure 5.44: Creep rate versus time across selected load steps for P11
- Figure 5.45: Development of the total creep settlement at the pile head during selected load steps for P11
- Figure 5.46: Strain versus depth profile for P11 at the end of each load step.

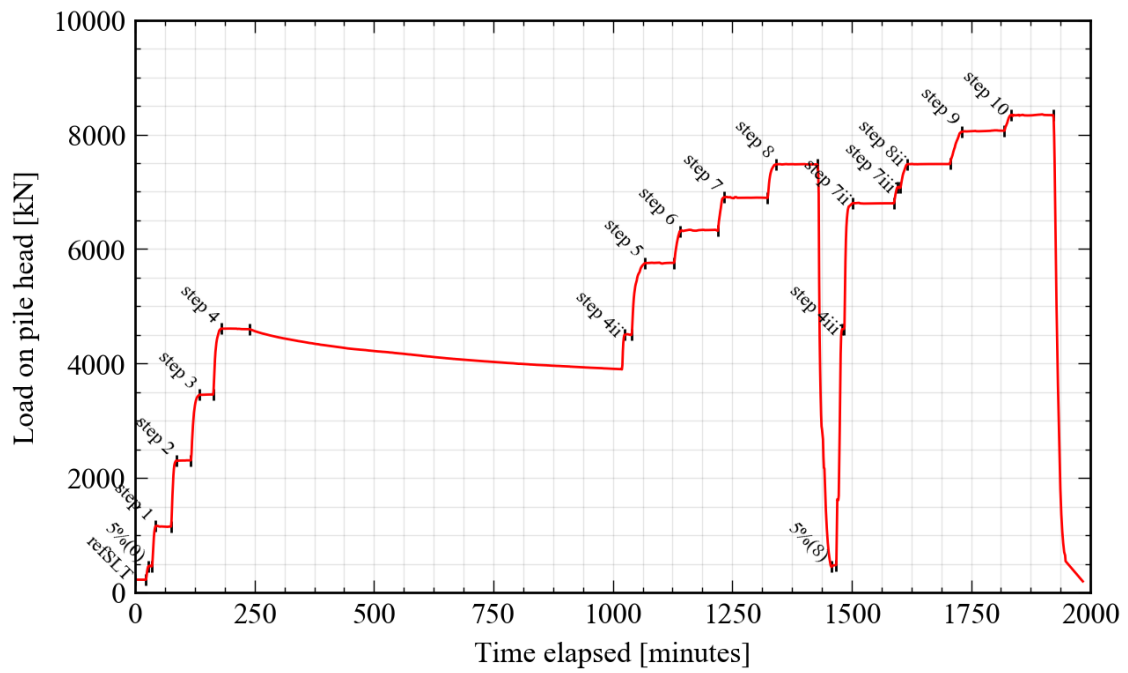


Figure 5.36: Plot of load exerted on pile head against the time elapsed for P11

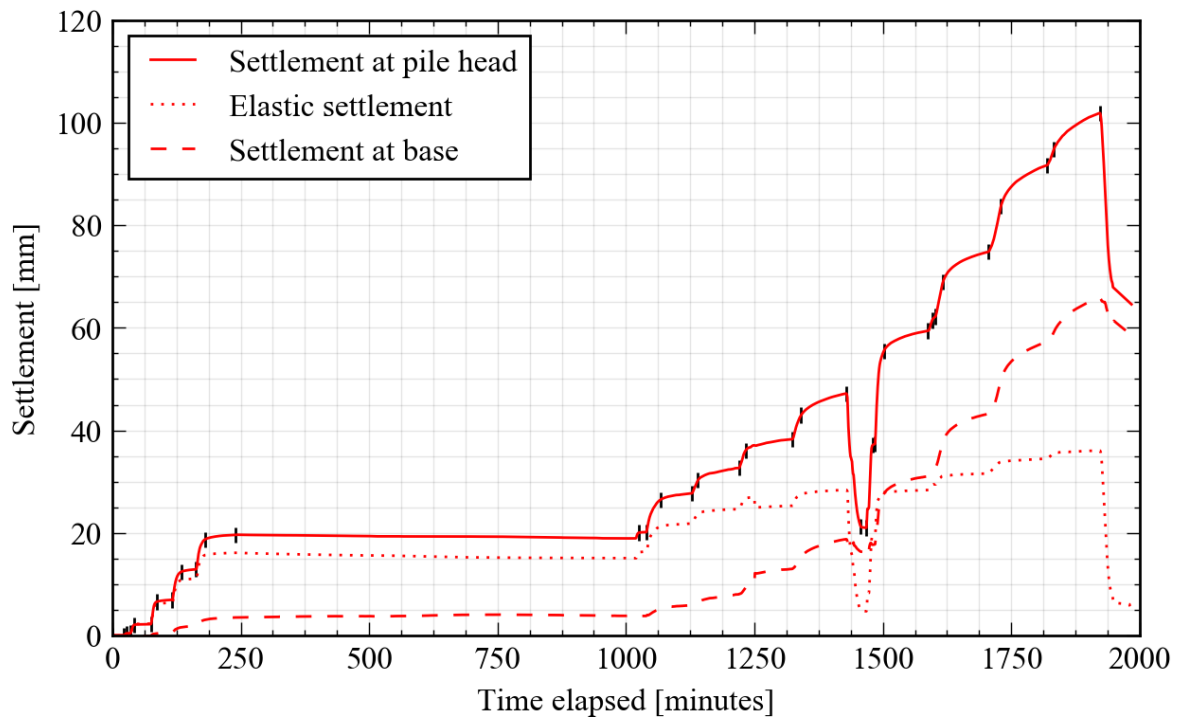


Figure 5.37: Plot of settlement measured at the pile head against the time elapsed for P11. The elastic settlement (and correspondingly the settlement at the pile base) readings shown have been derived from the FBG readings to provide more complete information over time

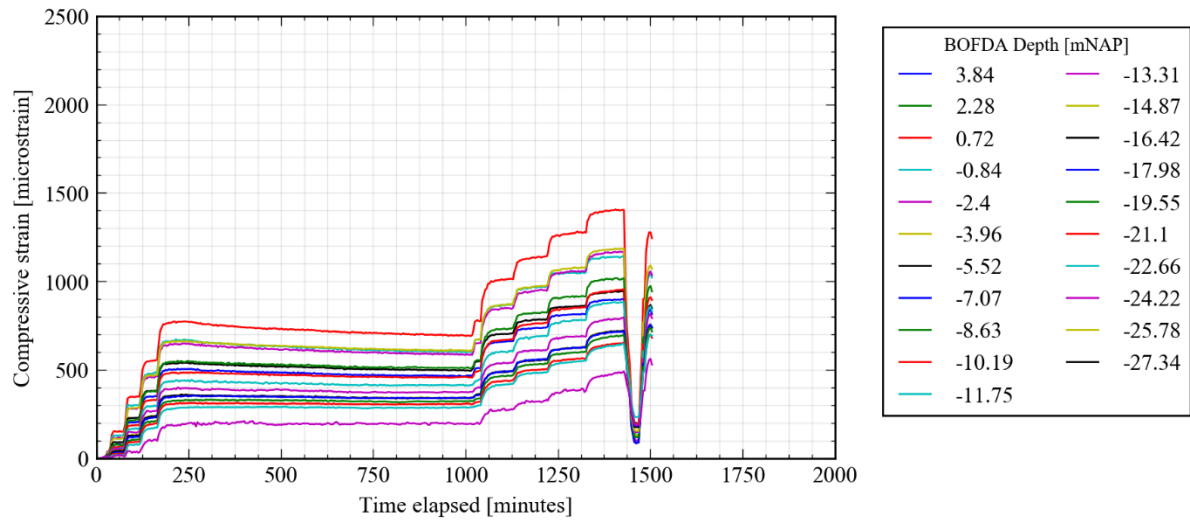


Figure 5.38: Plot of strain versus time for selected BOFDA gauges for P11

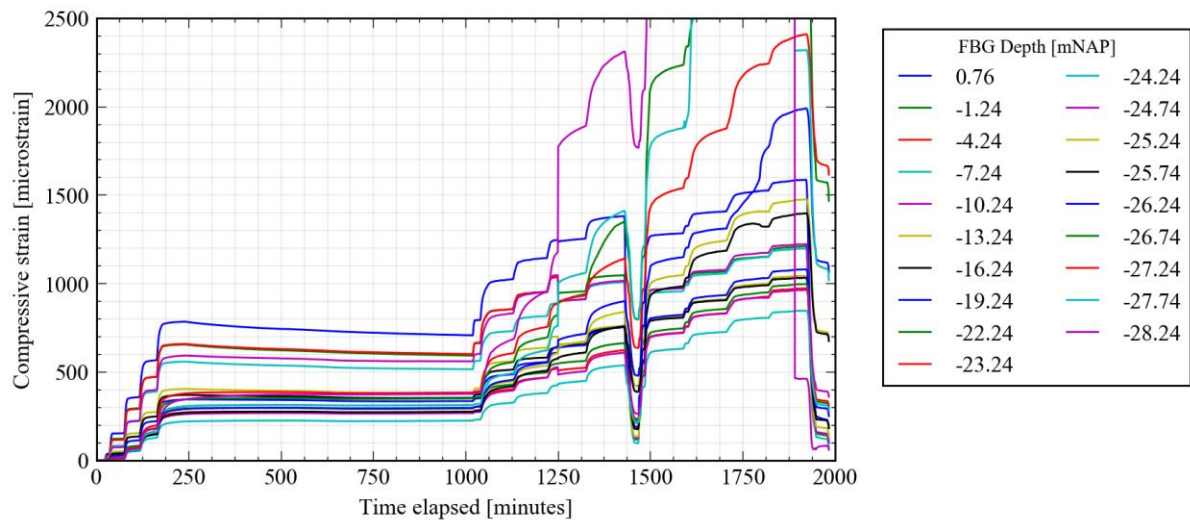


Figure 5.39: Plot of strain versus time for all FBG gauges for P11

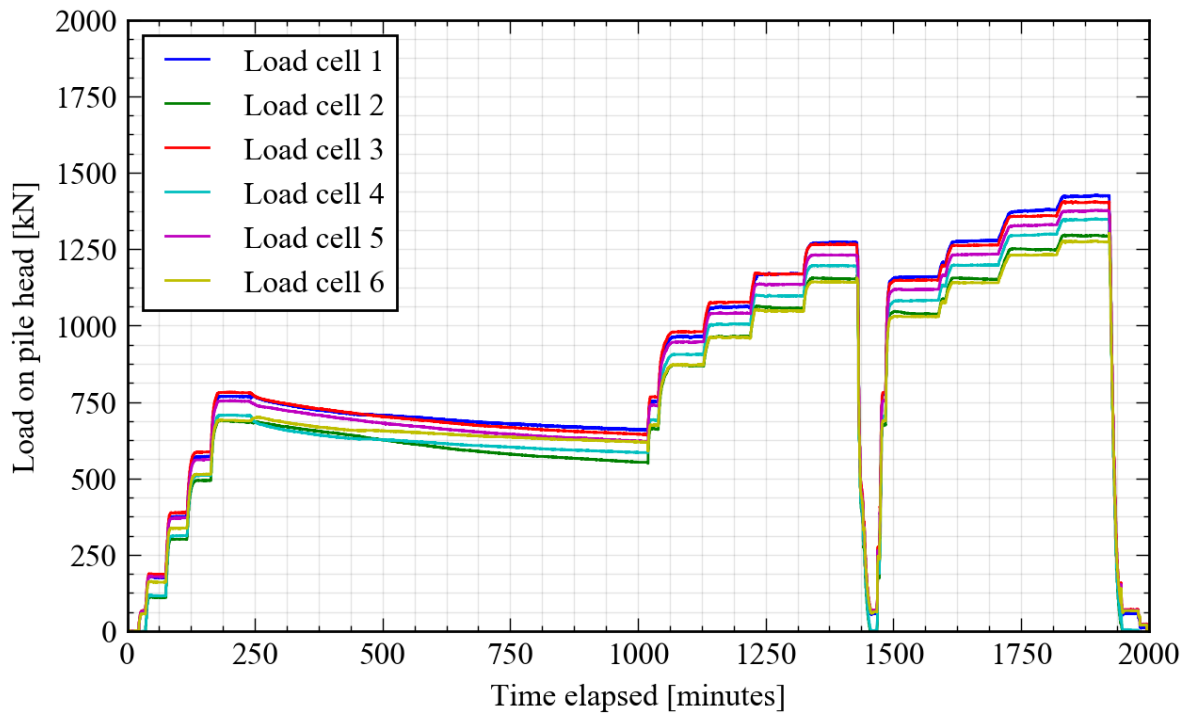


Figure 5.40: Load at pile head readings from each individual load cell for P11

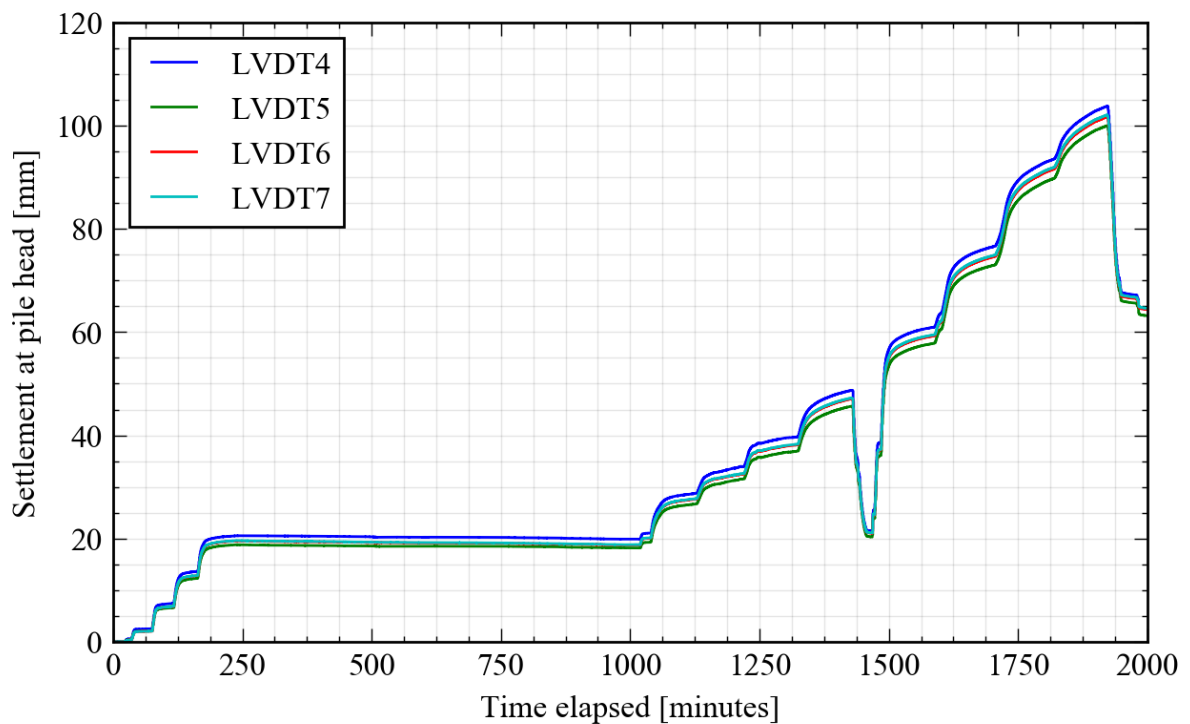


Figure 5.41: Settlement at pile head readings from each individual LVDT for P11

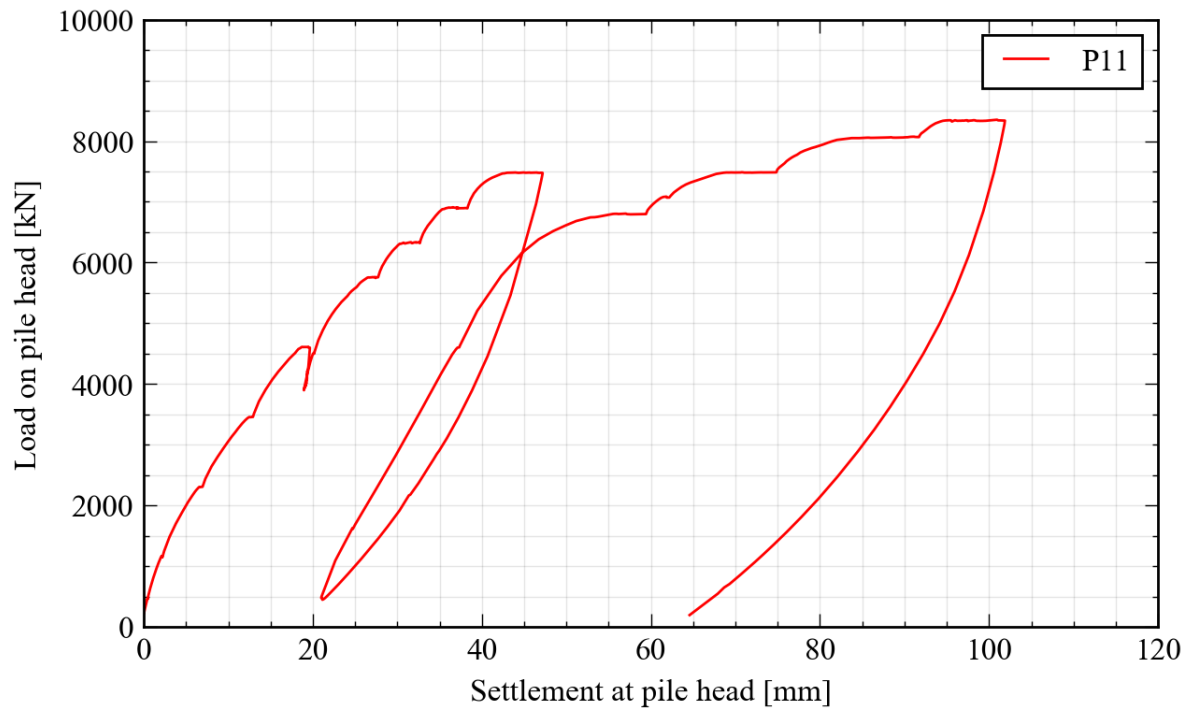


Figure 5.42: Plot of load versus settlement at pile head for P11

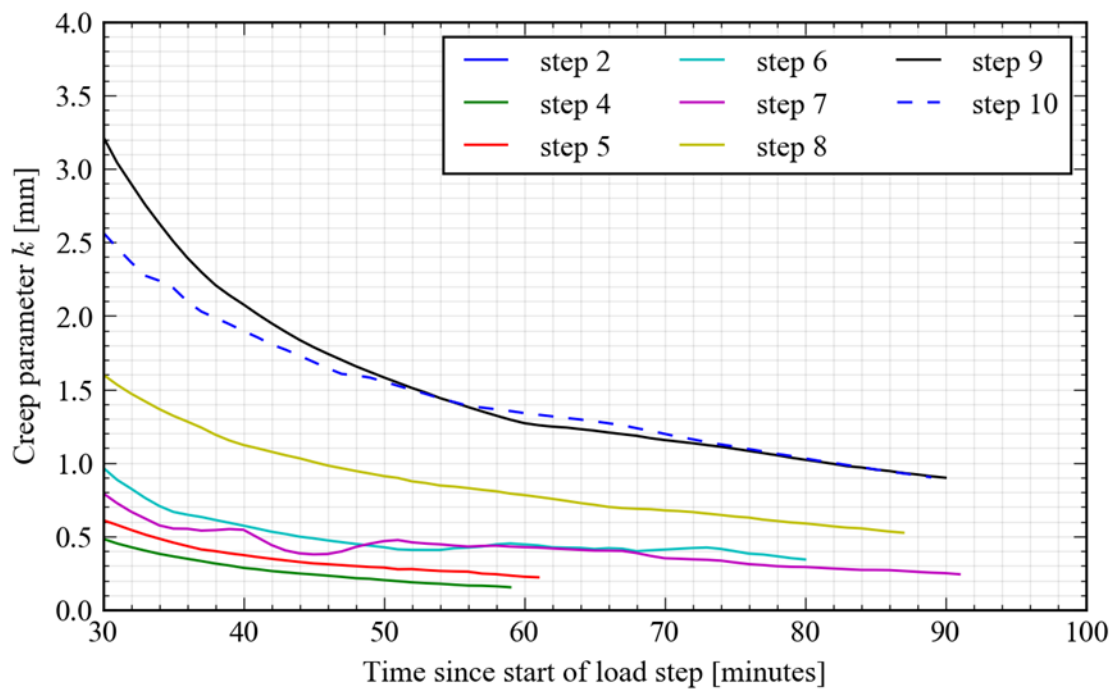


Figure 5.43: Creep parameter versus time across selected load steps for P11

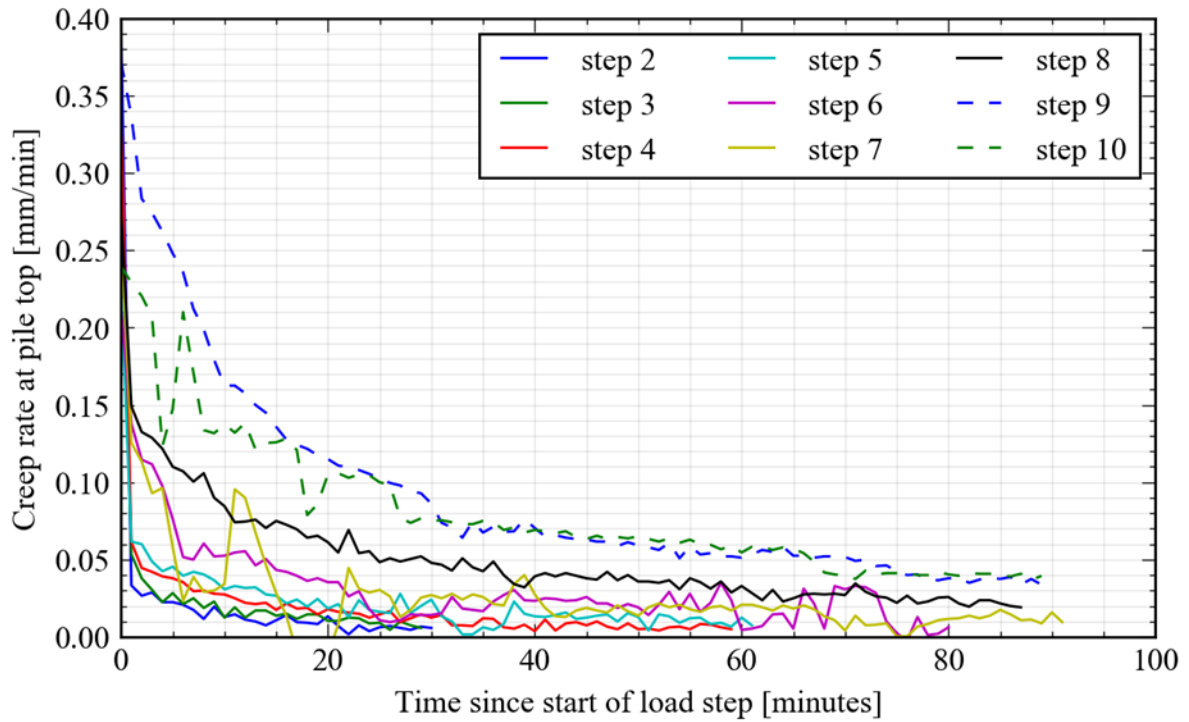


Figure 5.44: Creep rate versus time across selected load steps for P11

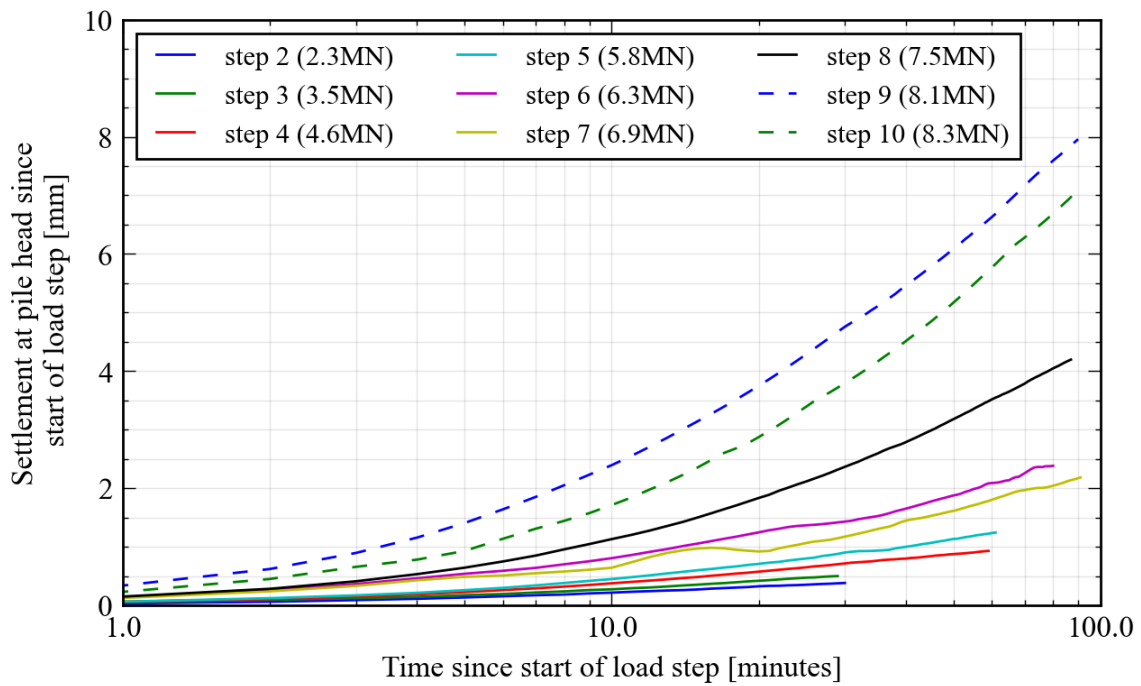


Figure 5.45: Development of the total creep settlement at the pile head during selected load steps for P11

Table 5.5: List of load steps and corresponding durations in pile test P11

Load Step	Start Time [DD/MM/YYYY hh:mm]	End Time [DD/MM/YYYY hh:mm]	Duration [hh:mm]	Average Load [kN]
refSLT	09/01/2020 14:35	09/01/2020 14:57	00:22	222.67
5%(0)	09/01/2020 15:03	09/01/2020 15:10	00:07	460.82
step 1	09/01/2020 15:18	09/01/2020 15:50	00:32	1152.11
step 2	09/01/2020 16:01	09/01/2020 16:31	00:30	2305.28
step 3	09/01/2020 16:49	09/01/2020 17:18	00:29	3455.55
step 4	09/01/2020 17:35	09/01/2020 18:34	00:59	4605.74
step 4ii	10/01/2020 07:40	10/01/2020 07:54	00:14	4504.92
step 5	10/01/2020 08:22	10/01/2020 09:23	01:01	5756.23
step 6	10/01/2020 09:35	10/01/2020 10:55	01:20	6327.74
step 7	10/01/2020 11:08	10/01/2020 12:39	01:31	6897.60
step 8	10/01/2020 12:56	10/01/2020 14:23	01:27	7480.21
5%(8)	10/01/2020 14:52	10/01/2020 15:02	00:10	467.58
step 4iii	10/01/2020 15:15	10/01/2020 15:19	00:04	4601.45
step 7ii	10/01/2020 15:37	10/01/2020 17:03	01:26	6798.30
step 7iii	10/01/2020 17:11	10/01/2020 17:17	00:06	7076.14
step 8ii	10/01/2020 17:32	10/01/2020 19:01	01:29	7484.04
step 9	10/01/2020 19:25	10/01/2020 20:55	01:30	8061.71
step 10	10/01/2020 21:08	10/01/2020 22:37	01:29	8339.70

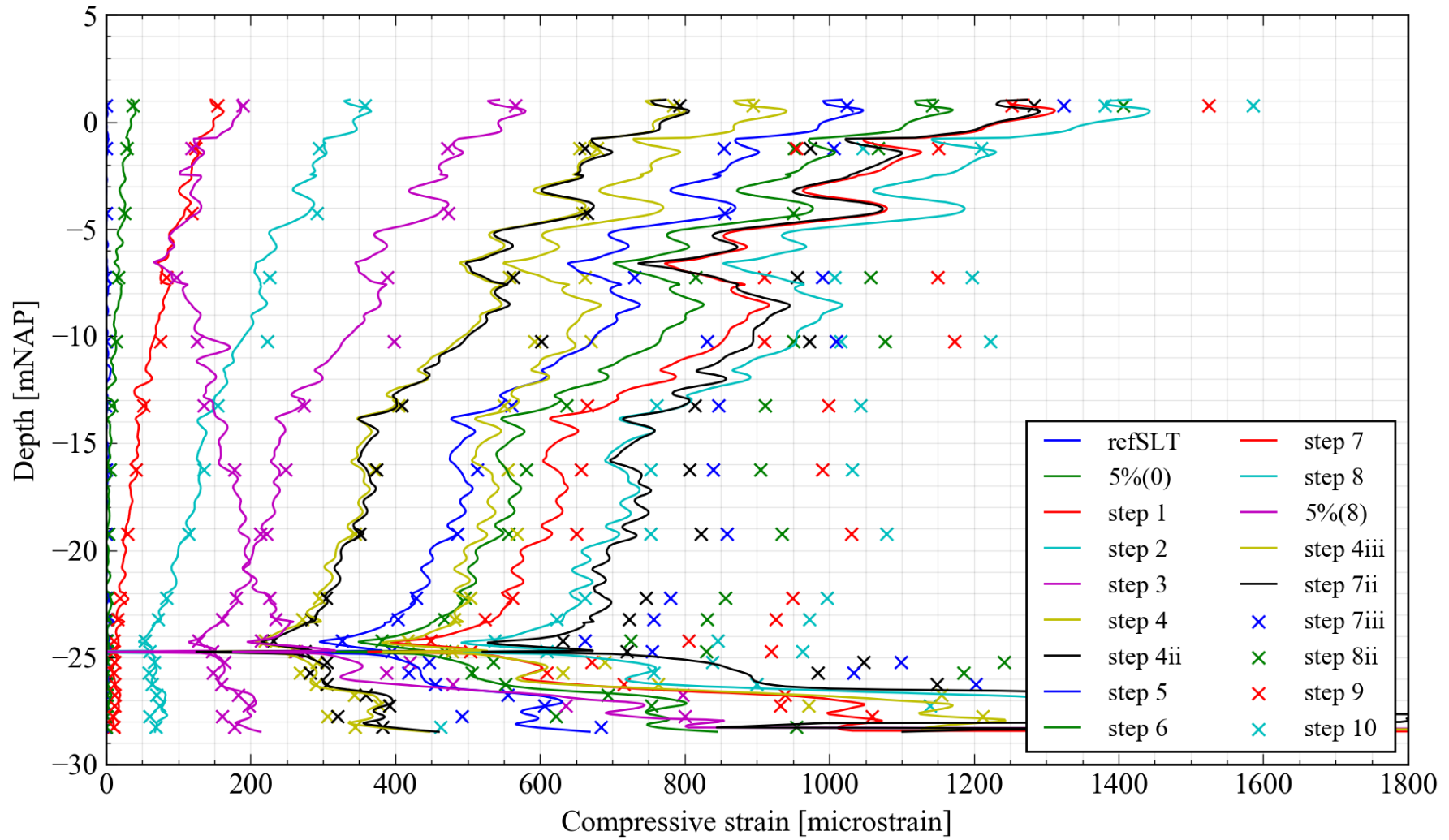


Figure 5.46: Strain versus depth profile for P11 at the end of each load step. Note that the BOFDA measurements are indicated by a continuous line whereas FBG readings are indicated by a discrete point

6. Interpretation & Analysis

6.1. Measurement Scatter

Evident in the strain results of all vibro piles, is the significant scatter in both the BOFDA and FBG readings in the lower part of the pile (e.g. Figure 5.11). This scatter is exhibited by an approximate three-fold increase in strains compared to the upper part of the pile. This may suggest a substantial change in stiffness in the lower part of the pile, redolent of a pile consisting of only the steel reinforcement ($EA_{reinf.} = 1610\text{MN}$) as opposed to the expected stiffness of a composite steel-concrete pile ($EA_{vibro} = 4453\text{MN}$); assuming a shaft diameter equal to the outer diameter of the auxiliary tube.

It is postulated that this is a result of segregation occurring within the concrete mix in the lower part of the pile i.e. the separation of certain aggregate sizes from the cement at particular locations across the pile, resulting in the deficiency of this aggregate grouping in certain areas of the pile and the overabundance of this grouping in other areas of the pile.

This problem has been observed in previous projects (BieTec B.V. Consultancy (2015), Geerling and Janse (1997), van Weele and Lencioni (1999)) where noticeable deterioration of concrete quality towards the pile base was observed (e.g. Figure 6.1) and numerous factors (be it a combination thereof or otherwise) have been identified as the possible cause of this segregation, notably with regards to the composition of the concrete mix (such as its workability and cohesiveness) and the placement of the reinforcement cage.



Figure 6.1: Photos of the piles after tension tests at the Gaag viaduct in Schipluiden. Noticeable deterioration of concrete towards the pile tip was observed (Geerling and Janse, 1997)

A couple of stipulations exist in the national standards with respect to the installation of the vibro piles. These stipulations state that the inside of the auxiliary tube must be dry after its installation (i.e. no ingress of soil or water) and that the reinforcement cage must remain in suspension (i.e. not resting on the base plate) during the withdrawal of the auxiliary tube. Nonetheless, the number of these stipulations is relatively limited and the problem persists in a variety of projects across the country.

To account for the possible effect of segregation in the analysis of the pile test results, it is assumed that no shaft resistance was developed after the start depth of the apparent segregation (Table 6.1), i.e. primarily the Pleistocene sand. As a result, this assumption implies that the

axial load in the pile was transferred through the reinforcement cage and directly to the pile base plate from the start depth of the apparent segregation. Nonetheless, it should be stressed that this assumption has been made in order to make an interpretation of the base resistance from the existing pile test results and it is recommended that the extraction of one or more of the piles is carried out in order to obtain more certainty of the condition of the pile(s) and its behaviour in the Pleistocene sand.

A detailed memo (Timmermans, 2020) regarding this problem at Maasvlakte has been drafted with recommendations for future projects and stipulations.

Table 6.1: Estimate of the start depth of the scattered measurements and the depth of the Pleistocene for each pile. Note that in the instance of P03 and P06, the scatter in the BOFDA readings occurs at a shallower depth (at NAP -23.23m and NAP -23.29m respectively)

Pile	Depth of scattered measurements [mNAP]	Depth of Pleistocene sand [mNAP]
P01	-23.70	-24.05
P03	-24.73	-23.95
P06	-24.24	-23.50
P11	-23.50	-24.10

6.2. Strain to Force Conversion

The conversion of the strain readings measured by the fibre optics along the pile shaft to force has been carried out using a visual interpretation of the change in the tangent and secant stiffness moduli with increasing strain as per Fellenius (2001). The strain dependency of tangent stiffness modulus is given by the following first order polynomial equation:

$$E_t = \frac{d\sigma}{d\varepsilon} = m\varepsilon + c$$

where m = slope of the fitted tangent modulus line; c = y-intercept of the fitted tangent modulus line.

Given that $E_s = \sigma/\varepsilon$, can also be shown that for the same slope m and intercept c , the strain dependency of the secant stiffness modulus can be provided as:

$$E_s = \frac{m}{2}\varepsilon + c$$

The determination of an appropriate value for m and c has been interpreted based on both the tangent and secant stiffness plots shown in Figure 6.2 to Figure 6.5 and have been verified via an assessment of the force-depth profiles and the synchronisation of the uppermost strain gauge readings with the force measured by the load cells. For clarity, only a certain number of gauges have been presented in these tangent stiffness and secant stiffness plots, with priority given to the upper gauges which are less affected by the shaft resistance on the pile section above and thus the governing gauges for the interpretation of the strain-dependent stiffness equation.

Given the potential non-uniformity in the cross-section between each pile, a different strain-dependent stiffness equation has been chosen for all piles and are outlined in Table 6.2. As part of this analysis, no consideration of the pile stiffness on pile unloading or reloading has been considered however it is recommended that it is implemented in future analyses.

Table 6.2: Slope and intercept of the strain-dependent stiffness equations

Pile	Slope m	Intercept c
P01	-0.0010	5.50
P03	-0.0010	5.50
P06	-0.0012	5.20
P11	-0.0011	5.80

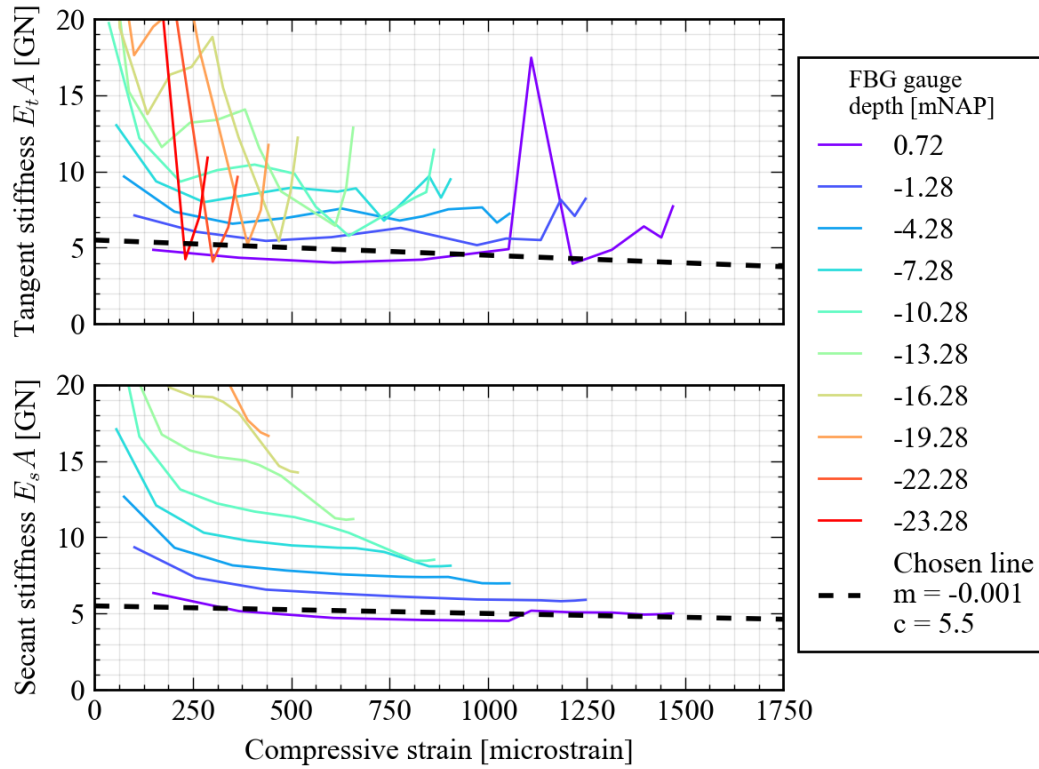


Figure 6.2: Fitted strain-dependent equation to the FBG data for the tangent and secant stiffness moduli of P01. Steps on the unload/reload cycle have been filtered out

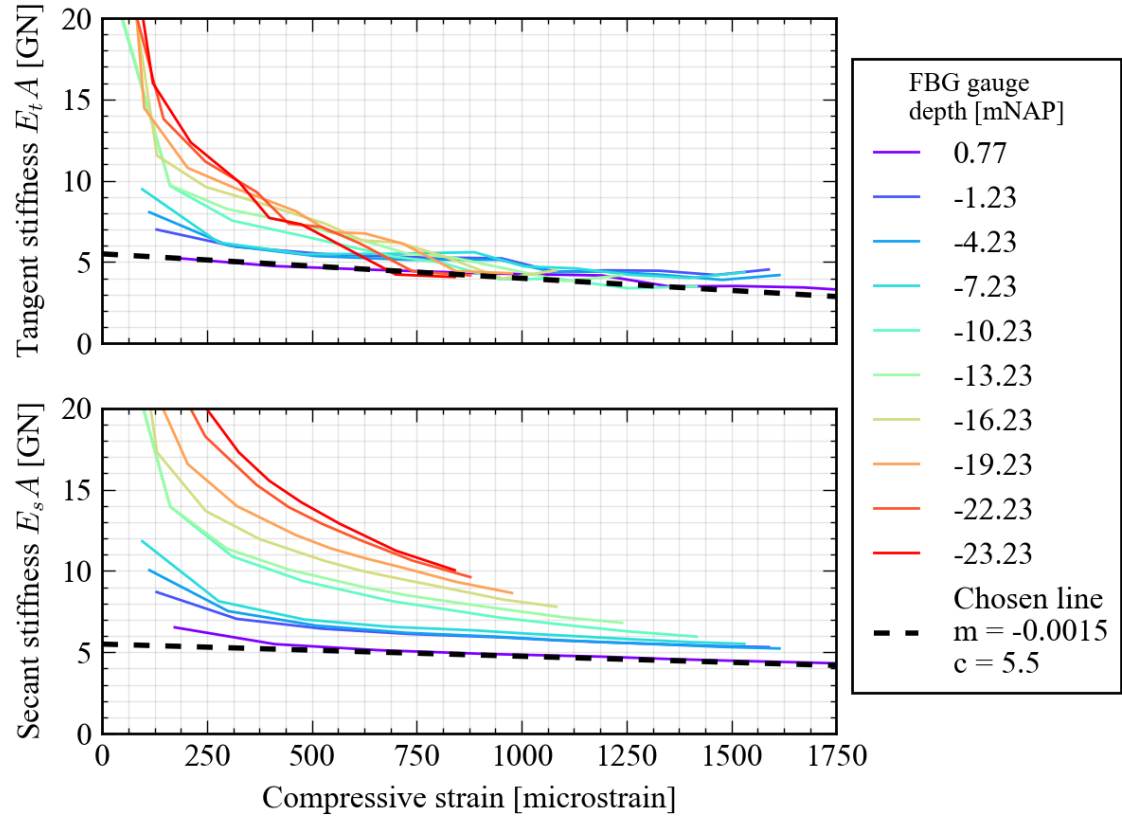


Figure 6.3: Fitted strain-dependent equation to the FBG data for the tangent and secant stiffness moduli of P03

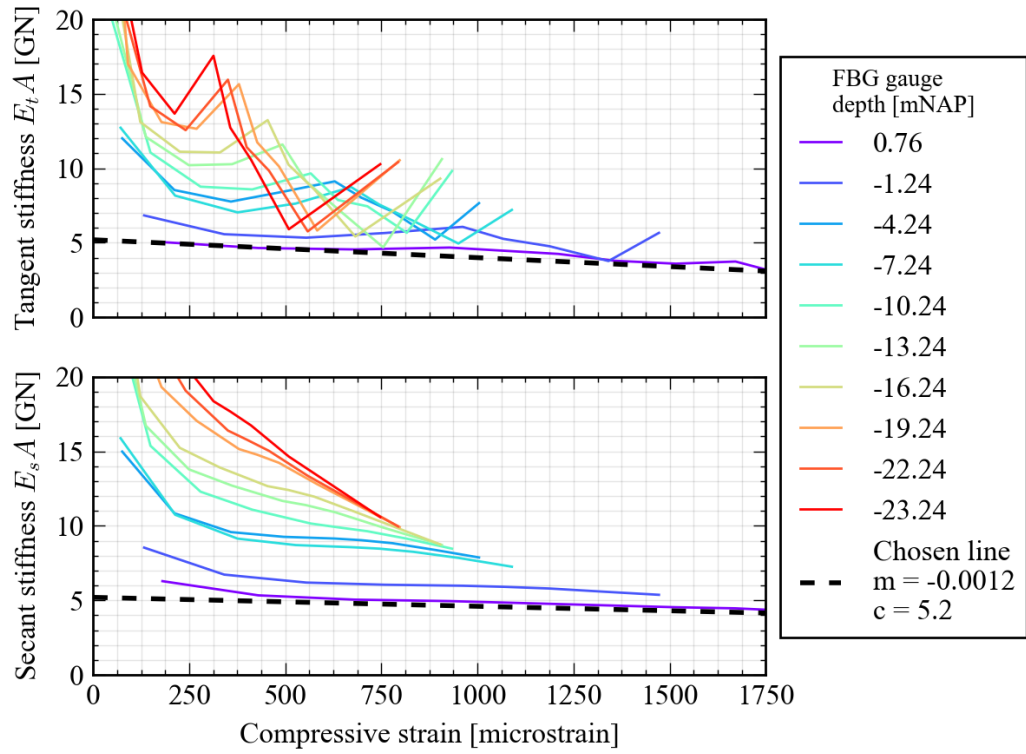


Figure 6.4: Fitted strain-dependent equation to the FBG data for the tangent and secant stiffness moduli of P06. Steps on the unload/reload cycles have been filtered out

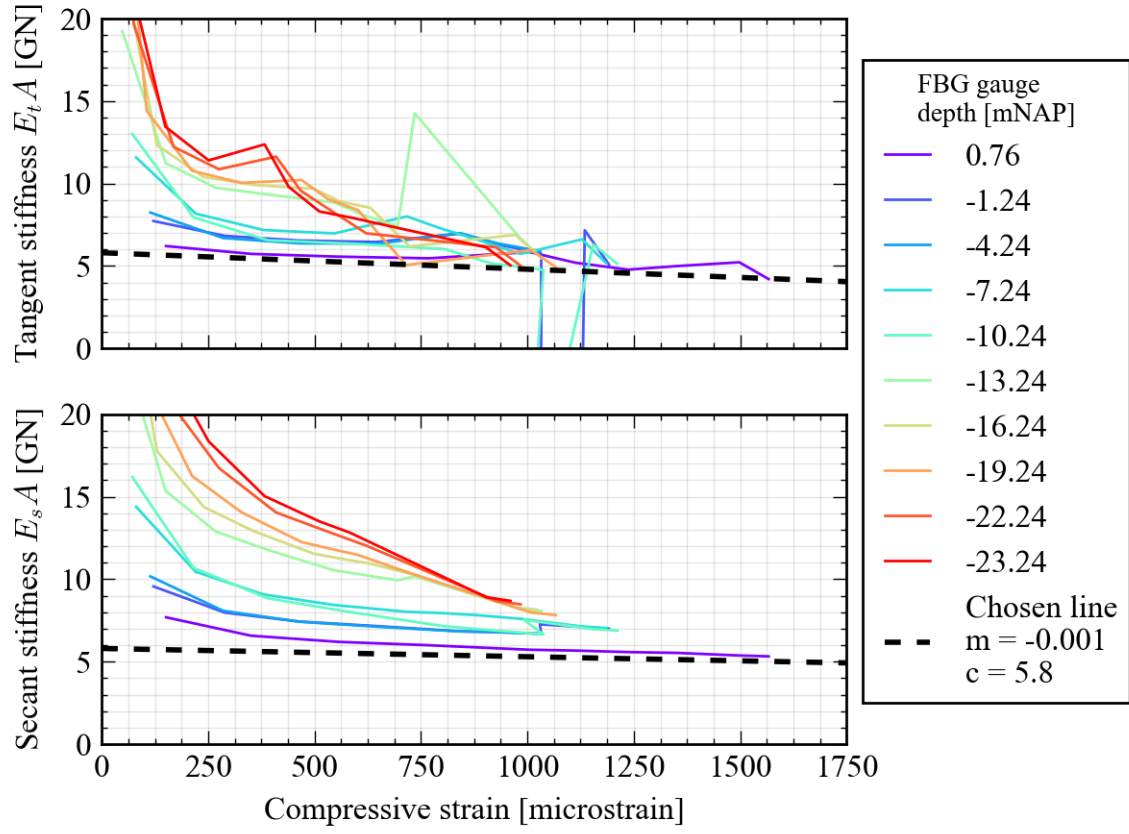


Figure 6.5: Fitted strain-dependent equation to the FBG data for the tangent and secant stiffness moduli of P11. Steps on the unload/reload cycle have been filtered out

6.3. Force/Depth Profiles

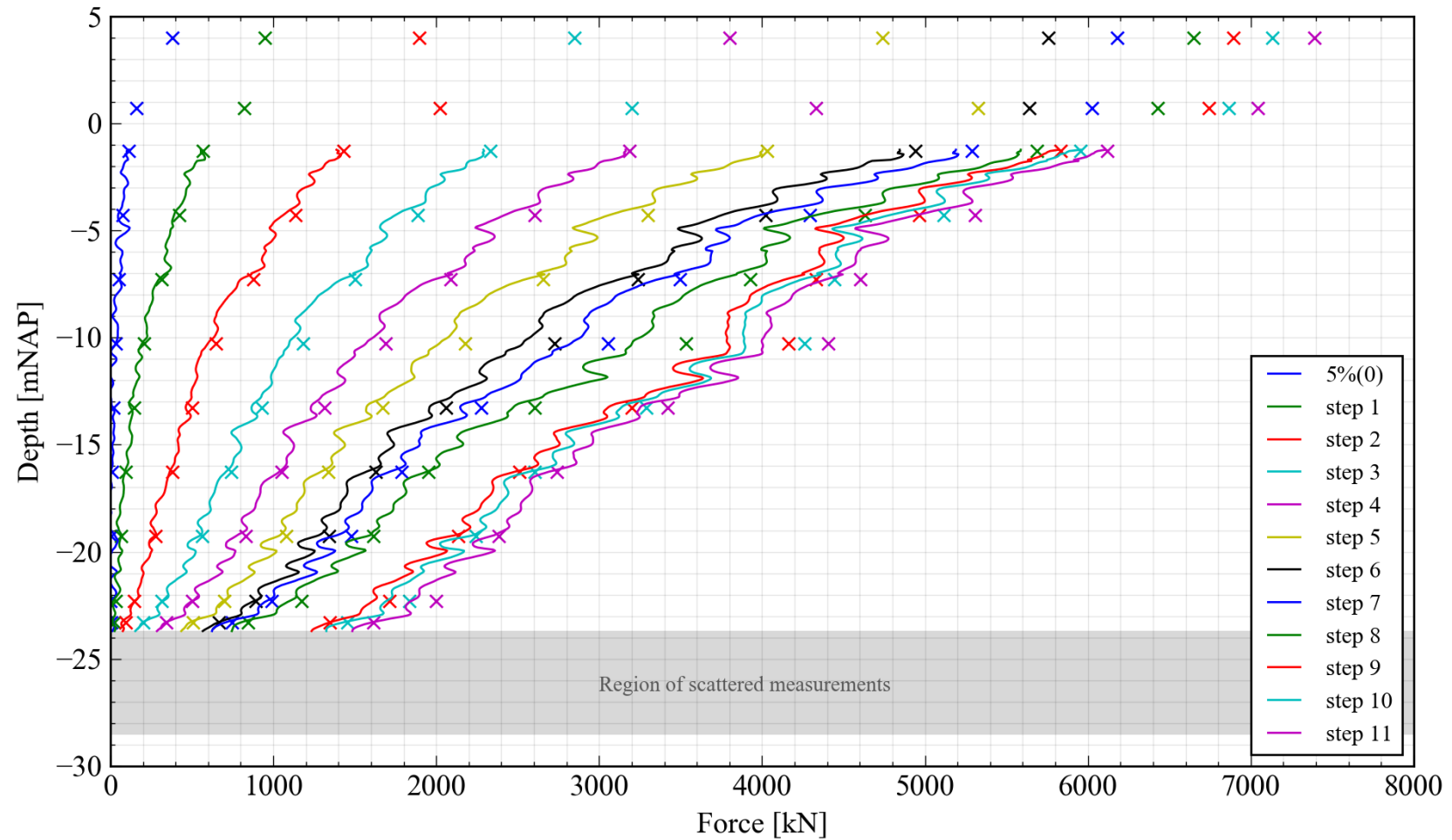


Figure 6.6: Force-depth profile of P01, taking the forces in the gauges at the end of the load step. Note that the BOFDA measurements are indicated by a continuous line whereas FBG readings are indicated by a discrete point and the force measured by the load cells has also been included as discrete points at NAP +4m. Steps within an unload/reload cycle have been omitted

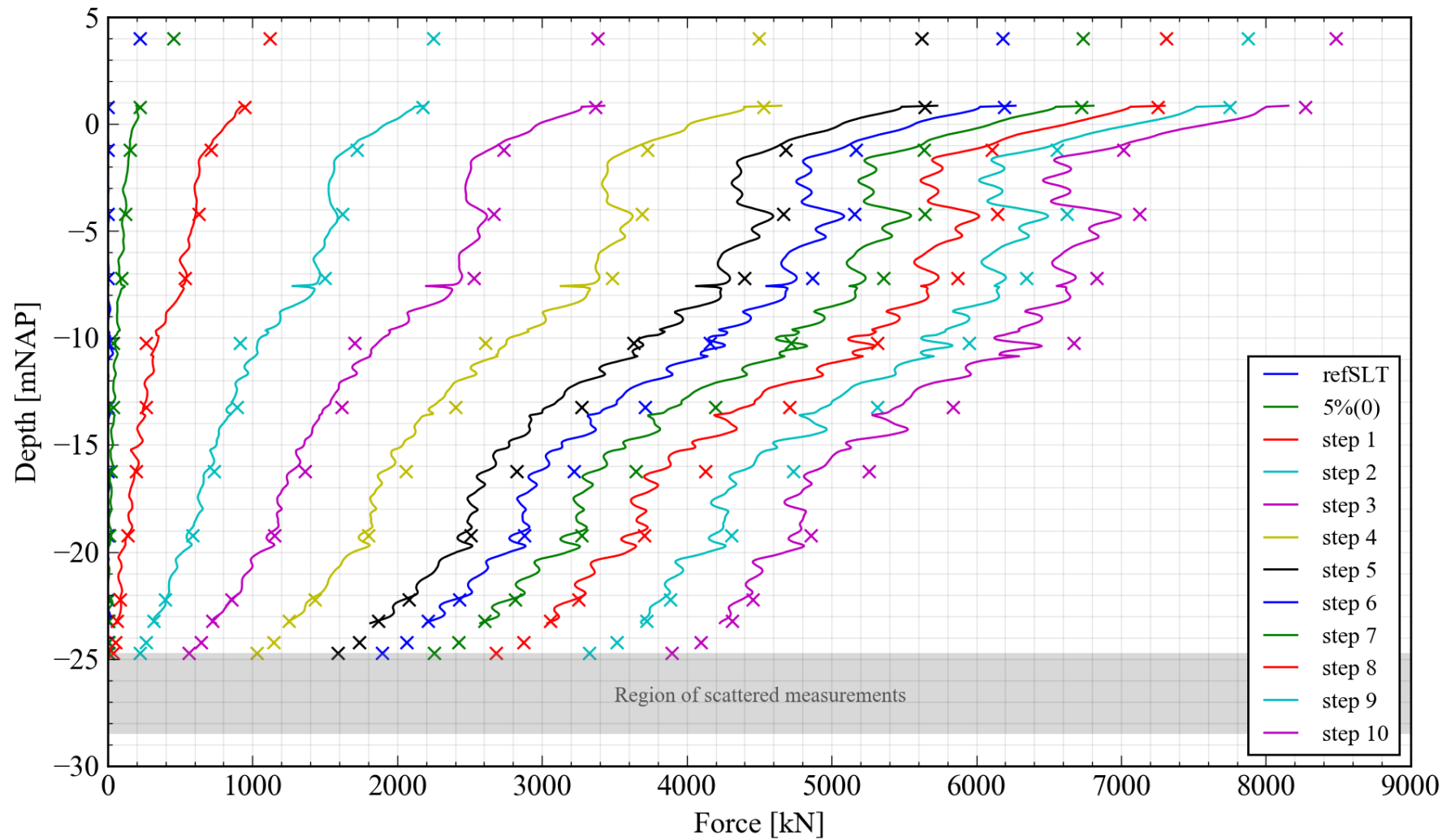


Figure 6.7: Force-depth profile of P03, taking the forces in the gauges at the end of the load step. Note that the BOFDA measurements are indicated by a continuous line whereas FBG readings are indicated by a discrete point and the force measured by the load cells has also been included as discrete points at NAP +4m. Steps within an unload/reload cycle have been omitted

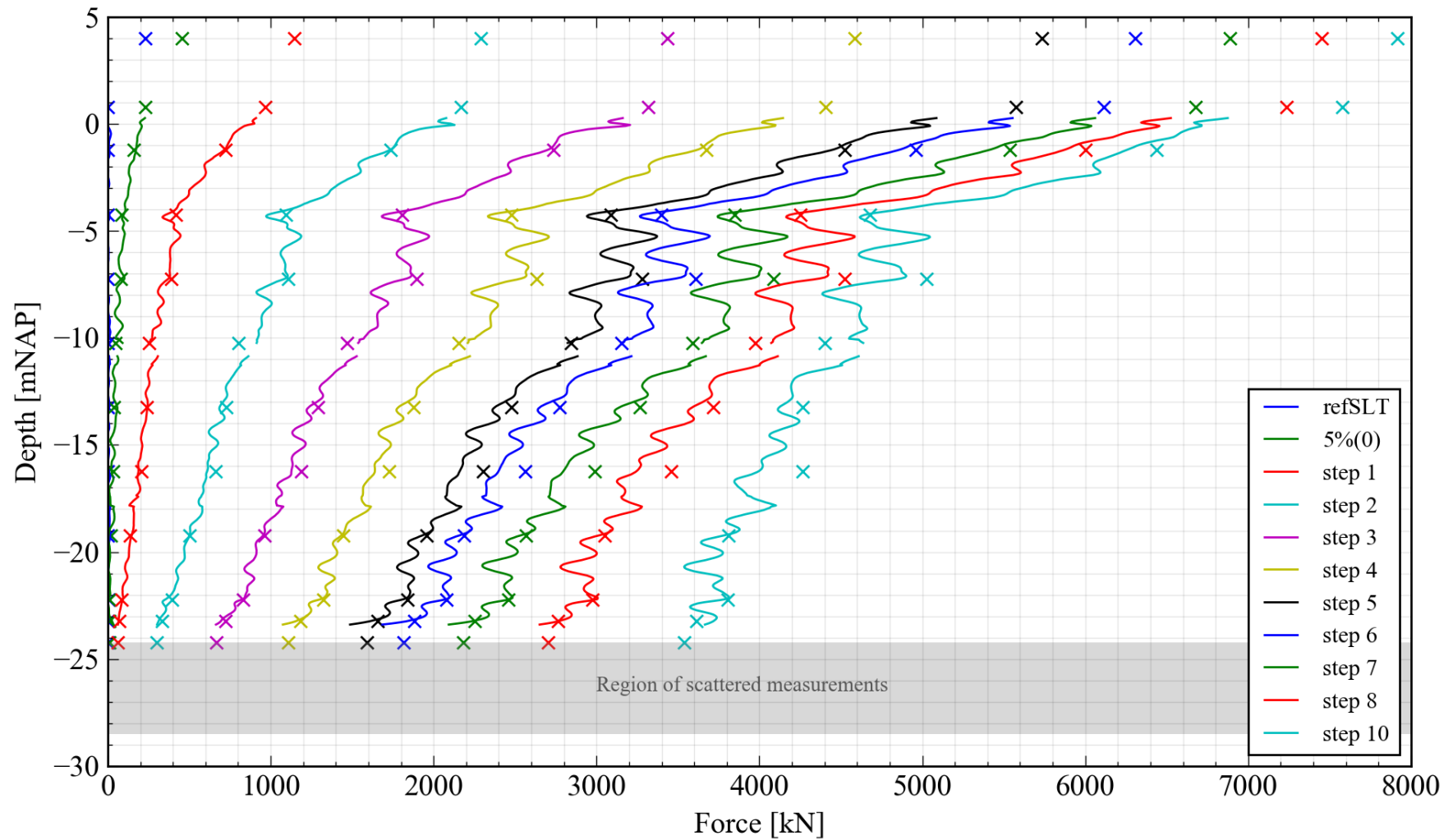


Figure 6.8: Force-depth profile of P06, taking the forces in the gauges at the end of the load step. Note that the BOFDA measurements are indicated by a continuous line whereas FBG readings are indicated by a discrete point and the force measured by the load cells has also been included as discrete points at NAP +4m. Steps within an unload/reload cycle have been omitted. The measurement gap in the BOFDA readings at approx. NAP -10.5m is as a result of the coupling sleeve on the reinforcement distorting the readings. This has been corrected for in the FBG measurement

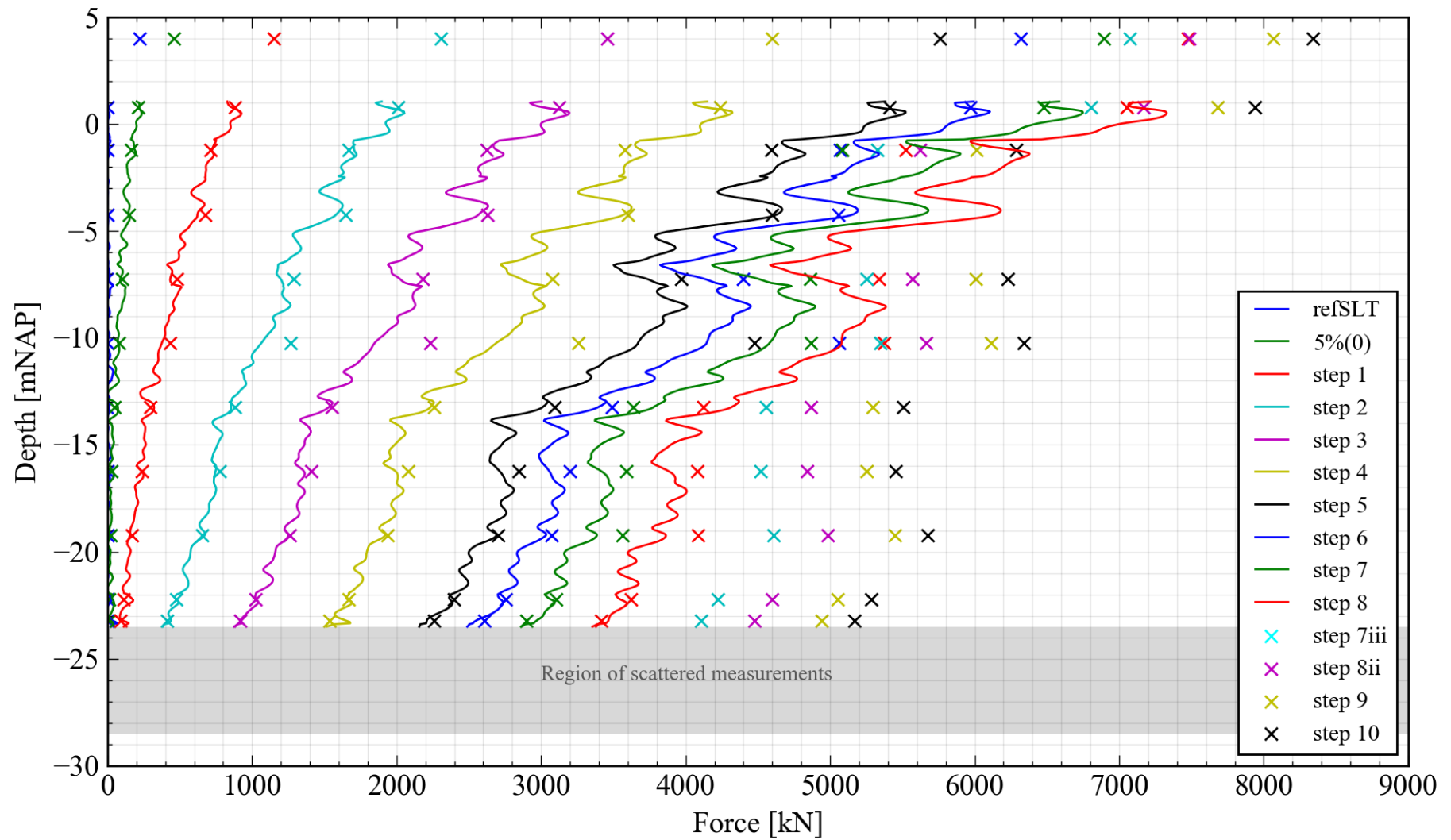


Figure 6.9: Force-depth profile of P11, taking the forces in the gauges at the end of the load step. Note that the BOFDA measurements are indicated by a continuous line whereas FBG readings are indicated by a discrete point and the force measured by the load cells has also been included as discrete points at NAP +4m. Steps within an unload/reload cycle have been omitted

6.4. Base Mobilisation

The following subsection visualises the mobilisation of base stress in terms of pile base settlement and provides the results received from both gauges in both a non-normalised and normalised fashion. As discussed in Section 6.1, the base pressure has been interpreted as the force returned from the lowermost gauge for both fibre optic systems with the region of scattered measurements filtered out (i.e. all depths lower than those listed in Table 6.1). In essence, it is assumed that across the region of segregation, the axial load is transferred through the reinforcing and directly to the base plate without the effect of shaft friction.

The normalising parameter $q_{c,avg}$ for the base pressure is based on the Koppejan averaging method (calculated values shown in Table 6.3) at the depth of the pile base plate, using a CPT profile of the average of all CPTs executed within two metres of each pile. The pile diameter for this calculation, in addition to the normalising parameter for the pile settlement, is the equivalent diameter D_{eq} and has been elected as the diameter of the base plate (480mm).

The figures are presented as follows:

Non-normalised

- Figure 6.10: BOFDA measurements
- Figure 6.11: FBG measurements

Normalised:

- Figure 6.12: BOFDA measurements
- Figure 6.13: FBG measurements

Patently, piles P03 and P11 develop the stiffest response of the four vibro piles, reaching a base stress of approximately 24MPa and 28MPa respectively, with both piles exhibiting almost identical stiffnesses. However, structural breakage in pile P03 resulted in the premature structural failure of the pile and was unable to reach a pile base settlement of $0.1D_{eq}$. Nonetheless, the base response of both piles is similar up until a base settlement of 7% of the equivalent pile diameter.

Weaker responses are evident in P01 and P06, substantially so in the case of P01. For pile P01, a peak base resistance of 8MPa was observed and for P06, a peak base resistance of 21MPa was attained. The resulting pile class factor α_p for both piles (Table 6.3) is in the range of 0.40-0.54, redolent of a continuous flight auger pile, as opposed to an α_p of 0.67 for P11, which is more in keeping with a driven precast pile according to the current NEN 9997-1 prescriptions.

Further discussion on the interpretation of the appropriate α_p to use for the site is provided in Section 7.

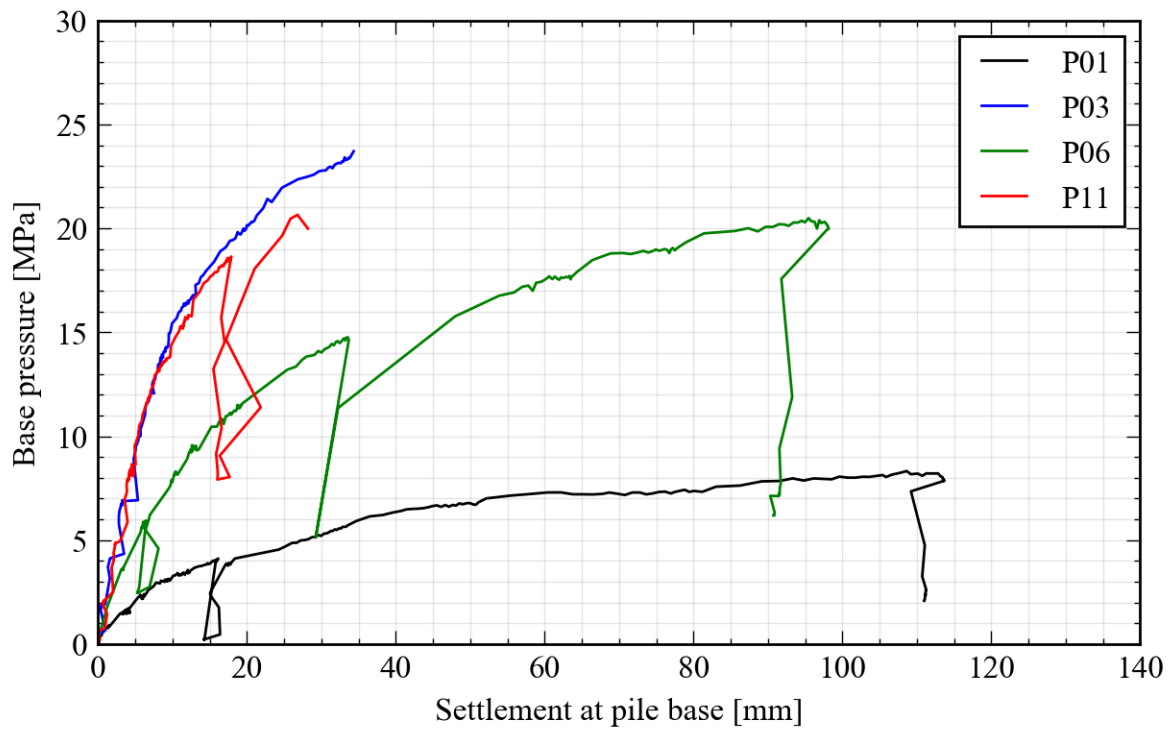


Figure 6.10: Mobilisation of the base capacity for all vibro piles (BOFDA measurements)

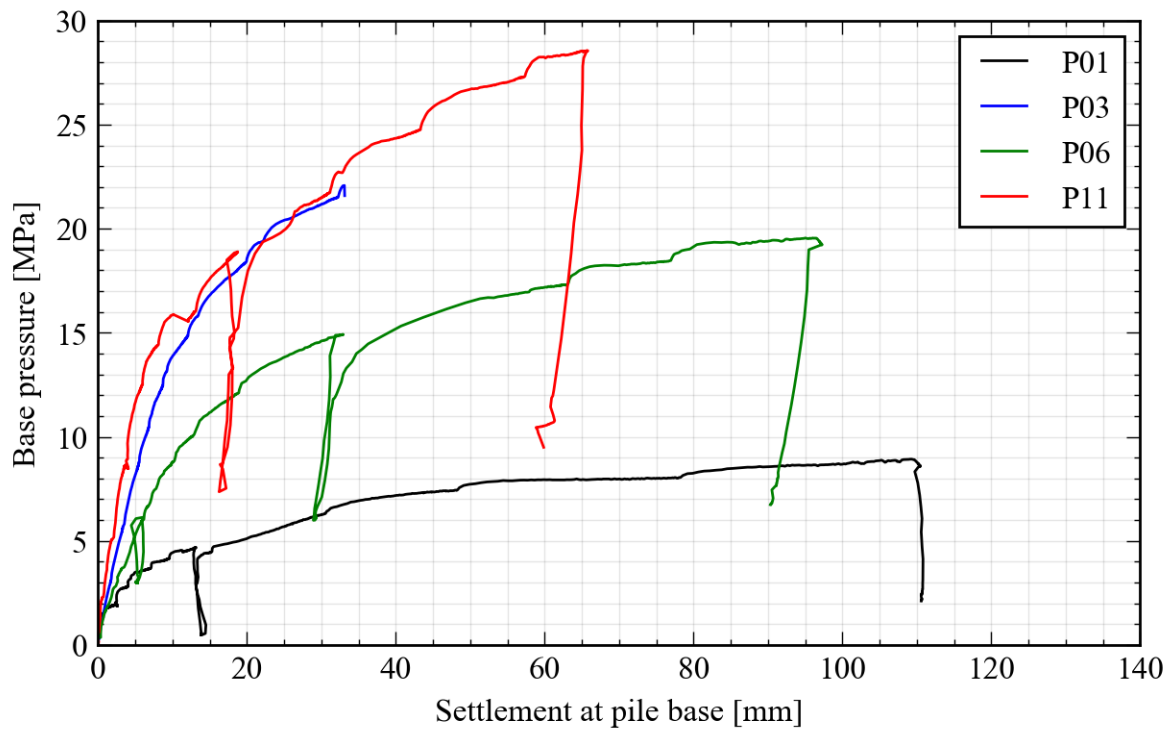


Figure 6.11: Mobilisation of the base capacity for all vibro piles (FBG measurements)

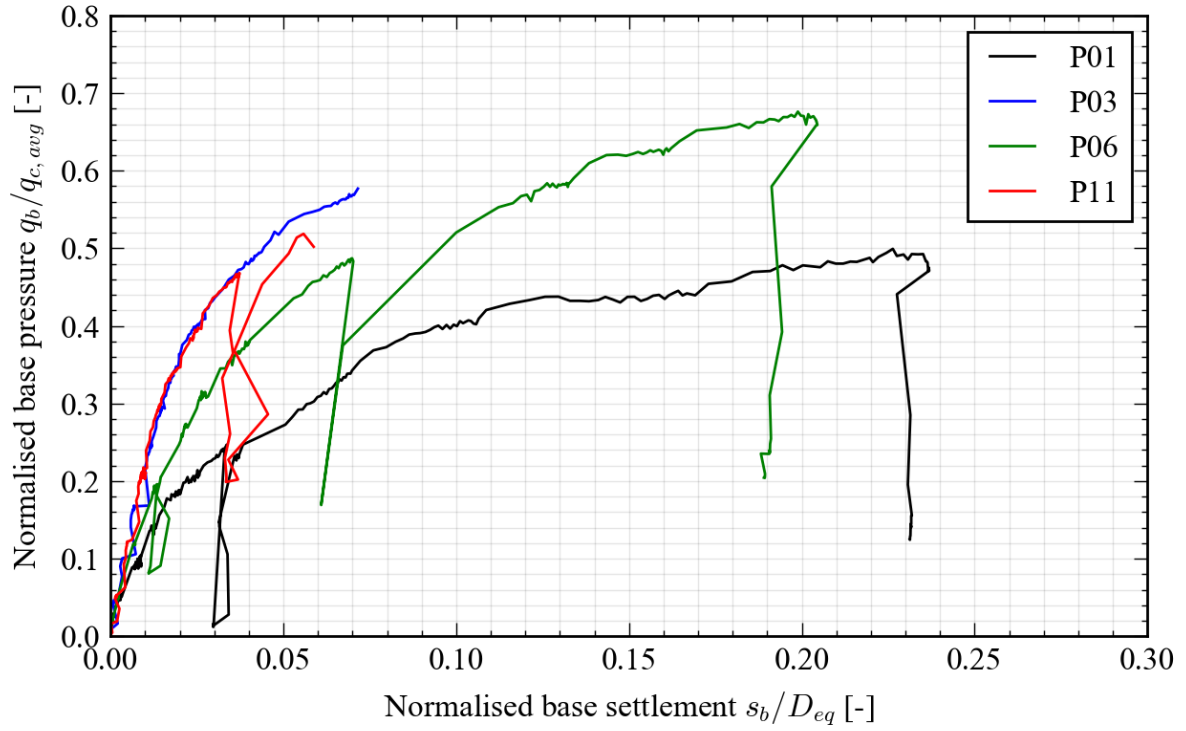


Figure 6.12: Mobilisation of the base capacity for all vibro piles (BOFDA measurements; normalised)

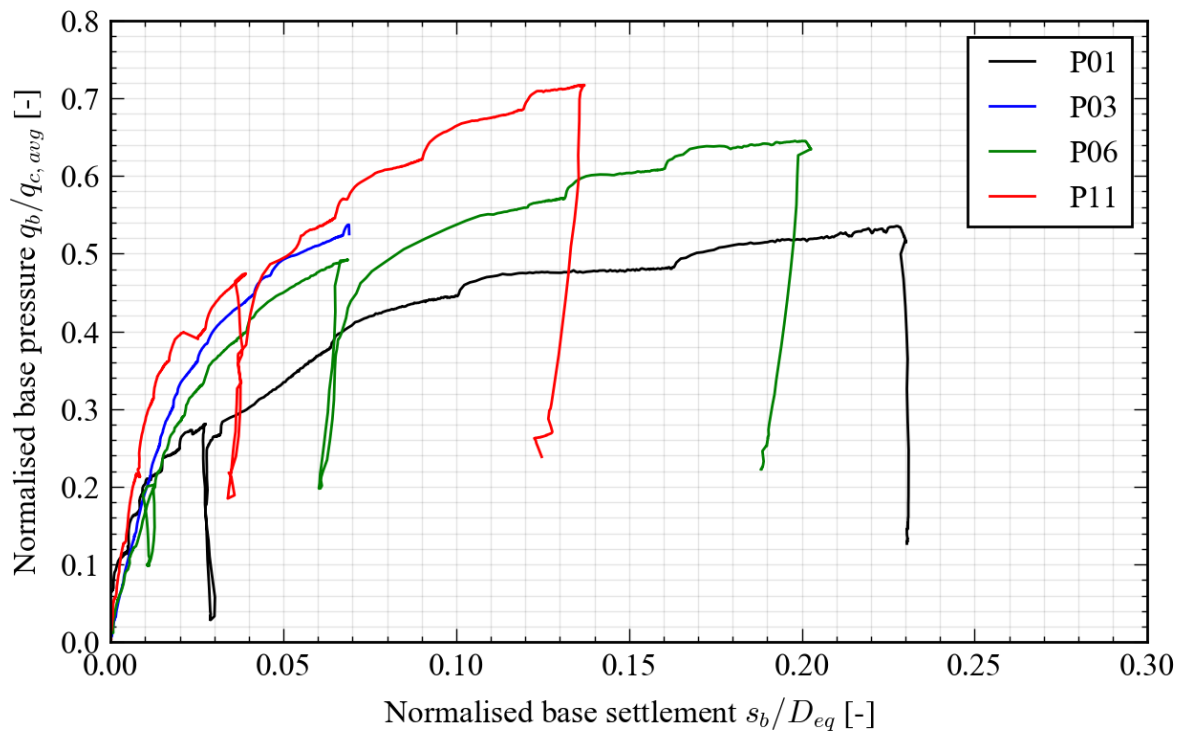


Figure 6.13: Mobilisation of the base capacity for all vibro piles (FBG measurements; normalised)

Table 6.3: Pile class factors for the base resistance of each pile retrieved directly from both measurement systems

Pile	Koppejan $q_{c,avg}$ [MPa]	$\alpha_p; 0.1D$ [-]	
		BOFDA	FBG
P01	16.68	0.40	0.44
P03*	41.09	0.58 [†]	0.54 [†]
P06	30.31	0.52	0.54
P11 [‡]	39.82	0.52 [†]	0.67

6.5. Shaft Mobilisation

Due to the lack of reliable measurements of the response of the vibro piles in the region of segregation, no assessment of the pile shaft response in the Pleistocene sand could be made. Notwithstanding an analysis of the shear stresses of the upper sand layer (from NAP +4m to NAP -14m) has been made and provides an insight into the shaft friction response of vibro piles in sand.

The mean shear stresses in Figure 6.14 to Figure 6.17 has been obtained by taking the difference in forces in the gauges at the top and the bottom of the upper sand layer and dividing by the surface area of that shaft increment. The outer diameter of the auxiliary tube (380mm) has been used, thus giving a conservative estimate of the local shear stresses. This has been plotted against the local shaft settlement which is based at the bottom of the shaft increment.

For completeness, readings from both the BOFDA and the FBG fibres have been provided in addition to the non-normalised and normalised plots. Normalisation of the shear stress has been carried out by taking the average cone resistance across the upper sand layer, as shown in Table 6.4 whereas normalisation of the settlement at the bottom of the shaft increment has been made using the diameter of the pile shaft, D_{eq} (380mm).

The figures are provided as follows:

Non-normalised

- Figure 6.14: BOFDA measurements in the upper sand layer
- Figure 6.15: FBG measurements in the upper sand layer

Normalised

- Figure 6.16: BOFDA measurements in the upper sand layer
- Figure 6.17: FBG measurements in the upper sand layer

From these figures, it is evident that a demonstrable reduction in the shaft friction has occurred in the piles which have incorporated an unload/reload cycle, resulting in a reduction of 10-20kPa across piles P01, P06 and P11. In the case of P01, the unload/reload cycle contributed to a reduction from 170-180kPa (the maximum shaft friction observed across all piles) to 150-170kPa. For pile P06 this shaft reduction reduced from a peak of 140-160kPa, to a post-peak of 120-150kPa and for pile P11, a reduction from a peak of 140-150kPa to a post-peak of

* Settlement at pile base failed to reach $0.1 \times D_{eq}$ due to structural failure of the pile

[†] Taken at peak load due to premature failure of gauge or pile

[‡] Only one FBG remained intact after step 7ii

around 115-130kPa. It should be noted that in the case of P11, this is based on the interpretation of one BOFDA line due to the breakage of the opposing cable and the FBG cables. Evidently, the incorporation of an unload/reload cycle has affected the interpretation of the appropriate α_s value in the upper layer across all three of these piles.

Pile P03, which was subjected to no unload/reload cycles and experienced sudden structural failure during the test, exhibits a gradual softening behaviour: reducing from 120-140kPa to 115kPa immediately before its failure.

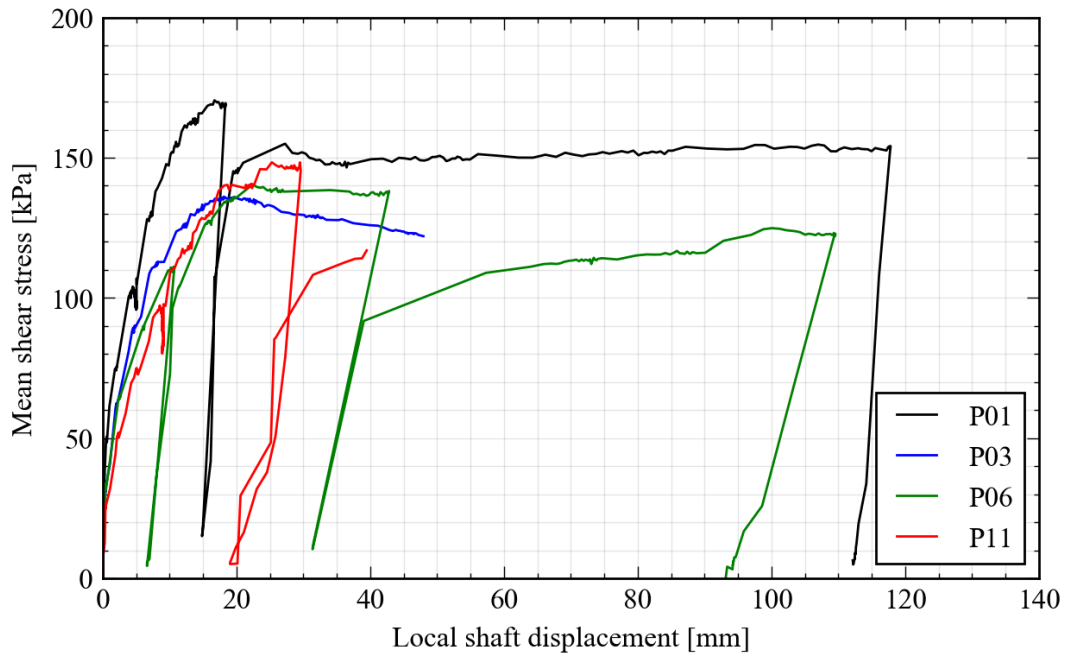


Figure 6.14: Mobilisation of the shaft capacity in the upper sand layer for all vibro piles (BOFDA measurements)

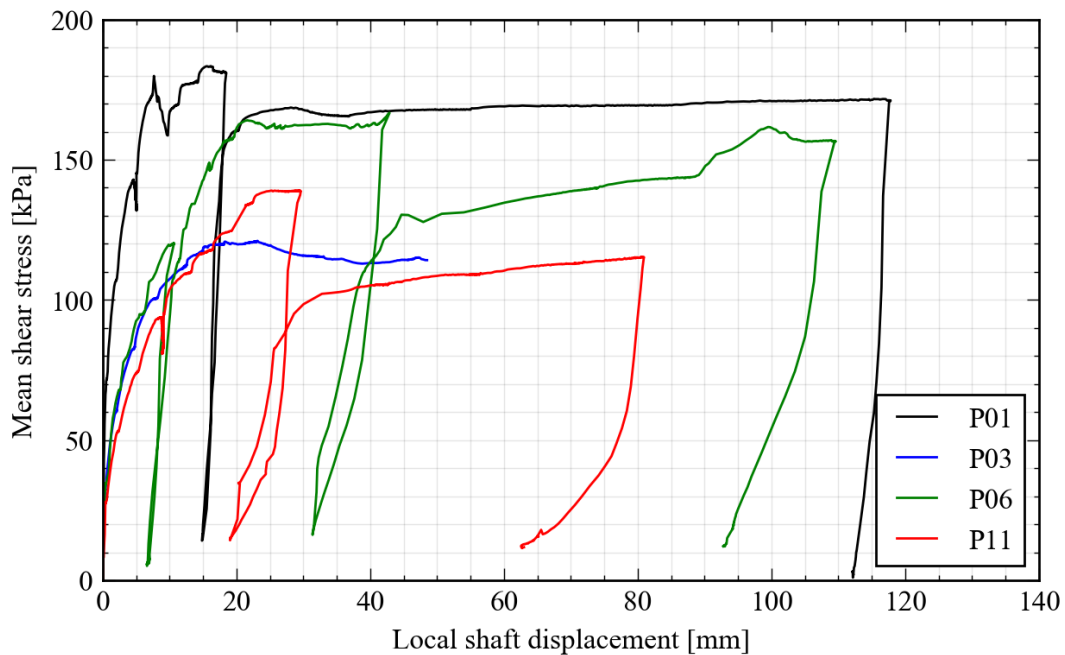


Figure 6.15: Mobilisation of the shaft capacity in the upper sand layer for all vibro piles (FBG measurements)

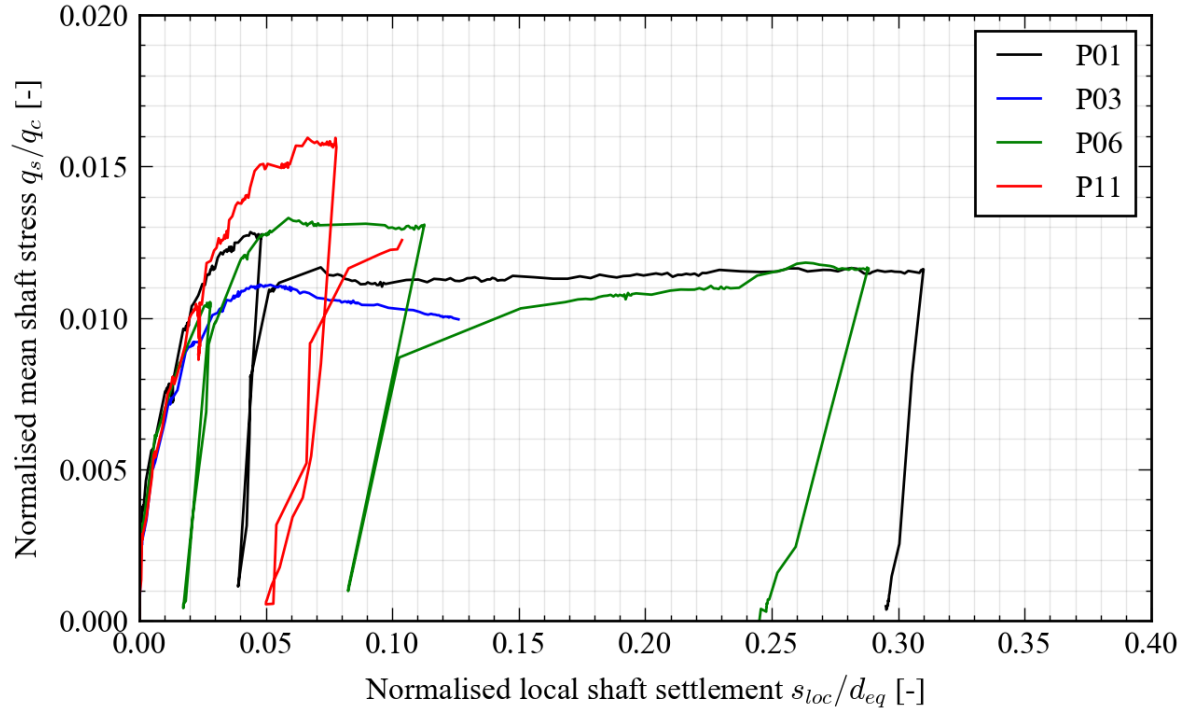


Figure 6.16: Mobilisation of the shaft capacity in the upper sand layer for all vibro piles (BOFDA measurements; normalised)

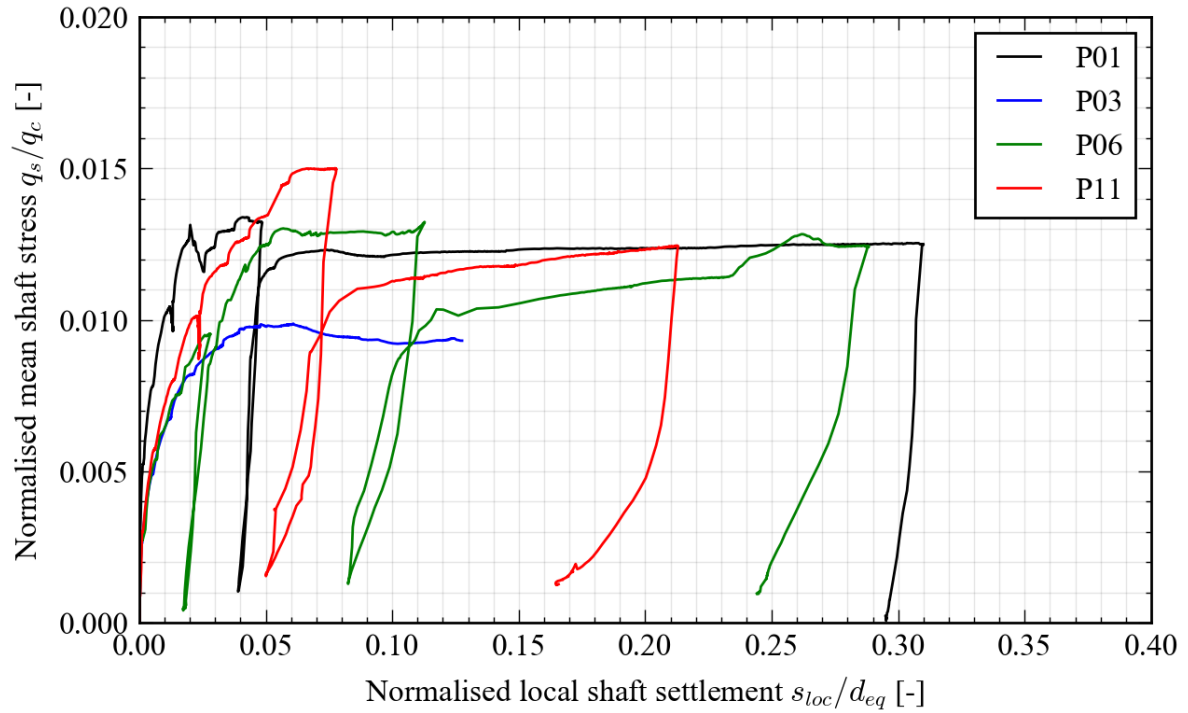


Figure 6.17: Mobilisation of the shaft capacity in the upper sand layer for all vibro piles (FBG measurements; normalised)

Table 6.4: Pile class factors for the shaft resistance in the upper sand layer of each pile retrieved directly from both measurement systems

Pile	$q_{c,avg}$ [MPa]	$\alpha_{s; 0.1D}$ [-]		$\alpha_{s; peak}$ [-]	
		BOFDA	FBG	BOFDA	FBG
P01	13.69	0.011	0.012	0.013	0.013
P03 [*]	12.26	0.010	0.009	0.011	0.010
P06	12.60	0.013	0.013	0.013	0.013
P11 [†]	9.27	0.012	0.011	0.016	0.015

* Settlement at pile base failed to reach $0.1 \cdot D_{eq}$ due to structural failure of the pile

† Only one FBG remained intact after step 7ii

7. Discussion & Recommendations

The overall load-settlement response of the four vibro piles tested is shown in Figure 7.1. The observed behaviour is consistent across all piles until a load of 6.5MN, with P01 exhibiting a slightly stiffer response compared to the three other piles before the implementation of an unload/reload cycle. P03 and P11 ended up developing slightly larger ultimate bearing capacities than P01 and P06, with P03 developing the largest capacity of 9MN before structural failure of the upper part of the pile occurred.

The presence of extremely scattered measurements in the lower part of the pile across the entirety of the Pleistocene sand layer has rendered it difficult to establish the behaviour of this sand layer under axial loading without full certainty of the cause of the scattered measurements or the shape of the pile in this region. For this report, it is postulated that the scattered measurements have occurred as a result of concrete segregation across this region (Section 6.1), however it is recommended that further investigation is carried out into this problem for future pile tests and projects, particularly with regards to the choice of concrete used and the pile installation parameters. This also comes with the recommendation of developing a more detailed and codified approach to the design and installation of vibro piles that describes the permissible range of a host of installation parameters (e.g. the hammer specifications and blow count, concrete composition, reinforcing size and/or offset between the base plate and pile shaft).

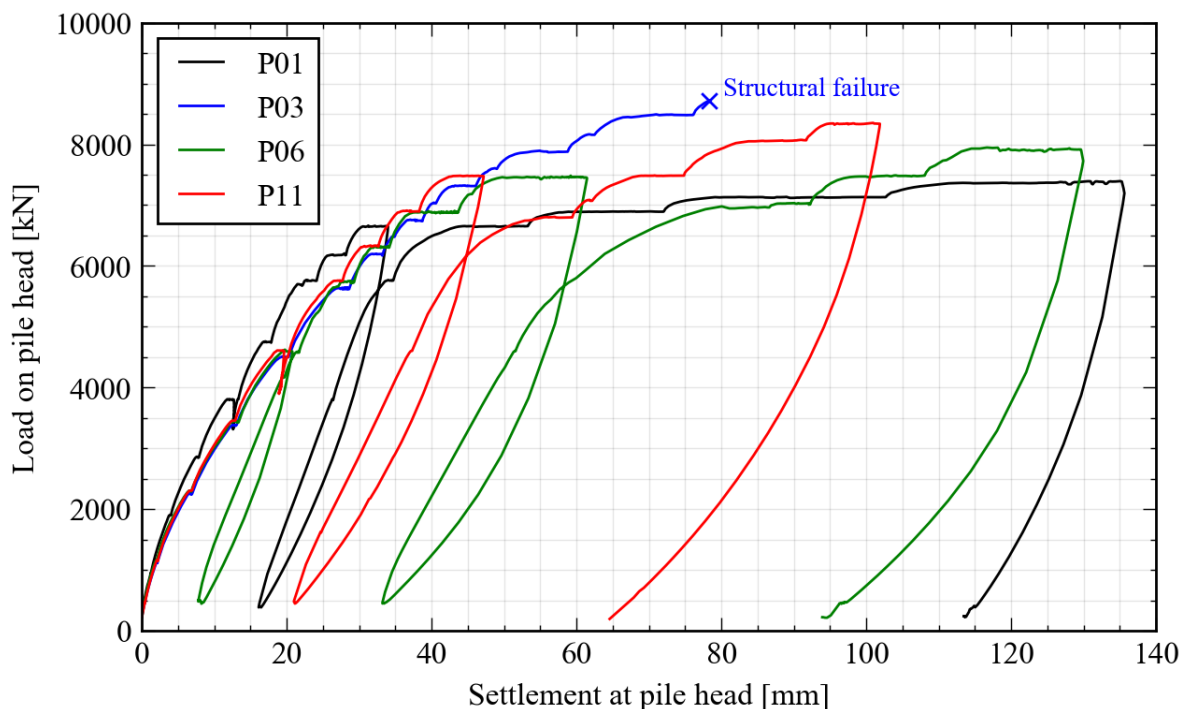


Figure 7.1: Load vs. settlement response of all vibro piles

7.1. Base Capacity

In order to make an interpretation of the base capacity from the results of the test programme, this analysis has assumed that no shaft resistance was developed across the “segregated region” due to the disintegration of the pile body across this region. As a result, it is assumed that the axial load in the pile was transferred through the reinforcement cage and directly to the pile base plate.

Notably, diverging behaviour in the base resistance of all piles (see Figure 6.10 to Figure 6.13) is exhibited in spite of their ostensible similarities. It is postulated that this behaviour is due to the differences in soil or installation conditions between the piles, illustrated by a graph of the change in cumulative hammer energy versus depth, or in other words, the amount of energy needed to achieve a certain penetration. Across most of the installation depth, P01 experiences a higher energy than the three other piles and crucially, the energy imparted on this pile is significantly lower compared to the three other piles across the final three to four metres in the Pleistocene sand layer. This imparted energy also begins to reduce with depth over the final metre.

Pile P06 has also been subjected to similar installation conditions, albeit to a slightly lesser extent. On the contrary, piles P03 and P11 were subjected to a continuously increasing amount of energy as the piles approached their respective target depths. The differences in the imparted hammer energies is reflected in the base resistance of the piles (Section 6.4), with P01 and P06 developing the least base capacity compared to P03 and P11. The latter grouping experienced very similar installation conditions and consequently exhibit very similar base stiffnesses.

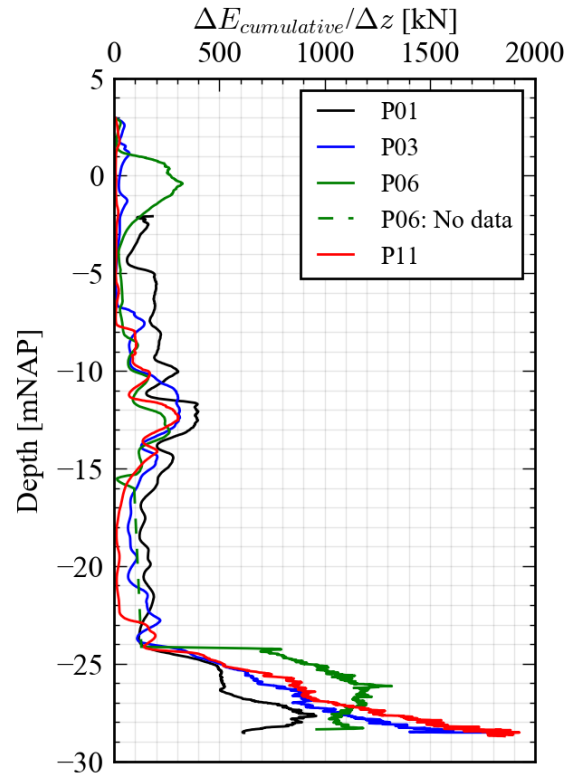


Figure 7.2: Change in imparted hammer energy with depth for the vibro piles

As a result, given that the magnitude of this base stress can be extremely sensitive to the soil or installation conditions, it is recommended for future projects that the vibro piles are driven to a minimum set as opposed to a prescribed depth to minimise the effect of the soil or installation conditions on the capacity of the piles.

These base resistances are all significantly lower than the driven precast piles tested at the pile test site. It is believed that this can be explained by the pile response immediately following installation. In the case of the driven precast piles at the test site, these piles developed large residual stresses towards the end of installation, induced by the pile driving process where the pile underwent vertical compression during a hammer blow and elastic decompression when the load is removed. As the pile rebounds, the end-bearing resistance decreases, however, the rebound of the pile is resisted by shear stresses mobilised at the pile-soil interface. As the pile is attempting to move upwards, these negative shear stresses allow some positive end bearing stress to be locked-in at the pile base as the pile reaches equilibrium after the hammer blow.

Whilst it may be anticipated that similar residual stresses might develop during the installation of the vibro piles, the subsequent removal of the auxiliary tube and replacement with wet concrete would result in the only means of equilibrium being the upward movement of the base plate until the residual base stress dissipated. Consequently, it'd be expected that the base stiffness of a vibro pile responds differently to that of a driven precast pile, with more displacement of the pile required in order to mobilise more of the base resistance. As a result an α_p below the lower-bound α_p value for a precast pile with no residual load is expected.

Based on this and the results shown in Section 6.4, it is recommended that to determine the base resistance $\alpha_p \times \beta$ is equal to 0.5, where β is a shape factor (see Figure 7i, NEN 9997-1) which accounts for differences (and consequent scale effects) between the areas of the pile shaft and the pile base. To align this with the results of the pile test, an α_p of 0.60 is thus recommended, based on a $q_{c,avg}$ obtained from the Koppejan averaging technique. This recommendation of α_p is also supported by the pile tests carried out by Flynn (2014), Ligthart & Timmer (2019) and Geerling & Janse (1993). As an additional safety factor, a limiting base resistance of 20MPa should be applied – a conservative value given that a higher maximum base capacity was measured during the field test.

7.2. Shaft Capacity

The local shaft resistance values measured across the piles' length, normalised by the local q_c value, are shown in Figure 7.3a. In addition to the NEN 9997-1 method, a comparison has also been made to the UWA-05 method which incorporates a friction fatigue term $h/D^{-0.5}$. A recent update to the UWA-05 model (Lehane *et al.*, 2021) has been utilised whereby:

$$q_s = 0.03q_c \left(\frac{h}{D_{eq}} \right)^{-0.5} \tan(\delta_f)$$

where: q_s is the shear stress at failure; h is the distance from the pile base; δ_f is the interface friction angle, taken as 35°.

Whilst significant scatter is evident in Figure 7.3a, the data does not seem to support the assumption that friction fatigue affects the shaft resistance, but rather a constant α_s value seems to fit better than the variable approach suggested by UWA-05. These measurements have also

been compared to those reported by Flynn and McCabe (2015) who carried out a series of tests on driven cast-in-situ piles in medium-dense to dense sand deposits the United Kingdom (Figure 7.3b) and proposed the inclusion of a friction fatigue term into the axial capacity prediction of driven cast-in-situ piles. If the datasets were combined, it would suggest that a constant α_s is appropriate and the data-point at $h/D_{eq} = 13$ in Figure 7.3b is in fact as a result of the scatter evident in Figure 9a, rather than friction fatigue. Figure 7.4, based on a fitted line through both the BOFDA and FBG data also corroborates the use of a constant α_s of 0.012, showing a direct linear relationship between shear stress and average cone resistance across the range of shear stresses experienced.

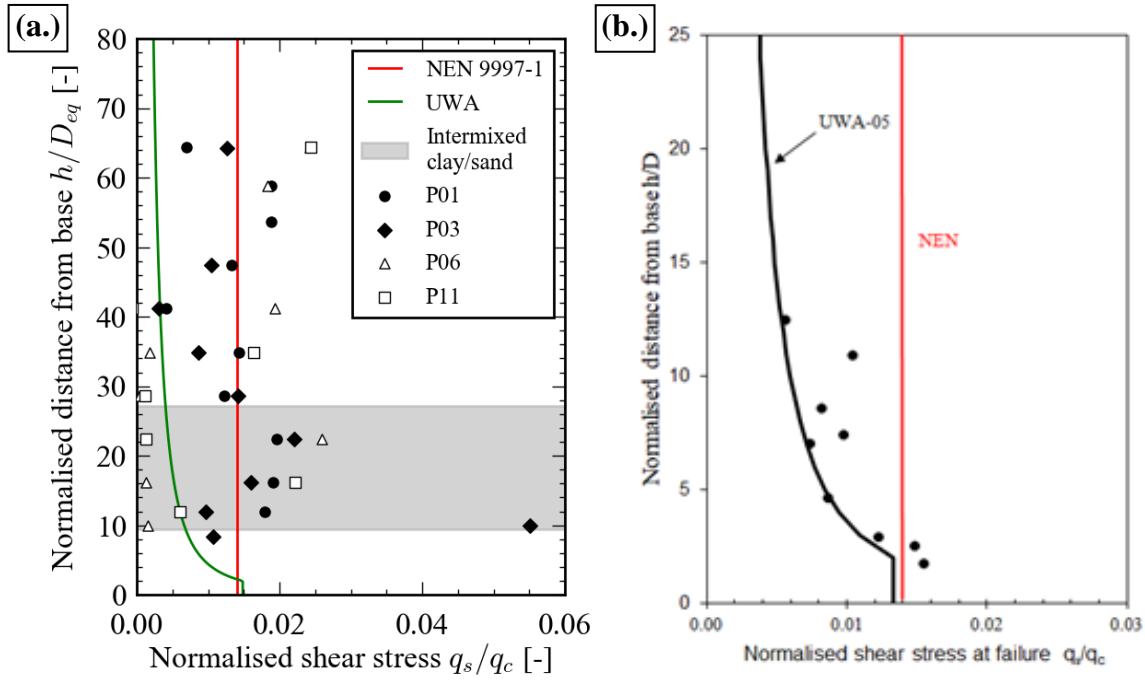


Figure 7.3: (a.) Comparison of the measured (FBG gauges) and the predicted q_s/q_c at a pile base settlement of $0.1D_{eq}$. The layer of intermixed clay/sand has been plotted relative to CPT P01 and the base depth of pile P01 (b.) Comparison of measured and predicted q_s/q_c at peak load from Flynn and McCabe (2015) with the UWA-05 and NEN predictions (where $\delta_f = 33^\circ$ as opposed to 35°)

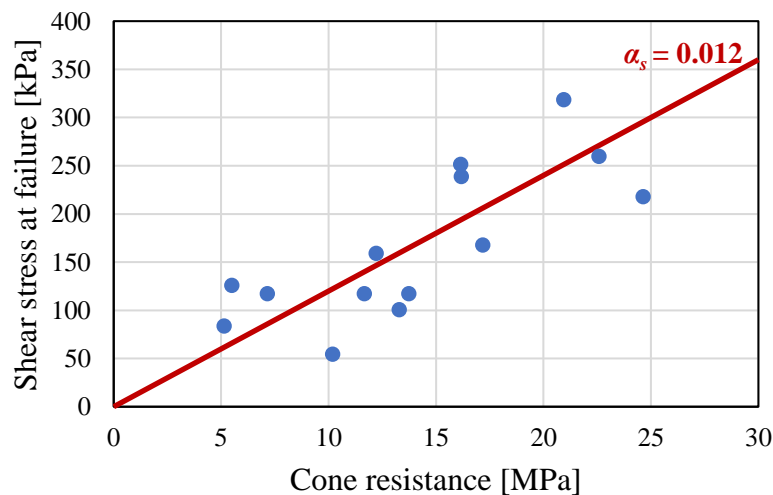


Figure 7.4: Range of shaft resistances along the pile shaft at pile failure ($s_b = 0.1D_{eq}$) plotted against the corresponding average cone resistance of that shaft increment

Furthermore, if the load-depth profiles across all vibro piles is considered (Figure 7.5), it is clear that a prediction model with a friction fatigue term (UWA-05; shown as the green line) would significantly underestimate the shaft resistance developed and provide a misleading load distribution in each pile (i.e. an overestimation of the base resistance). The adoption of a constant α_s as used in the NEN 9997-1 approach is more consistent with the measurements, however, the best-fit of the data (consistently across the range of q_c values encountered) is achieved with $\alpha_s = 0.012$. This is slightly lower than the current NEN value of 0.014, however both predict similar force profiles as the NEN approach also includes a limiting upper-bound q_c .

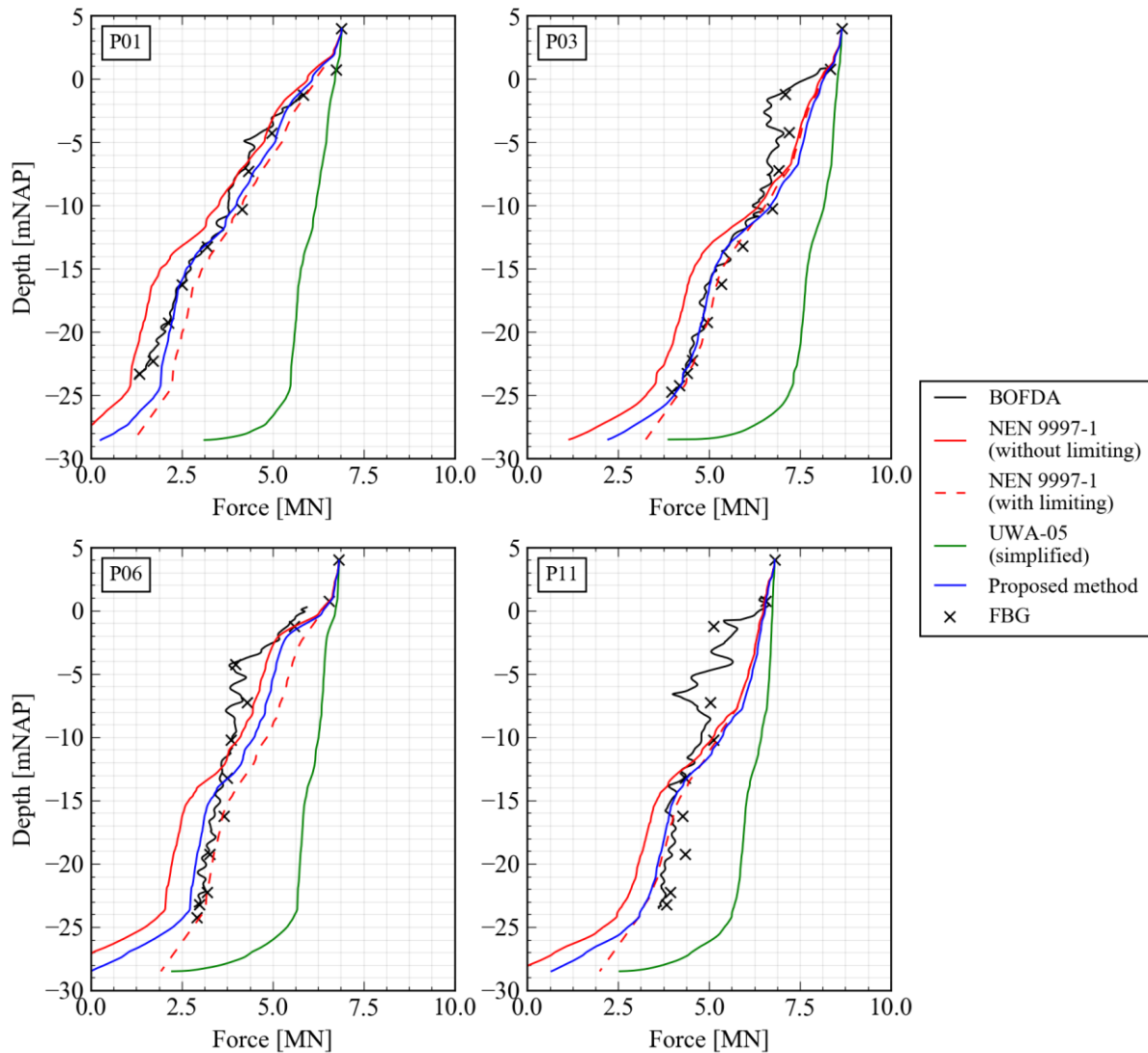
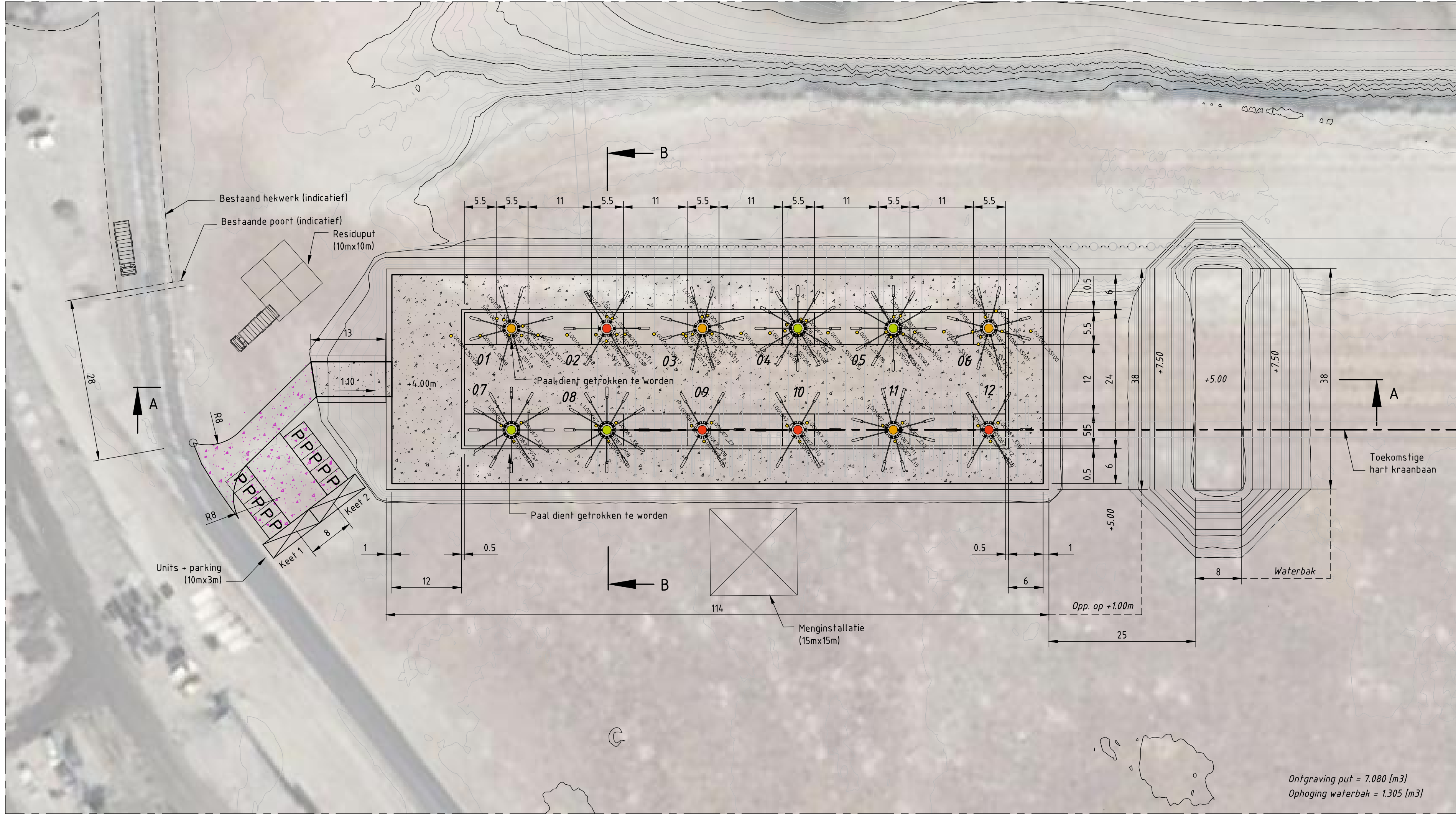


Figure 7.5: Predictions for the pile capacity at peak load compared to the true measurements. The CPT on the piles' central axes was used, with the simplified UWA-05 method and the current NEN 9997-1 with and without limiting resistances included for comparison. A constant α_s was used for the entire profile

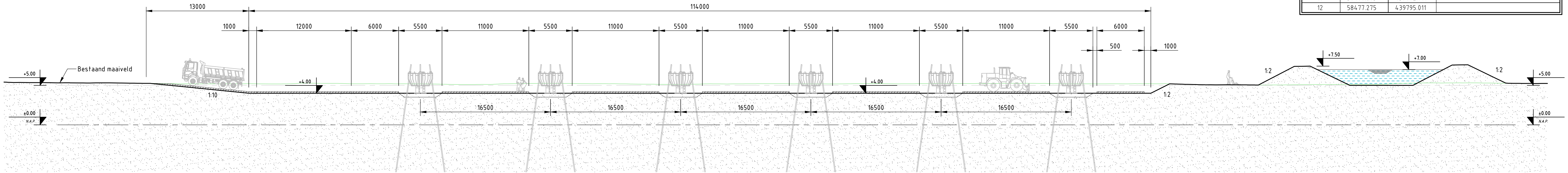
References

- BieTec B.V. Consultancy (2015) *Elke Paal een Heipaal?*, Archidat BouwKosten. Available at: <https://bouwkosten.bouwformatie.nl/nieuws/elke-paal-een-heipaal> (Accessed: 5 October 2020).
- de Boorder, M. (2019) *Development of a new CPT averaging technique and review of existing CPT based methods for the calculation of total pile capacity*. M.Sc. Thesis. TU Delft.
- CUR (2008) *CUR Rapport 166:2008 Damwandconstructies (deel 1)*.
- Fellenius, B. (2001) 'From strain measurements to load in an instrumented pile', *Geotechnical News Magazine*, pp. 35–38.
- Flynn, K. (2014) *Experimental investigations of driven cast-in-situ piles*. PhD Thesis. NUI Galway.
- Flynn, K. N. and McCabe, B. A. (2015) 'Shaft resistance of driven cast-in-situ piles in sand', *Canadian Geotechnical Journal*. doi: 10.1139/cgj-2015-0032.
- Geerling, J. and Janse, E. (1993) *Proefbelastingen op twee typen grondverdringende funderingspalen*. CO-330890/56. Delft, The Netherlands: Grondmechanica Delft.
- Geerling, J. and Janse, E. (1997) *Tekpalenonderzoek locatie de Gaag proefbelastingen op 9 palen*. CO-351310/195. Delft, The Netherlands: Grondmechanica Delft.
- Lehane, B. *et al.* (2021) 'A New "Unified" CPT-Based Axial Pile Capacity Design Method for Driven Piles in Sand', in: *International Symposium on Frontiers in Offshore Geotechnics (ISFOG)*, Austin, Texas: Deep Foundations Institute.
- Ligthart, S. and Timmer, P. (2019) *Proefbelasting Alblasserdam*. 23738. Oosthuizen, The Netherlands: Vroom Funderingstechnieken.
- Netherlands Standardisation Institute (2017a) *NEN 9997-1+C2:2017*. Delft, The Netherlands.
- Netherlands Standardisation Institute (2017b) *NPR 7201:2017 - Geotechniek - Bepaling van het axiaal draagvermogen van funderingspalen door middel van proefbelastingen*. Delft, The Netherlands.
- Piccolo, A. *et al.* (2020) 'Mechanical Properties of Optical Fiber Strain Sensing Cables under γ -Ray Irradiation and Large Strain Influence', *Sensors*, 20(3), pp. 696–709. doi: 10.3390/s20030696.
- Timmermans, A. (2020) *Vibropalen en maatregelen om segregatie te voorkomen*. i. 001347-MAR-FO-DPP-MEM-001. MariTeam.
- van Weele, A. F. and Lencioni, B. M. L. G. (1999) 'Het mislukken van een paalfundering is duur, maar leerzaam (SPECIAL)', *Geotechniek*.



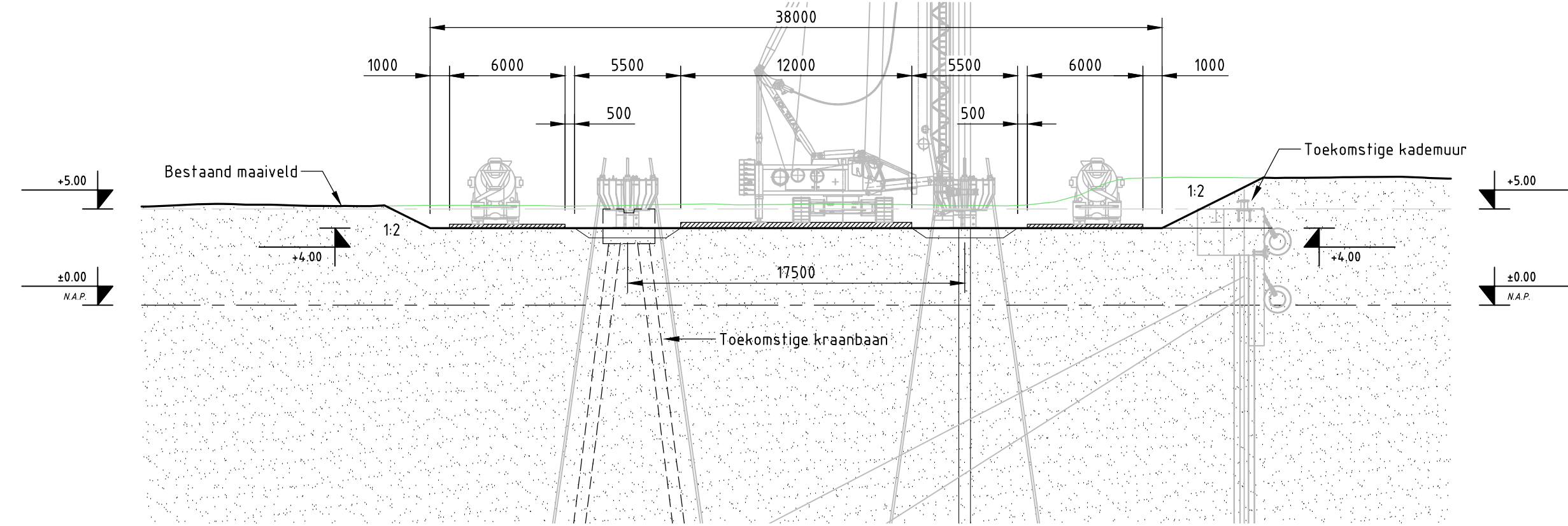
LOCATIE & OVERZICHT: DRUKPALENPROEF

(schaal 1:500)
- Maatvoering in m weergegeven



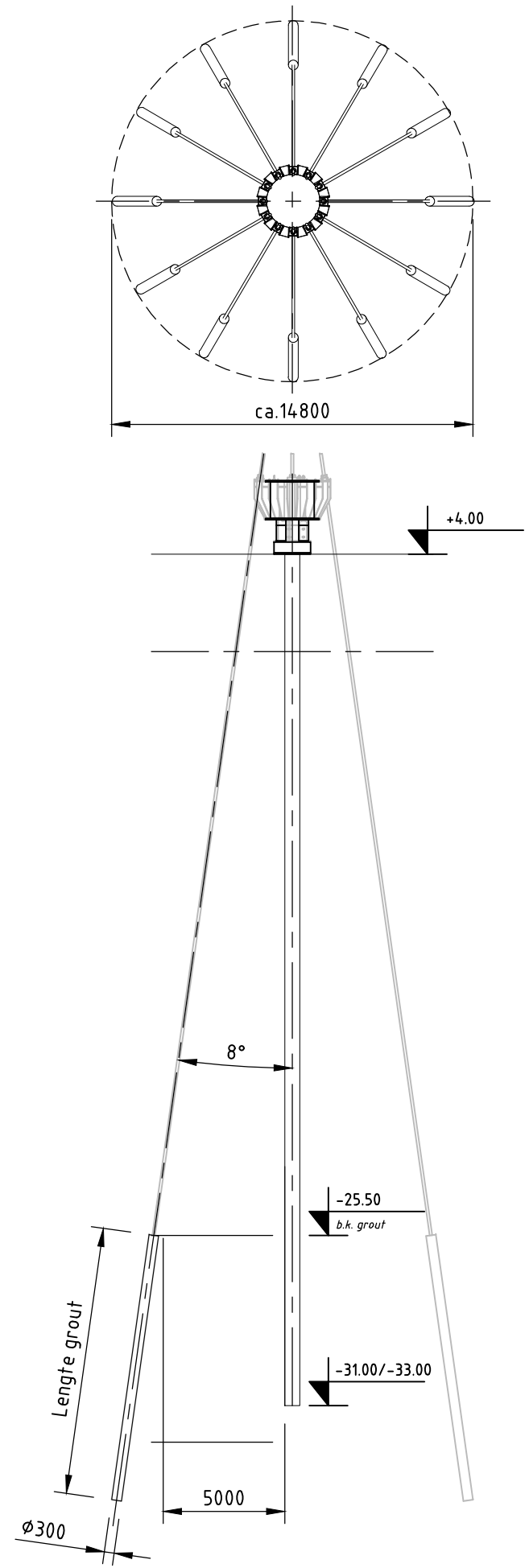
DOORSNEDE A-A

(schaal 1:250)



DOORSNEDE B-B

(schaal 1:250)



PRINCIPE DOORSNEDE TESTOPSTELLING

(schaal 1:250)
- SI-Paal weergegeven

Repac (keet 1 = uitvoeringskeet // keet2 = schaffkeet)
= Ruimte voor transport en/of heistelling (verharding n.t.b.)

Snede	Ankertype	Anker-hoek	Insteekn. [mm]	Testbelast. [kN]	Lanker [m]	Lgrout [m]	Boorkop [m]	Aantal totaal
Betonpaal	H 2800-108	8°	+4.00	1658	38.0	8.0	310	24
Vibropaal	H 2800-108	8°	+4.00	1547	38.0	7.5	310	32
SI-paal	H 3200-108	8°	+4.00	1875	40.0	9.5	310	48

Type testpaal	B [mm]	H [mm]	Paalkop [mm]	P.P.N. [mm]	Beton kwal.	Testbel. [kN]	Aantal ankers per kop
Betonpaal (02)	400	400	+4.00	-28.00	C90/105	9950	6
Betonpaal (09)	400	400	+4.00	-27.50	C90/105	9950	6
Betonpaal (10)	400	400	+4.00	-28.00	C90/105	9950	6
Betonpaal (12)	400	400	+4.00	-28.00	C90/105	9950	6
SI-paal (04)	D [mm]	Schacht [mm]	Punt [mm]				
SI-paal (05)	609	850	+4.00	-33.00	C35/45	22500	12
SI-paal (07)	609	850	+4.00	-31.00	C35/45	22500	12
SI-paal (08)	609	850	+4.00	-30.00	C35/45	22500	12
Vibropaal (01)	356	480	+4.00	-28.50	C35/45	12375	8
Vibropaal (03)	356	480	+4.00	-28.50	C35/45	12375	8
Vibropaal (06)	356	480	+4.00	-28.50	C35/45	12375	8
Vibropaal (11)	356	480	+4.00	-28.50	C35/45	12375	8

Additionalen inbreng voorwaarden bovenop de standaard voorwaarden van het moederbestek Port of Rotterdam:

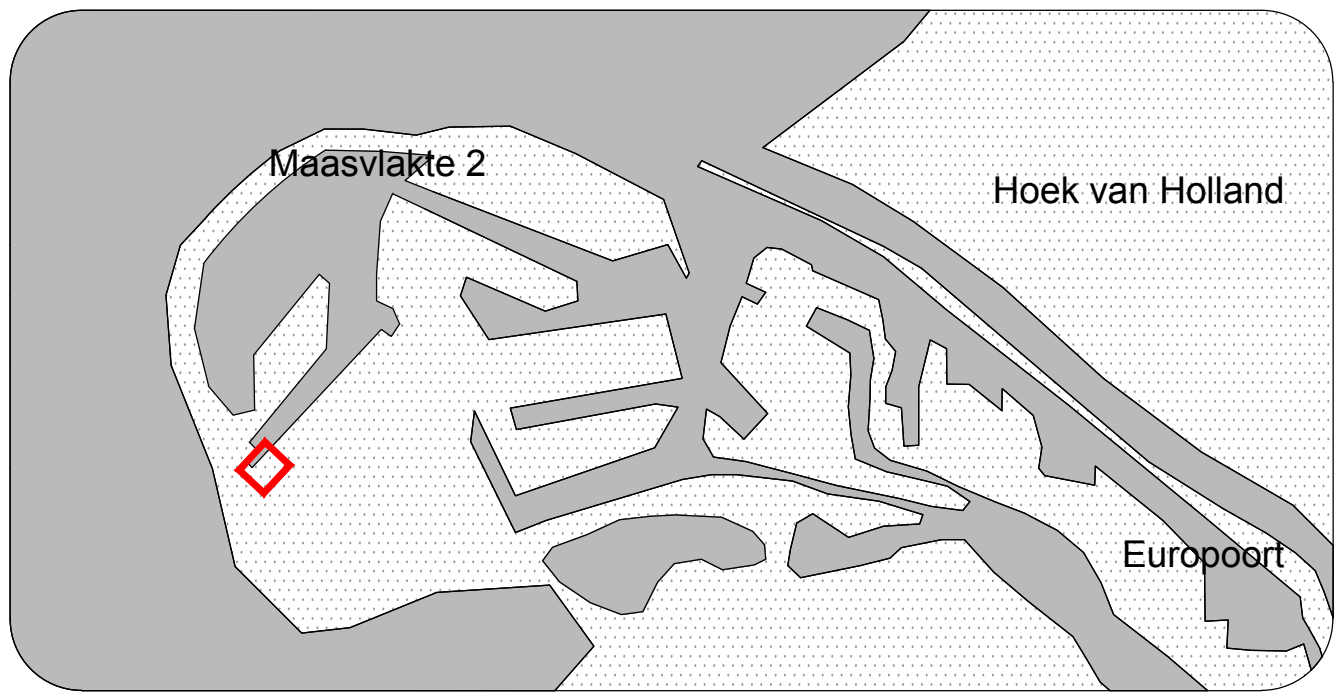
- × Prefab betonpaal
 - Spuitend op diepte brengen tot bovenzijde kleilaag ca. N.A.P. -23.0m
 - Mutsvullingen Wisselen na 500 klappen
 - Start heien: Palen minimaal 4 weken oud
- × Vibropaal
 - Trekken heibuis: Heibuis heidend trekken (vanwege beschikbaarheid materieel op de markt) Mogelijkheid onderzoeken om ring vibrator op het werk standby te hebben
 - Heibuis: Minimaal 2 heibuisen op het werk. Wanddikte heibuis ter goedkeuring aan directie voorleggen
 - Leffer: Leffer gereed staan om de paal om bij refusal trekken heibuis direct te kunnen bijspringen
- × SI-Paal
 - Schroefpunt: Gegoten schroefpunt
 - Gegevens zoals WBF, druksterkte en debiet ter goedkeuring aan directie voorleggen
 - Wijze inbrengen: Tijdens het inbrengen is het niet toegestaan om de boorbuis omhoog te trekken. Links- of rechtsomdraaien is wel toegestaan



Proefpaal	X-Coordinaat	Y-Coordinaat	Opmerking:
01	58412.536	439741.190	Dient getrokken te worden
02	58422.736	439754.121	
03	58432.935	439767.053	
04	58443.135	439779.985	
05	58453.335	439792.916	
06	58463.534	439805.848	
07	58473.734	439818.780	
08	58483.934	439831.712	
09	58494.134	439844.644	
10	58504.334	439857.576	
11	58514.534	439870.508	
12	58524.734	439883.440	

RENVOL:

ALGEMEEN:

-Alle maten in mm en 360° cirkel, tenzij anders vermeld
-Alle niveau's in m t.o.v. N.A.P., tenzij anders vermeld
-Alle coördinaten in m en in RD-stelsel, tenzij anders vermeld



A	10-10-2019	Eerste uitgifte - definitief	B.T.	A.T.	L.T.	ST
REV.	DATUM	OMSCHRIJVING REVISIE	GETEKEND	GECONTR.	GEZIEN	
OPDR. GEVER			Port of Rotterdam			
PROJECT			<div> Port of Rotterdam</div> <div>Havenbedrijf Rotterdam N.V. Postbus 6622 3062 AP Rotterdam 010 - 252 10 10 www.portofrotterdam.com</div>			
ONDERDEEL			<div> MariTeam</div> <div>Noordhoek 37 3351 LD Papendrecht Postbus 1155 3350 CD Papendrecht Nederland Telefoon +31(0)78 644 81 11 Fax +31(0)78 644 81 12</div>			
OMSCHRIJ. / VERSIE			Eerste uitgifte			
DATUM	10-10-2019	GECONTROLEERD:		A. Timmermans		
GETEKEND	B. Theunis	GEZIEN:		L. Tuurter		
STATUS:	DEFINITIEF		SCHAAL:		Zie tek.	
DEZE TEKENING IS EIGENDOM VAN MariTeam			FORMAAT: A1 (841x594)			
ZONDER SCHRIFTELIJKE TOESTEMMING VAN DE EIGENAAR MAG DEZE OP GEENREKELIJK WIJZE WORDEN GECOPYEERD OF OVERNOMMEN (GEMAKT)						
PROJECTNR.			I.001347-MAR-FO-DPP-TEK-001			
TEKENINGNR.						

Appendix B Site Investigation Data

B.1 CPTs

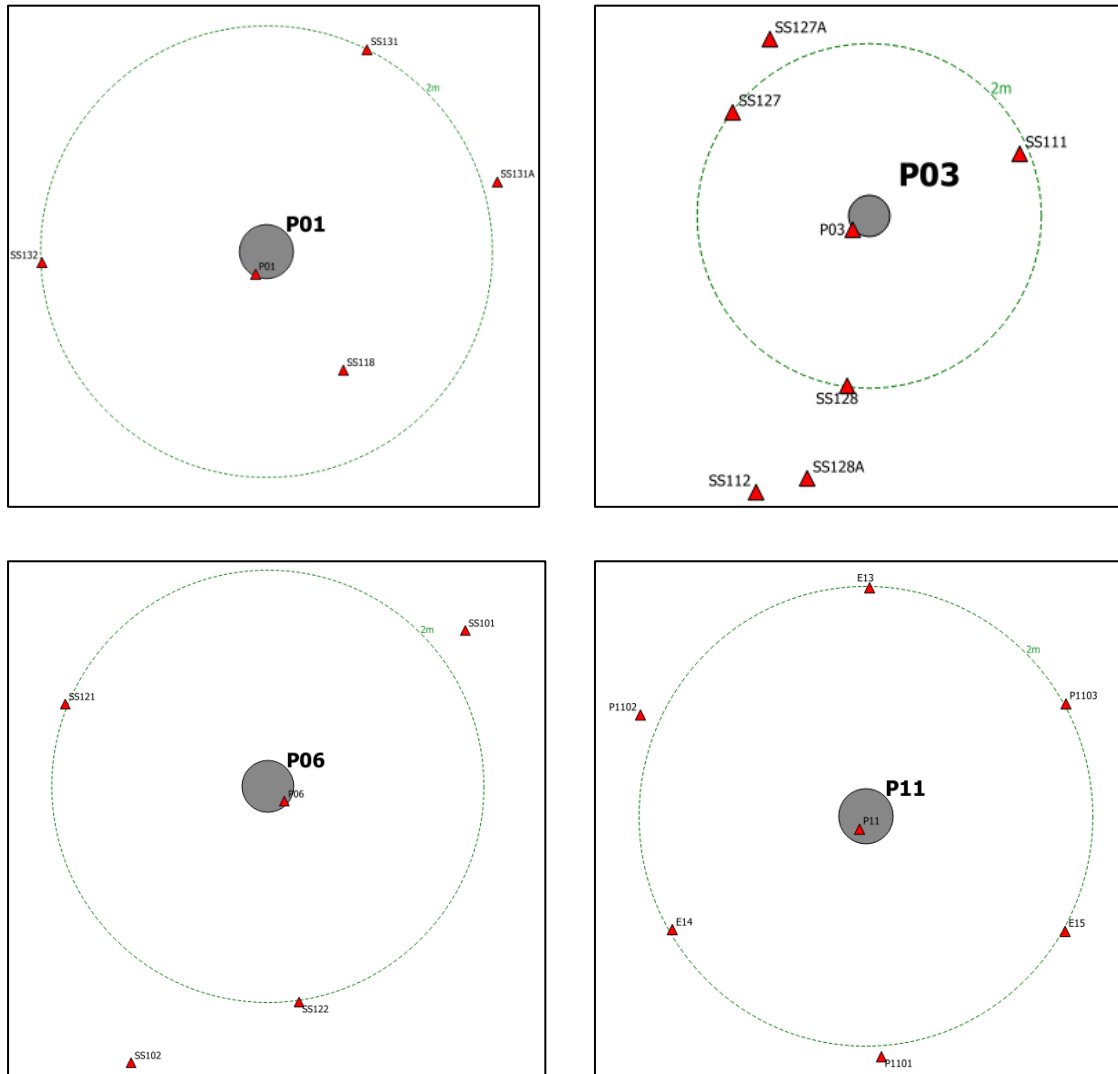


Figure B.1: Relative positions of the CPTs around each pile

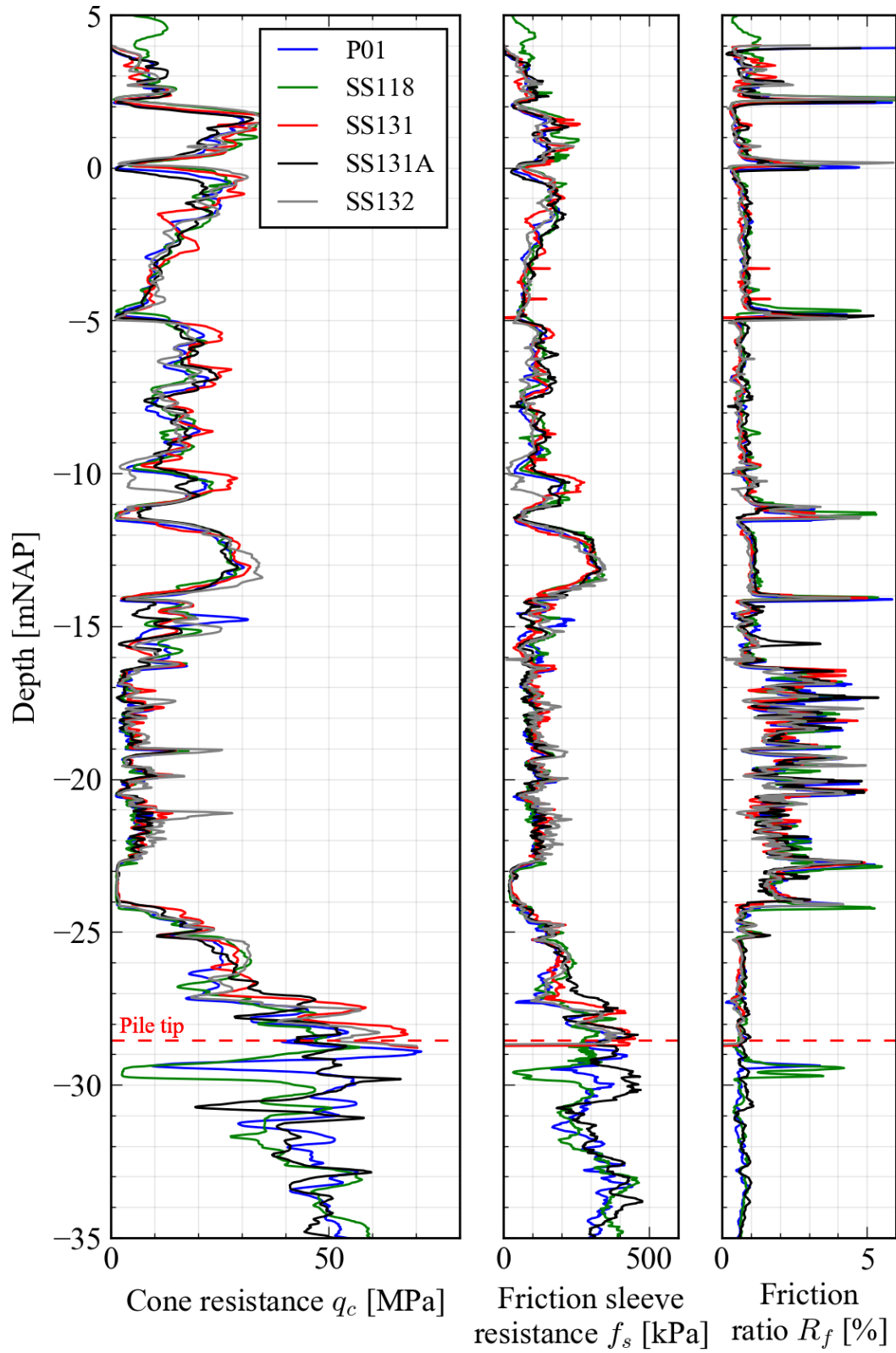


Figure B.2: CPTs executed around pile P01

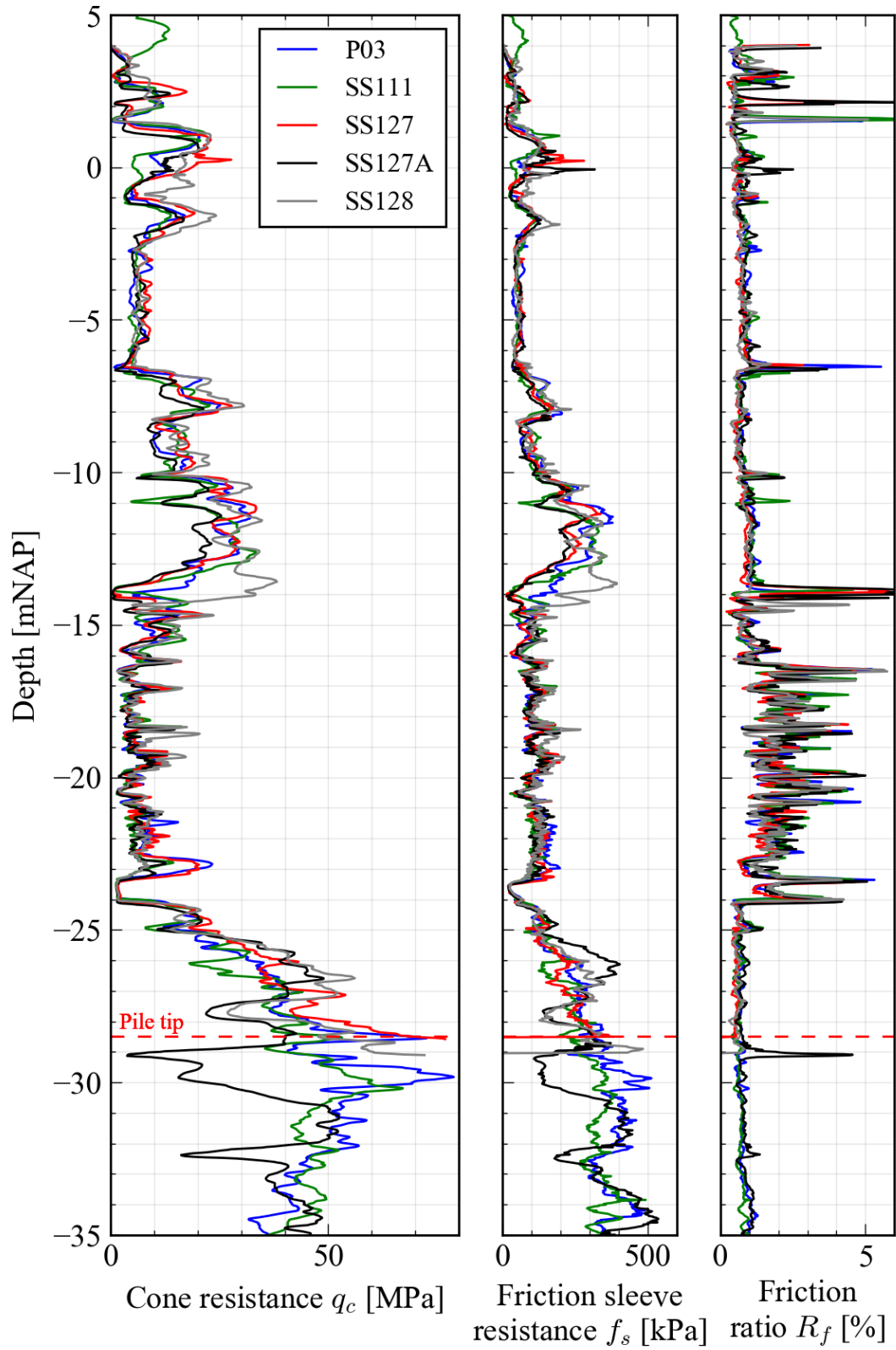


Figure B.3: CPTs executed around pile P03

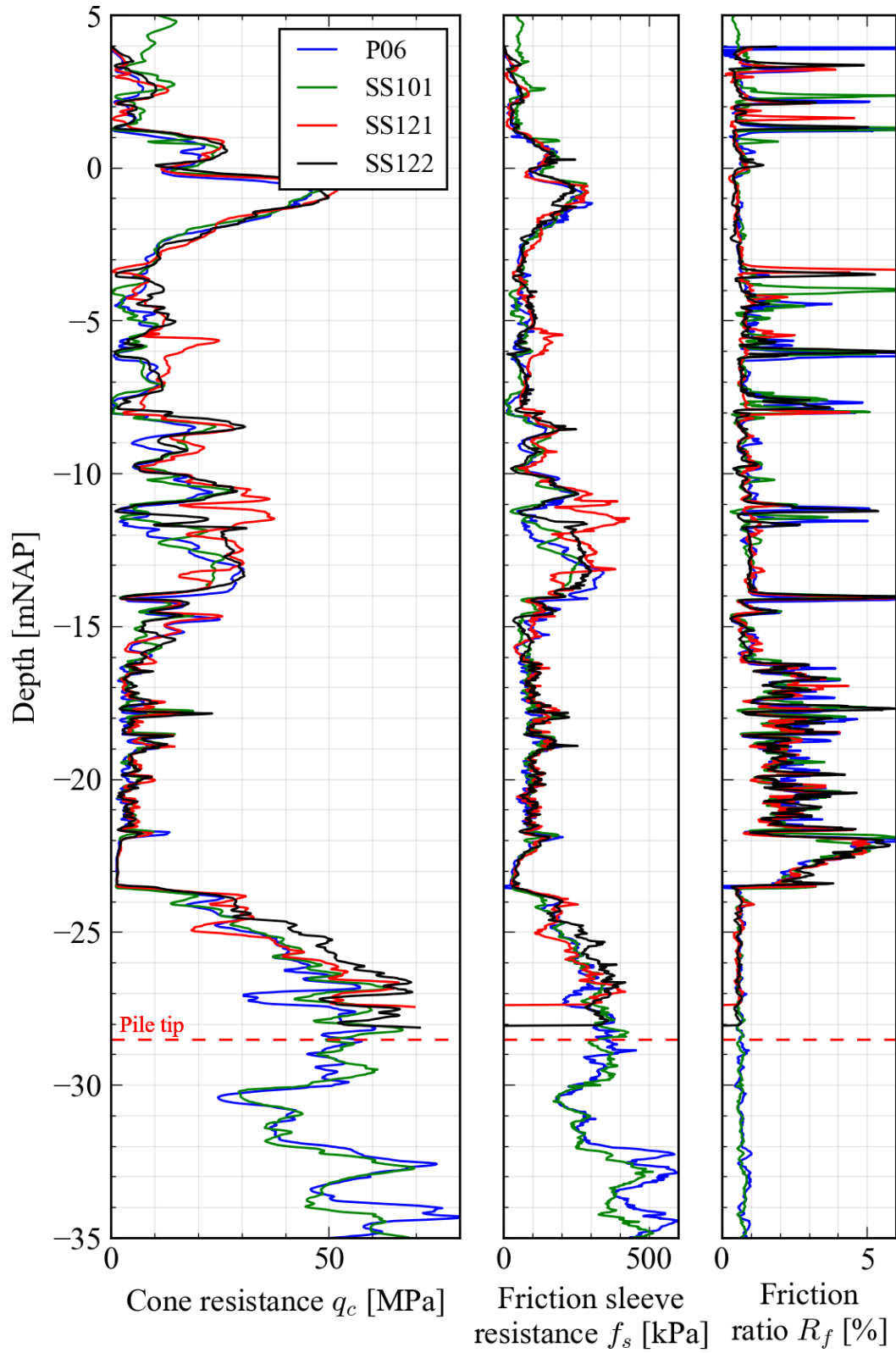


Figure B.4: CPTs executed around pile P06

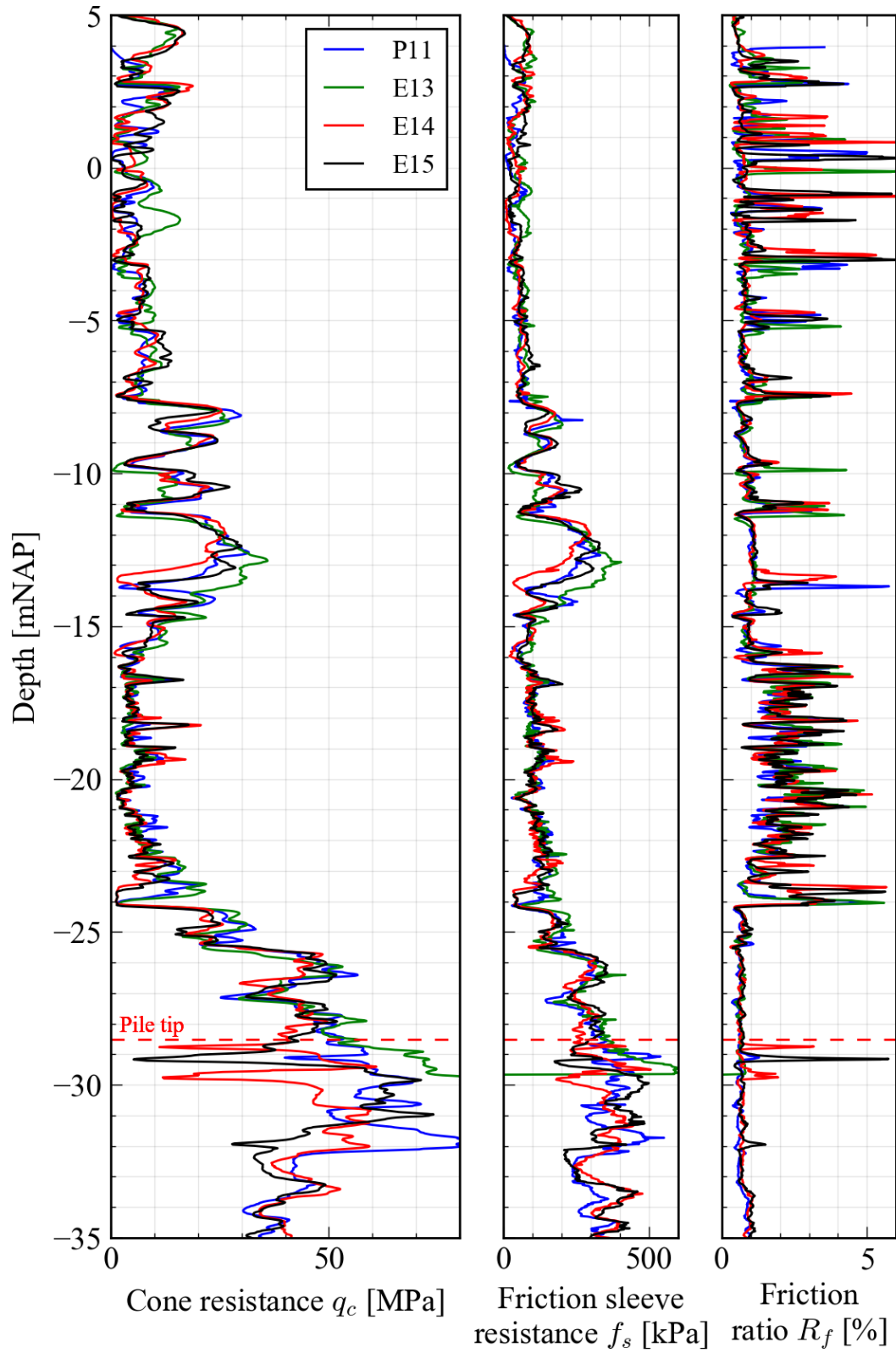


Figure B.5: CPTs executed around pile P11, excluding post-installation CPTs

B.2 Boreholes

BORING : BB20

Datum : 27-05-2019 X : 58454.410 Boormethode : Puls/Ack
GWS : NAP +0.68 m Y : 439757.910 Boormeester : CH
Maaiveld : NAP +5.13 m Beschrijver : CH
Opmerking : Definitieve boorstaat.

Boorprofiel	Laag nr.	Diepte [m t.o.v. NAP] van tot	Omschrijving grondlaag	Kleur
	1	1 +5.13 +4.13	Zand (matig fijn), zwak siltig	bruin
	2	2 +4.13 +3.13	Zand (matig grof), zwak siltig	bruin
	3	3 +3.13 +2.33	Zand (matig fijn), sterk siltig	grijs
	4	4 +2.33 +2.03	Zand (matig fijn), sterk siltig	grijs
	5	5 +2.03 +1.64	Monster nr. 5406k	grijs
	6	6 +1.64 +1.63	Zand (matig fijn), sterk siltig	grijs
	7	7 +1.63 +1.25	Monster nr. 5407k	grijs
	8	8 +1.25 +1.23	Zand (matig fijn), sterk kleilig	grijs
	9	9 +1.23 +0.85	Monster nr. 5408k	grijs
	10	10 +0.85 +0.83	Zand (matig fijn), sterk kleilig	grijs
	11	11 +0.83 +0.45	Monster nr. 5409k	grijs
	12	12 +0.45 -0.37	Zand (matig grof), zwak siltig	grijs
	13	13 -0.37 -0.87	Zand (matig grof), zwak siltig, zwak puinhoudend	grijs
	14	14 -0.87 -1.87	Zand (matig grof), zwak siltig, zwak grindig (matig grof)	grijs
	15	15 -1.87 -2.77	Zand (matig grof), zwak siltig, zwak grindig (matig grof)	grijs
	16	16 -2.77 -3.04	Monster nr. 5410k	grijs
	17	17 -3.04 -3.17	Zand (matig fijn), matig siltig	grijs
	18	18 -3.17 -3.44	Monster nr. 5411k	grijs
	19	19 -3.44 -3.57	Zand (matig fijn), matig siltig	grijs
	20	20 -3.57 -3.82	Monster nr. 5412k	grijs
	21	21 -3.82 -3.87	Zand (matig fijn), matig siltig	grijs
	22	22 -3.87 -4.87	Zand (matig fijn), matig siltig	grijs
	23	23 -4.87 -5.87	Zand (matig fijn), matig siltig	grijs
	24	24 -5.87 -6.87	Zand (matig fijn), matig siltig, bevat resten van klei	grijs
	25	25 -6.87 -7.87	Zand (matig fijn), matig siltig	grijs
	26	26 -7.87 -8.87	Zand (matig fijn), matig siltig	grijs
	27	27 -8.87 -9.21	Monster nr. 5413k	grijs
	28	28 -9.21 -9.27	Zand (matig fijn), sterk siltig, bevat resten van klei	grijs
	29	29 -9.27 -9.54	Monster nr. 5414k	grijs
	30	30 -9.54 -9.67	Zand (matig fijn), sterk siltig, bevat resten van klei	grijs
	31	31 -9.67 -10.01	Monster nr. 5415k	grijs
	32	32 -10.01 -10.87	Zand (matig fijn), sterk siltig, zwak schelpengruishoudend	grijs
	33	33 -10.87 -11.87	Zand (matig fijn), sterk siltig	grijs
	34	34 -11.87 -12.87	Zand (matig fijn), sterk siltig	grijs
	35	35 -12.87 -13.87	Zand (matig fijn), sterk siltig, zwak schelpengruishoudend	grijs
	36	36 -13.87 -14.87	Zand (matig fijn), sterk siltig, bevat resten van klei, zwak schelpengruishoudend	grijs
	37	37 -14.87 -15.87	Zand (matig fijn), sterk siltig, bevat resten van klei, zwak schelpengruishoudend	grijs
	38	38 -15.87 -15.97	Zand (matig fijn), matig kleilig, zwak schelpengruishoudend	grijs
	39	39 -15.97 -16.32	Monster nr. 5416k	grijs
	40	40 -16.32 -16.37	Zand (matig fijn), matig kleilig, zwak schelpengruishoudend	grijs
	41	41 -16.37 -16.76	Monster nr. 5417k	grijs
	42	42 -16.76 -16.77	Zand (matig fijn), matig kleilig, zwak schelpengruishoudend	grijs
	43	43 -16.77 -17.12	Monster nr. 5418k	grijs
	44	44 -17.12 -17.87	Zand (zeer fijn), matig kleilig	grijs

BORING : BB20 - vervolg -

Datum : 27-05-2019 X : 58454.410 Boormethode : Puls/Ack
 GWS : NAP +0.68 m Y : 439757.910 Boormeester : CH
 Maaiveld : NAP +5.13 m Beschrijver : CH
 Opmerking : Definitieve boorstaat.

Boorprofiel	Laag nr.	Diepte [m t.o.v. NAP] van tot	Omschrijving grondlaag	Kleur
	45	45 -17.87 -18.87	Zand (zeer fijn), matig kleilig	grijs
	46	46 -18.87 -19.77	Zand (zeer fijn), zwak kleilig	grijs
	47	47 -19.77 -20.17	Monster nr. 5419k	grijs
	48	48 -20.17 -20.50	Monster nr. 5420k	grijs
	49	49 -20.50 -20.57	Zand (zeer fijn), matig kleilig	grijs
	50	50 -20.57 -20.96	Monster nr. 5421k	grijs
	51	51 -20.96 -21.87	Zand (zeer fijn), matig kleilig	grijs
	52	52 -21.87 -22.77	Zand (zeer fijn), zwak kleilig	grijs
	53	53 -22.77 -23.17	Monster nr. 5422k	grijs
	54	54 -23.17 -23.54	Monster nr. 5423k	grijs
	55	55 -23.54 -23.57	Klei, matig siltig	grijs
	56	56 -23.57 -23.89	Monster nr. 5424k	grijs
	57	57 -23.89 -23.97	Klei, matig siltig	grijs
	58	58 -23.97 -24.27	Monster nr. 5425k	grijs
	59	59 -24.27 -24.37	Klei, matig siltig	grijs
	60	60 -24.37 -24.61	Monster nr. 5426k	grijs
	61	61 -24.61 -25.57	Zand (matig grof), zwak siltig	grijs

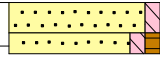
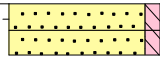
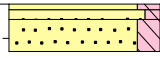


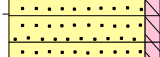
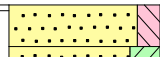
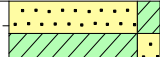
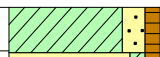
Afwerking boorgat

Diepte [m t.o.v. NAP] van tot	Aanvulmateriaal
-14.87 -24.87	kleistop

Boorprofiel	Monsternr.	Diepte [m t.o.v. NAP] van tot	Omschrijving grondlaag	Kleur
	5406k	+2.03 +1.70	Zand (zeer fijn), matig siltig	grijs
		+1.70 +1.64	Zand (zeer fijn), zwak siltig, bevat brokken van klei	grijs
	5407k	+1.63 +1.41	Zand (zeer fijn), zwak siltig, bevat laagjes van klei	grijs
		+1.41 +1.29	Klei, zwak zandig (zeer fijn)	grijs
		+1.29 +1.25	Zand (zeer fijn), zwak siltig	grijs
	5408k	+1.23 +0.89	Zand (zeer fijn), zwak siltig, bevat sporen van klei	grijs
		+0.89 +0.85	Klei, matig siltig	grijs
	5409k	+0.83 +0.78	Zand (zeer fijn), zwak siltig	grijs
		+0.78 +0.71	Klei, matig zandig (zeer fijn)	grijs
		+0.71 +0.60	Klei, matig siltig	grijs
		+0.60 +0.45	Zand (zeer grof), zwak siltig, zwak grindig (fijn)	grijs

BORING : BB20 - vervolg -

Datum : 27-05-2019 X : 58454.410 Boormethode : Puls/Ack
 GWS : NAP +0.68 m Y : 439757.910 Boormeester : CH
 Maaiveld : NAP +5.13 m Beschrijver : CH
 Opmerking : Definitieve boorstaat.

Boorprofiel	Monsternr.	Diepte [m t.o.v. NAP] van tot		Omschrijving grondlaag	Kleur
	5410k	-2.77	-2.93	Zand (matig fijn), zwak siltig	grijs
		-2.93	-3.04	Zand (zeer fijn), zwak siltig, zwak humeus	grijs
	5411k	-3.17	-3.31	Zand (zeer fijn), zwak siltig	grijs
		-3.31	-3.44	Zand (uiterst fijn), zwak siltig	grijs
	5412k	-3.57	-3.60	Zand (uiterst fijn), matig siltig	grijs
		-3.60	-3.65	Zand (uiterst fijn), zwak siltig	grijs
		-3.65	-3.82	Zand (uiterst fijn), matig siltig	grijs
	5413k	-8.87	-9.21	Zand (zeer fijn), zwak siltig	grijs
	5414k	-9.27	-9.54	Zand (zeer fijn), zwak siltig	grijs
	5415k	-9.67	-9.76	Zand (zeer fijn), zwak siltig	grijs
		-9.76	-9.90	Zand (zeer fijn), zwak siltig, bevat brokken van klei	grijs
		-9.90	-10.01	Zand (uiterst fijn), zwak siltig, bevat sporen van klei	grijs
	5416k	-15.97	-16.19	Zand (zeer fijn), matig siltig, schelpengruis, bevat brokken van klei	grijs
		-16.19	-16.25	Zand (zeer fijn), sterk kleiig, schelpengruis	grijs
		-16.25	-16.32	Zand (zeer fijn), matig kleiig, schelpengruis	grijs
	5417k	-16.37	-16.54	Zand (uiterst fijn), matig kleiig	grijs
		-16.54	-16.68	Klei, matig zandig (uiterst fijn)	grijs
		-16.68	-16.76	Zand (uiterst fijn), matig kleiig	grijs
	5418k	-16.77	-17.01	Klei, matig zandig (zeer fijn), zwak humeus	grijs
		-17.01	-17.12	Zand (zeer grof), zwak kleiig, zwak humeus	grijs

Opdracht : 1802965
Plaats : Rotterdam
Project : Aanvullend grondonderzoek APMT-MV2 I.001067

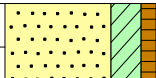


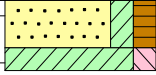
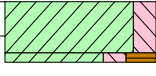
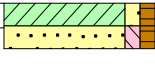
BOORBESCHRIJVING

Identificatie

NEN5104

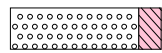
BORING : BB20 - vervolg -

Datum : 27-05-2019 X : 58454.410 Boormethode : Puls/Ack
GWS : NAP +0.68 m Y : 439757.910 Boormeester : CH
Maaiveld : NAP +5.13 m Beschrijver : CH
Opmerking : Definitieve boorstaat.

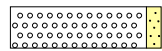
Boorprofiel	Monsternr.	Diepte [m t.o.v. NAP] van tot		Omschrijving grondlaag	Kleur
	5419k	-19.77	-20.17	Zand (zeer fijn), sterk kleiig, zwak humeus	grijs
	5420k	-20.17	-20.50	Leem, matig zandig (zeer fijn)	grijs
	5421k	-20.57	-20.69	Klei, matig zandig (zeer fijn), zwak humeus	grijs
		-20.69	-20.73	Zand (zeer fijn), zwak siltig, zwak humeus	grijs
		-20.73	-20.82	Zand (zeer fijn), zwak kleiig, zwak humeus	grijs
		-20.82	-20.96	Klei, matig zandig (zeer fijn), zwak humeus	grijs
	5422k	-22.77	-23.17	Zand (zeer fijn), zwak siltig, matig humeus, bevat laagjes van veen, bevat laagjes van klei	grijs
	5423k	-23.17	-23.42	Zand (zeer fijn), matig kleiig, matig humeus, bevat laagjes van veen	grijs
		-23.42	-23.54	Klei, matig siltig	grijs
	5424k	-23.57	-23.84	Klei, matig siltig	grijs
		-23.84	-23.89	Klei, matig siltig, sterk humeus	bruin
	5425k	-23.97	-24.10	Klei, matig siltig	grijs
		-24.10	-24.15	Klei, matig siltig, sterk humeus	bruin
		-24.15	-24.27	Klei, matig siltig, zwak humeus	grijs
	5426k	-24.37	-24.49	Klei, zwak zandig (zeer fijn), zwak humeus	grijs
		-24.49	-24.61	Zand (matig fijn), zwak siltig, zwak humeus	grijs

Legenda

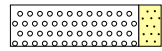
Grind



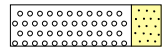
Grind, siltig



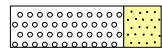
Grind, zwak zandig



Grind, matig zandig

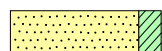


Grind, sterk zandig

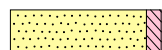


Grind, uiterst zandig

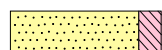
Zand



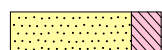
Zand, kleiig



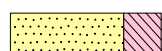
Zand, zwak siltig



Zand, matig siltig

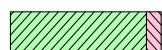


Zand, sterk siltig



Zand, uiterst siltig

Klei



Klei, zwak siltig



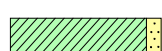
Klei, matig siltig



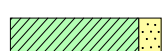
Klei, sterk siltig



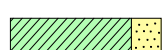
Klei, uiterst siltig



Klei, zwak zandig



Klei, matig zandig



Klei, sterk zandig

Veen



Veen, mineraalarm



Veen, zwak kleiig



Veen, matig kleiig



Veen, sterk kleiig



Veen, uiterst kleiig

Leem

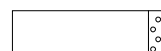


Leem, zwak zandig



Leem, sterk zandig

Overige toevoegingen



Zwak grindig



Matig grindig



Sterk grindig

Overig



Puin



Slib



Water



Kleistoep / afdichtpellets



Lege monsterbus



Bus met ongeroerd monster



Grondwaterstand tijdens boren



Stijghoogte in peilbuis



Peilbuisfilter

Afkortingen

CRS Constant Rate of Strain test

DSS Direct Simple Shear test

SDR Samendrukkingsproef

TRX Triaxiaalproef

VGM Bepaling volumegewicht monster (zonder verdere beproeving)

VGB Bepaling totaal volumegewicht bus

Appendix C General Photos



Figure C.1: Head of the steel auxiliary tube lying on the test site prior to pile installation



Figure C.2: IHC S-120 hammer used for the installation of the auxiliary tube



Figure C.3: Annular space around the auxiliary pile during pile driving



Figure C.4: Lifting of the reinforcement cage for P11 using a mobile crane and the drilling rig crane (left)



Figure C.5: Concrete replenishment during the withdrawal of the auxiliary tube



Figure C.6: Vibro pile prepared with pile cap, awaiting installation of the reaction frame



Figure C.7: Close-up of the pile head and pile cap

Appendix D Prediction of Pile Behaviour

D.1 Prediction of Failure Load

In advance of pile installation and testing, the failure load was predicted in order to devise the load test programme. This was done using the following prediction methods:

Base capacity

1. NEN 9997-1 (2017 alpha factors)
2. NEN 9997-1 (pre-2017 alpha factors)
3. LCPC (“French method”)
4. LCPC method with $q_{c,avg}$ obtained using the De Boorder (2019) technique

Shaft capacity

1. NEN 9997-1 (2017)
2. UWA-05 (simplified)

For all piles, the CPT along their respective central axes was used, the diameter of the base plate was used to determine the shaft capacity and no limitation of the pile base capacity or cone resistances were applied. The target installation level was used as the elevation of the pile toe.

Table D.1: Overview of the alpha factors used for calculation of the pile base and shaft capacities

Combination	Base capacity				Shaft capacity	
	NEN 9997-1 (2017)	NEN 9997-1 (pre-2017)	LCPC	De Boorder (2019)	NEN 9997-1 (2017)	UWA-05 (simplified)
1	0.70				0.014	
2		1.0			0.014	
3			0.60			0.030
4				0.60		0.030

Table D.2: Overview of the predicted base and shaft capacities at failure

Pile	Base capacity [MN]				Shaft capacity [MN]	
	NEN 9997-1 (2017)	NEN 9997-1 (pre-2017)	LCPC	De Boorder (2019)	NEN 9997-1 (2017)	UWA-05 (simplified)
P01	3.4	2.4	5.3	4.6	9.7	3.0
P03	6.9	4.9	5.1	5.6	9.5	3.3
P06	5.5	3.8	5.7	5.5	10.1	3.7
P11	6.8	4.8	5.6	5.7	9.0	3.4

Table D.3: Overview of the predicted failure capacities

Pile	Pile tip level [mNAP]	Combination 1 [MN]	Combination 2 [MN]	Combination 3 [MN]	Combination 4 [MN]
P01	-28.5	12.1	13.1	8.3	7.6
P03	-28.5	14.4	16.4	8.4	8.9
P06	-28.5	13.9	15.5	9.4	9.2
P11	-28.5	13.8	15.9	9.0	9.2

D.2 Prediction of Pile Settlement

In accordance with the stipulations of the NPR 7201 and NEN 9997-1, the following load-settlement diagrams have been predicted in advance of pile testing using the combinations of prediction methods, outlined in Table D.1.

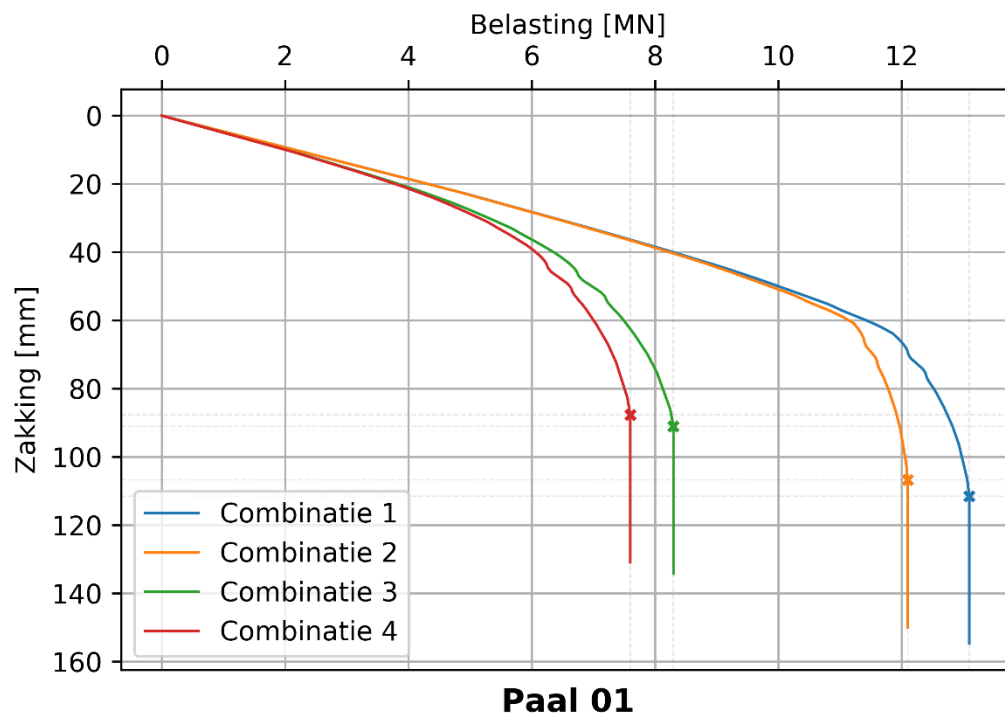


Figure D.1: Predicted load-settlement graph for pile P01 for the aforementioned combinations

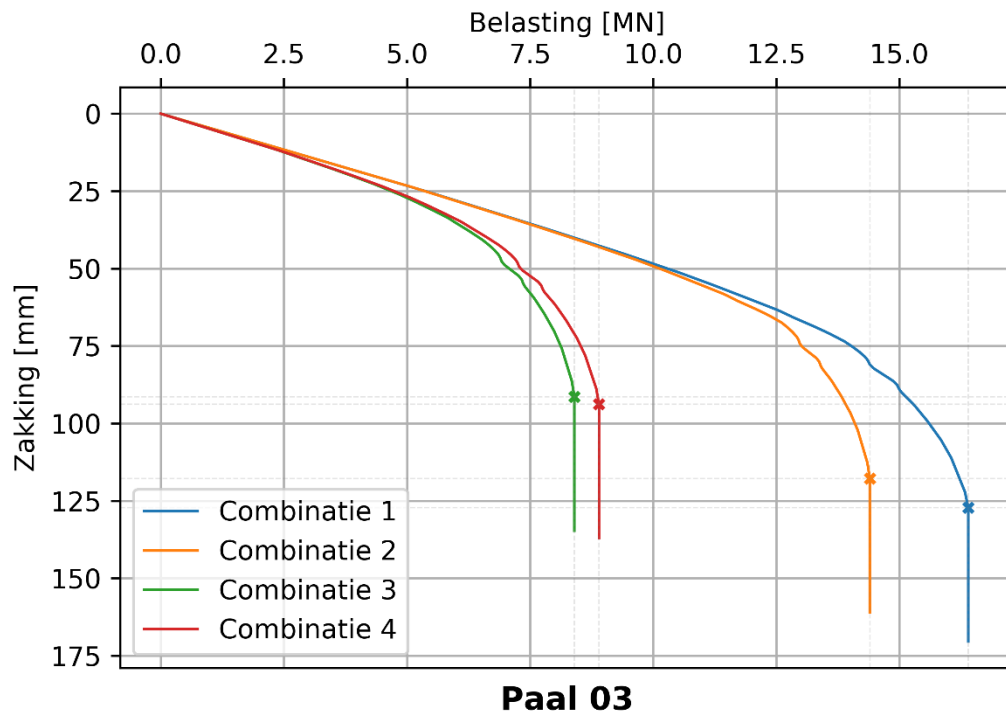


Figure D.2: Predicted load-settlement graph for pile P03 for the aforementioned combinations

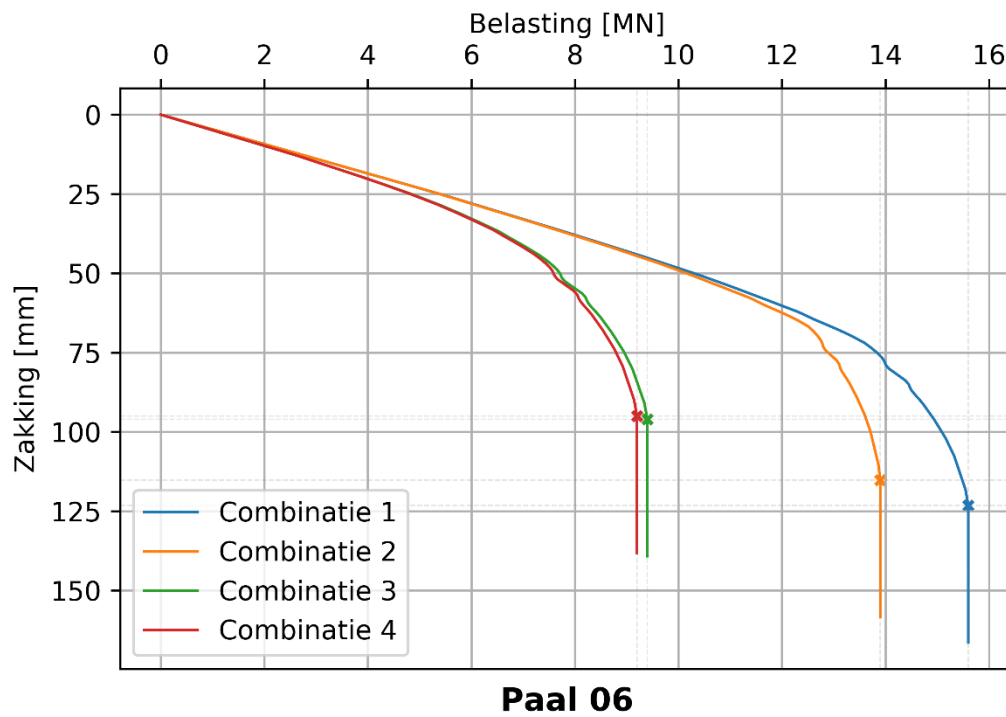


Figure D.3: Predicted load-settlement graph for pile P06 for the aforementioned combinations

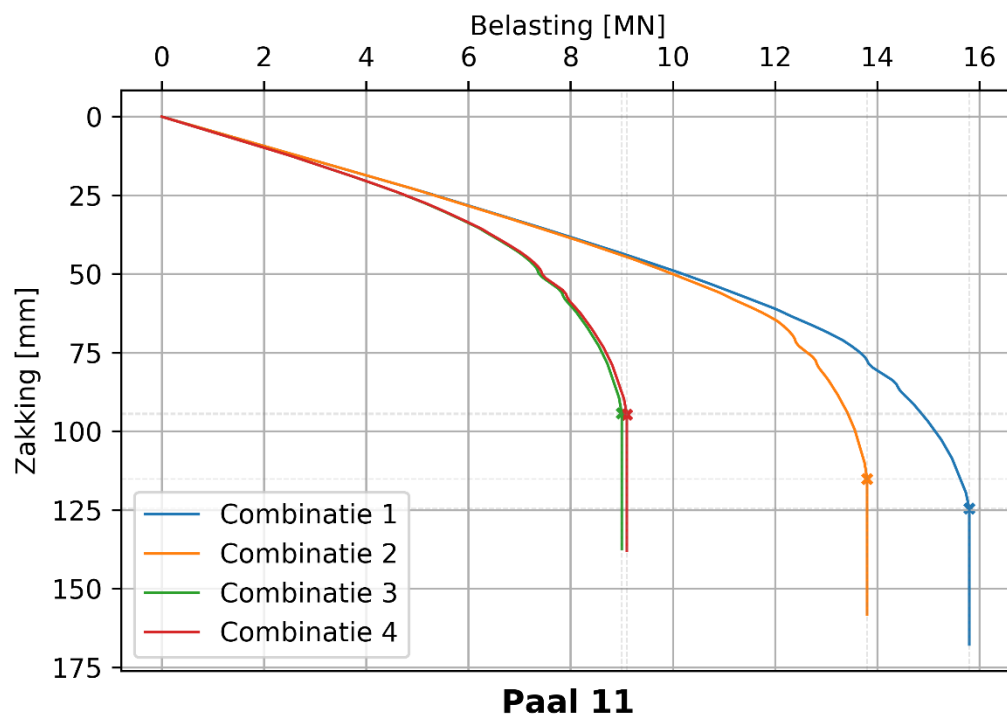


Figure D.4: Predicted load-settlement graph for pile P11 for the aforementioned combinations

Appendix E Detailed Drawings

E.1 Reinforcement Cage

BUIGSTAAT : 2019-92558 - paalkorven

Project 2019-00566 - Terracon 2019 Q3
Dossier 2019-05467 - 3.19.13 - Maasvlakte 2
Samengesteld D.H.J. Drent

Klant 2020 - Terracon Funderingstechniek B.V.
Referentie 3.19.13 - Maasvlakte 2
Afdruk datum Tuesday, October 29, 2019

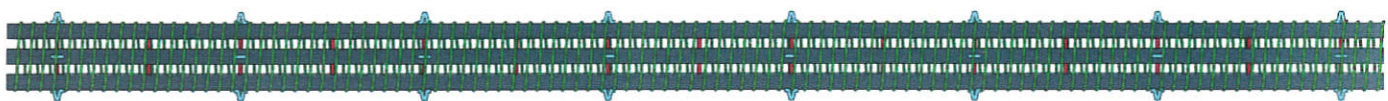
Product : 001 - VK 250 4ø50 l=32250

Aantal : 4 Gewicht/st : 2052,2 kg

korf lengte=32250

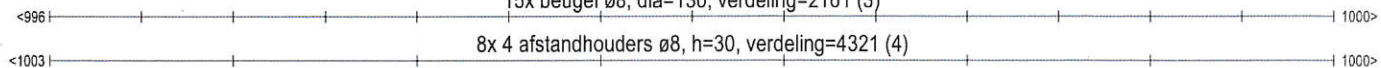
4 ø50, l=32250 (1)

spiraal ø10, dia=250, spoed=300, l=32250 (2)



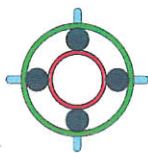
15x beugel ø8, dia=130, verdeling=2161 (3)

8x 4 afstandhouders ø8, h=30, verdeling=4321 (4)

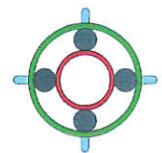


GEWI® staven 50 TR 670/800

afstandhouders 30mm Hoog



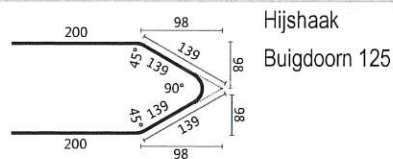
250



250

Onderdelenlijst

Merk	Aantal	Materiaal	Kwaliteit	Afmeting	Gewicht	Eigenschappen	Positie
HW	4	ø50		32250	1988,3	GEWI® staven 50 TR 670/800	1
SP	1	ø10	B500B	90380	55,8	spiraal ø10, dia=250, spoed=300, l=32250	2
R	15	ø8	B500A	408	2,4	beugels ø8, ring, dia=130, verdeling=2161	3
AH	32	ø8	B500A	250	3,2	8x 4 afstandhouders ø8, h=30, verdeling=4321	4
HH	1	ø25	B500B	678	2,6		



Hijshaak

Buigdoorn 125

Gewicht/stuk: 2052,2 kg Totaal gewicht: 8208,9 kg

BUIG CENTRALE STEENBERGEN B.V.

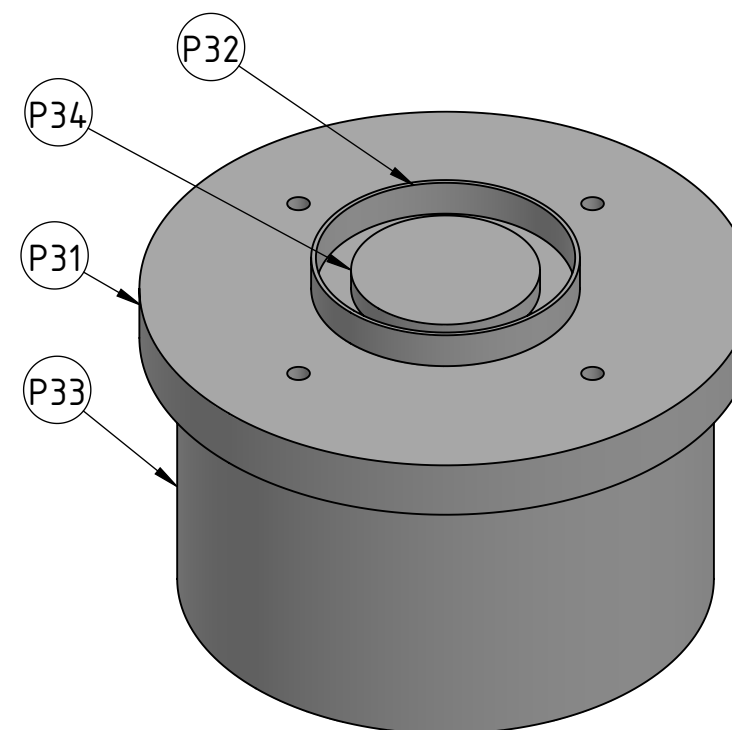
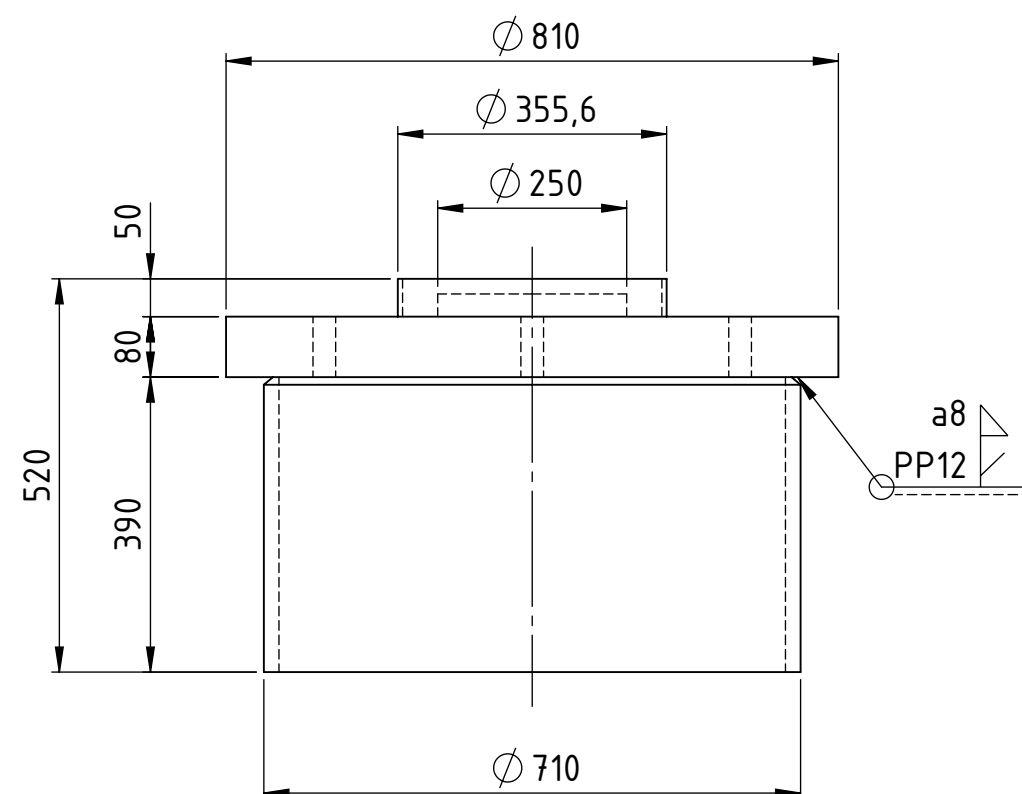
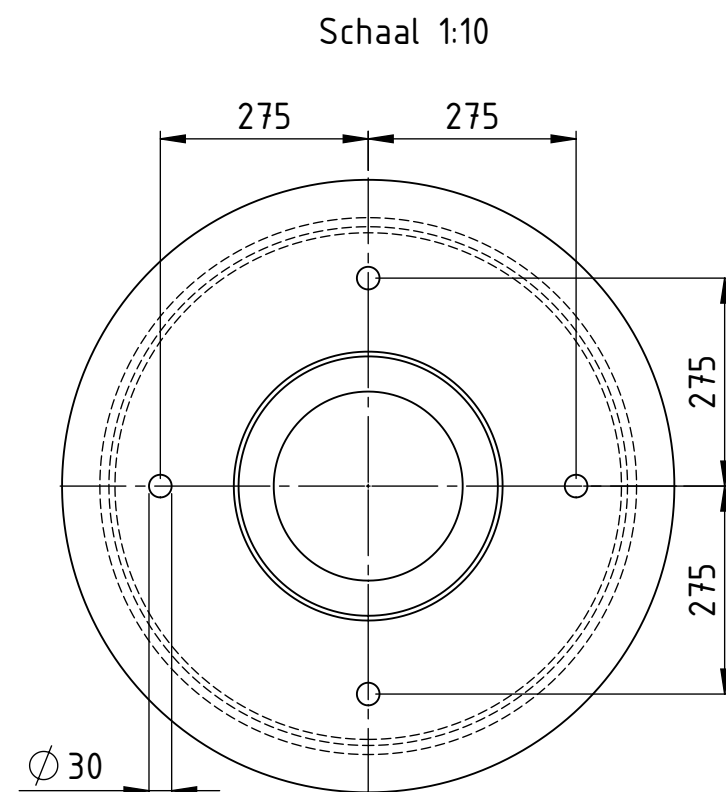
Dr. A. Philipsstraat 15
Postbus 54 - 7900 AB
Hoogeveen
Nederland

T : +31 528 229 400
F : +31 528 263 880
E : info@bcssteel.eu
I : www.bcssteel.eu

BTW : NL001266755B01
LB : 001266755L01
KVK : 04011733

CERTIFICATEN | ISO 9001 | KOMO K7230/04 | BENOR 117 VERDELER - 606 VLECHTER | DIN 4099

E.2 Pile Cap



Opmerkingen:

- 8x Uitvoeren
- Lassen t.a.v. a=5
- Gewicht: 467,79 kg

Conservering:

-

P34	1	Plaat t=30 (3)	Ø250x30		S355 J2	11,56	0
P33	1	Buis Ø710x20 (1)	Lg 390		S355 J2	131,68	A
P32	1	Buis Ø355,6x6,3 (2)	Lg 50		S355 J2	2,71	0
P31	1	Plaat t=80 (2)	Ø810x80		S355 J2	321,83	0
Posnr.	Aantal	Omschrijving	Afmeting	Lengte	Materiaal	Gewicht (kg)	Rev.

A	Lengte P33 gewijzigd			S. Maas	A. Versluis	10-10-2019
REV.	Omschrijving			Getekend	Akkoord	Datum

Getekend door S. Maas		Gecontroleerd door A. Versluis			Blad SHEET 1 OF 1	Documentstatus
Bestek- / Contractnummer	Schaal Zie tekening	Formaat A3	Documenttype Tekening	Exc. 2	Datum uitgifte 20-9-2019	Documentnummer A31

Project
19S33 - Spinnenkop MV2

Opdrachtgever
B.V. Aannemingsbedrijf de Klerk

Onderdeel
Lassam. kop 2 voor prefab-&vibropaal

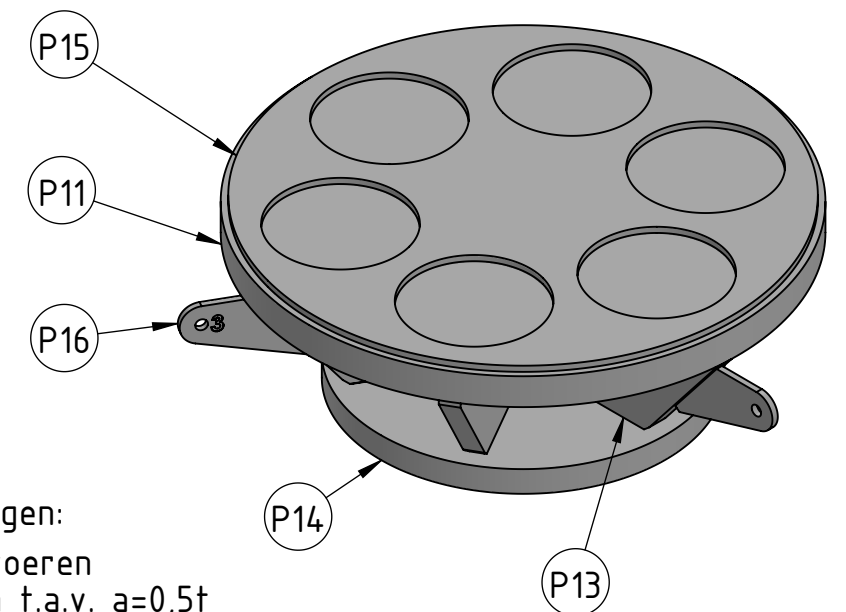
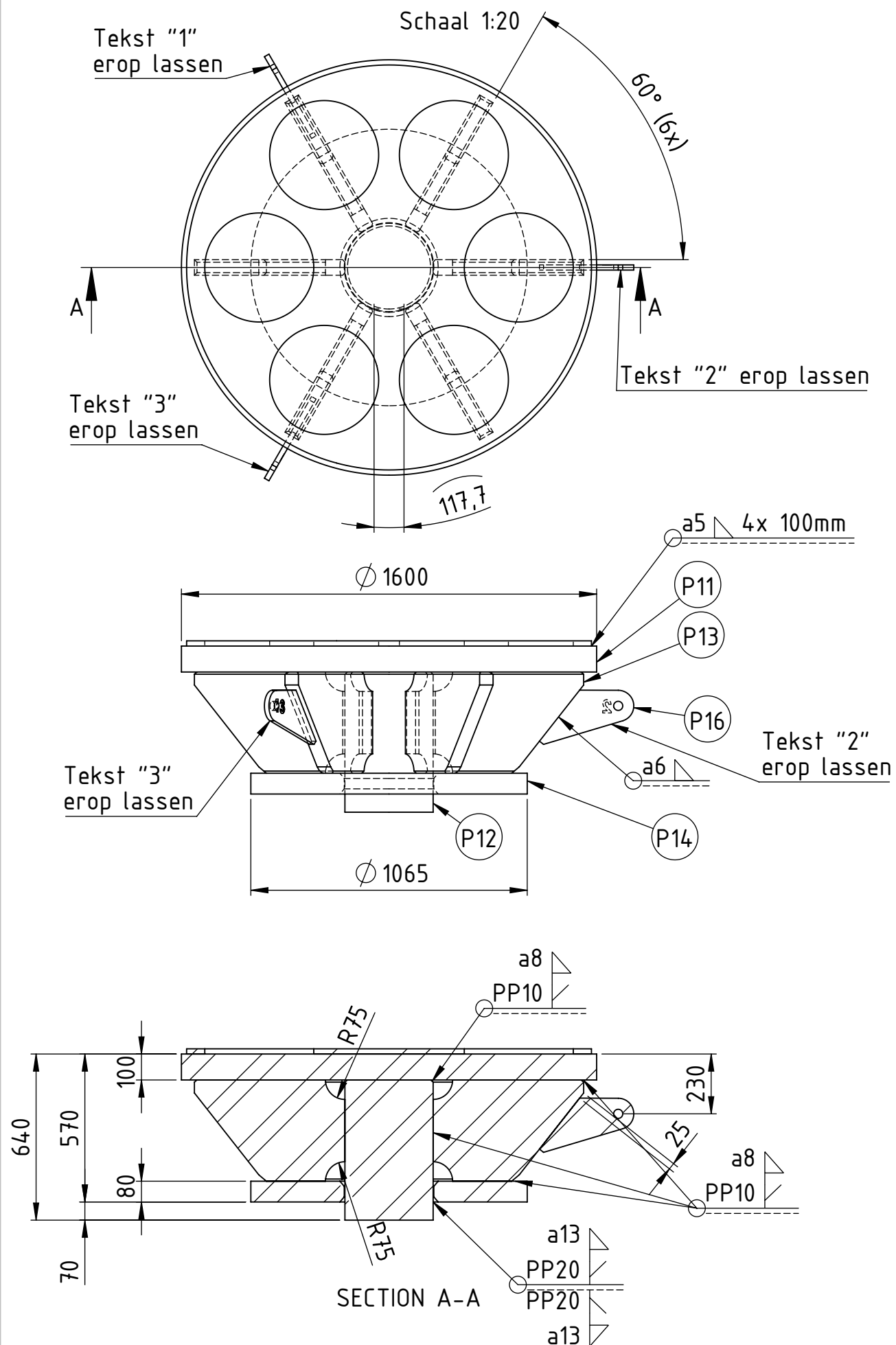


Postbus 21, 4250 DA Werkendam

T 0183 508666
F 0183 502402

E info@deklerkbv.nl
I www.deklerkbv.nl

E.3 Transition Piece



Opmerkingen:

- 1x Uitvoeren
- Lassen t.a.v. a=0,5t
- Gewicht: 3130,69 kg

Conservering:

- Stralen Sa 2,5
- 1e laag: Primer, droge laagdikte 75mu, RAL n.t.b.
- 2e laag: Polyurethaan, droge laagdikte 75mu, RAL n.t.b.

P16	3	Plaat t=20 (3)	390x160x20		S355 J2	6,35	0
P15	1	Plaat t=20 (2)	Ø1560x20		S355 J2	169,57	0
P14	1	Plaat t=80 (1)	Ø1065x80		S355 J2	497,78	0
P13	6	Plaat t=60 (2)	580x390x60		S355 J2	80,24	0
P12	1	Rond Ø340 (1)	Lg 540		S355 J2	384,52	0
P11	1	Plaat t=100 (1)	Ø1600x100		S355 J2	1578,34	0
Posnr.	Aantal	Omschrijving	Afmeting	Lengte	Materiaal	Gewicht (kg)	Rev.

A	Diverse opmerkingen verwerkt			S. Maas	A. Versluis	10-10-2019
---	------------------------------	--	--	---------	-------------	------------

REV.	Omschrijving			Getekend	Akkoord	Datum
------	--------------	--	--	----------	---------	-------

Getekend door S. Maas		Gecontroleerd door A. Versluis		Blad SHEET 1 OF 1	Documentstatus
--------------------------	--	-----------------------------------	--	----------------------	----------------

Bestek- / Contractnummer	Schaal Zie tekening	Formaat A3	Documenttype Tekening	Exc. 2	Datum uitgifte 19-9-2019	Documentnummer A11
--------------------------	------------------------	---------------	--------------------------	-----------	-----------------------------	-----------------------

Project

19S33 - Spinnenkop MV2

Opdrachtgever

B.V. Aannemingsbedrijf de Klerk

Onderdeel

Lassam. stalen adapter

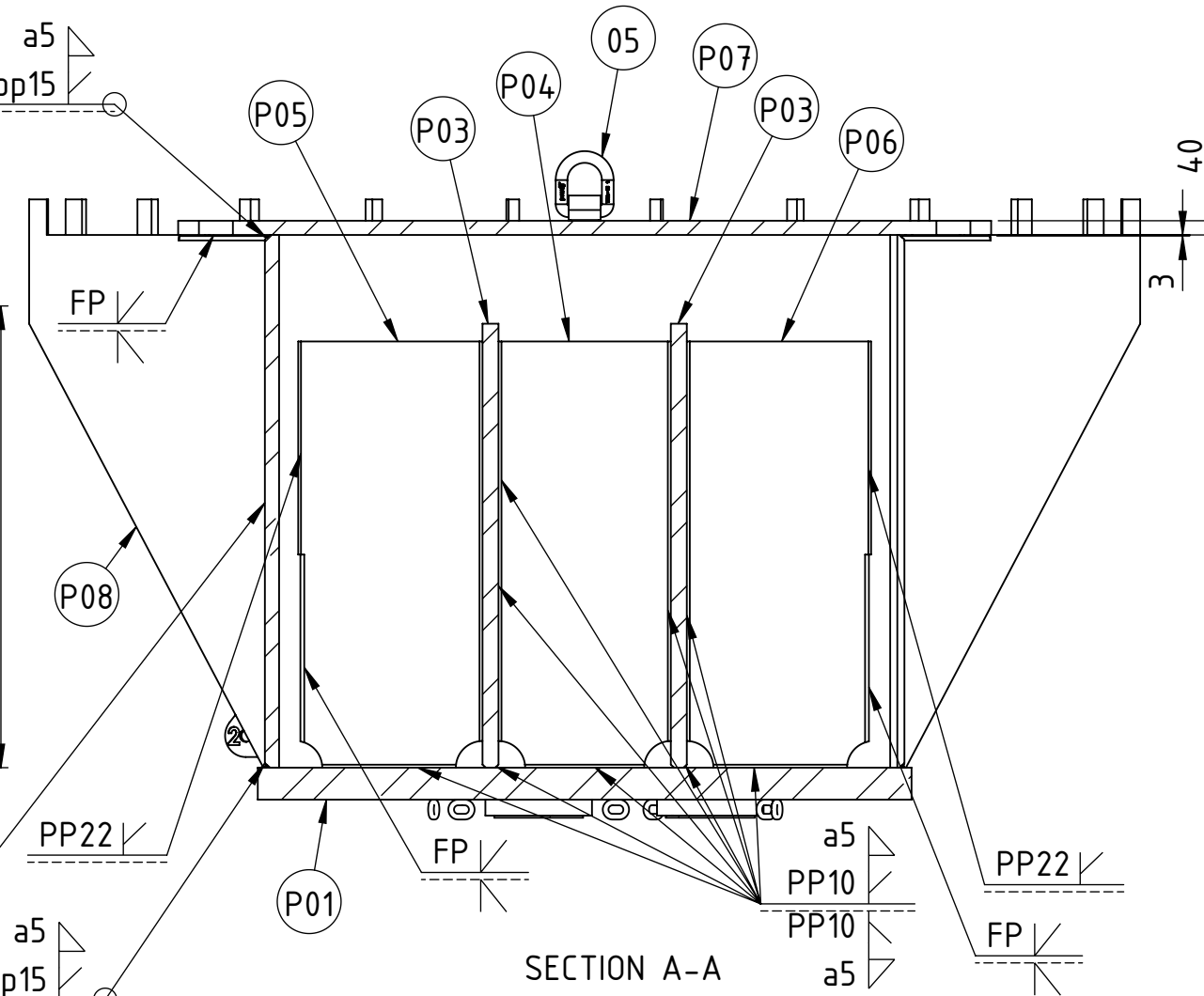
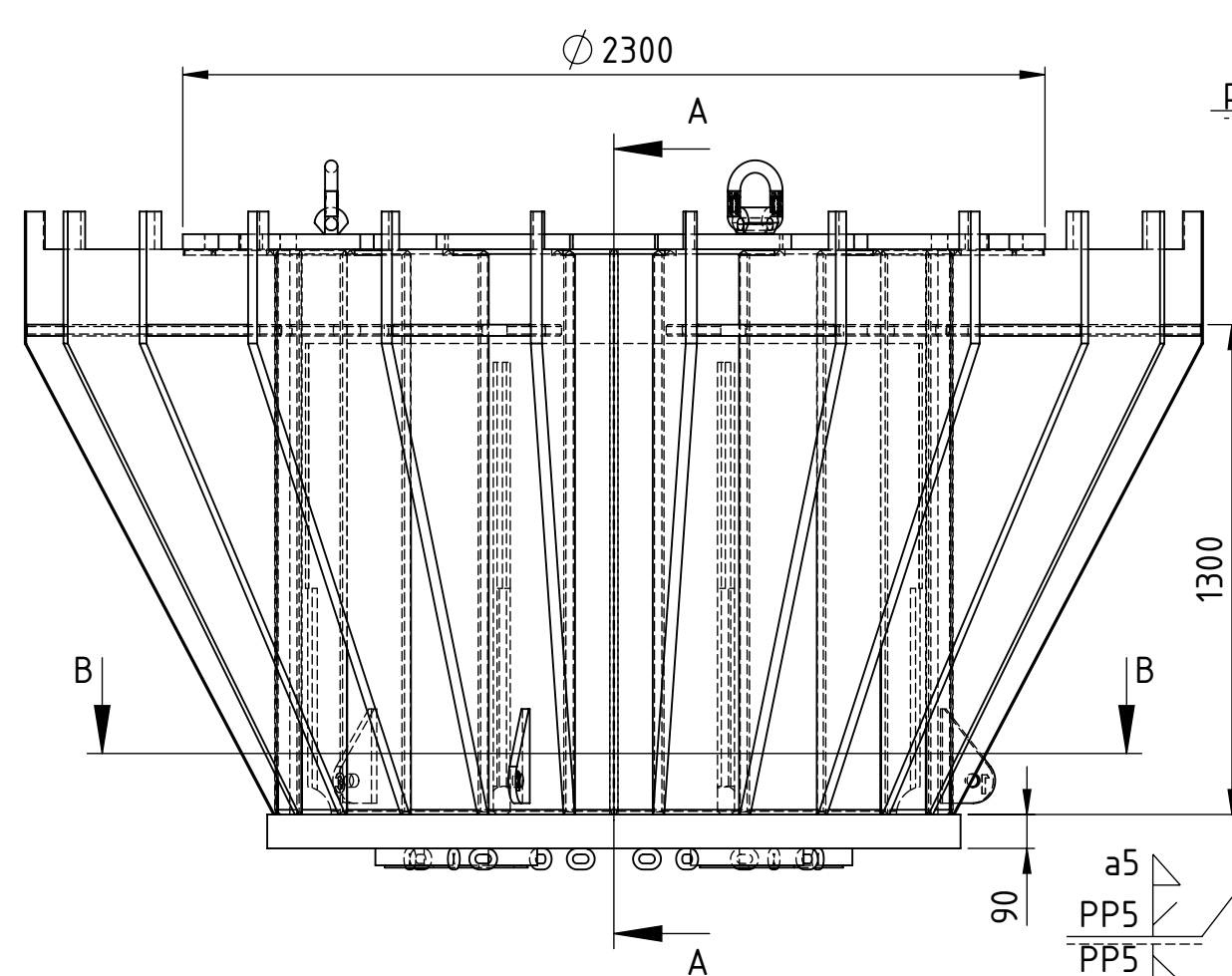
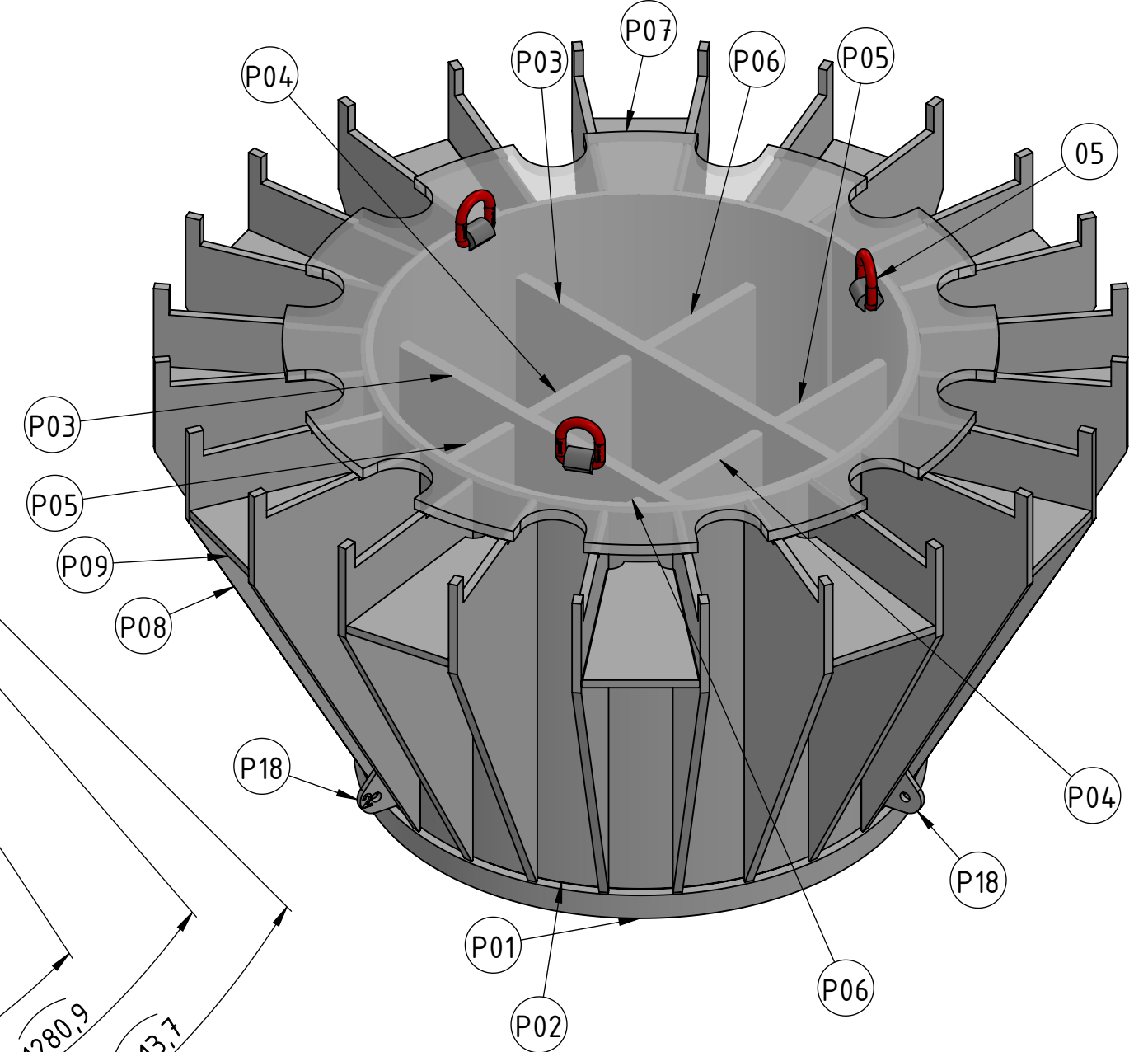
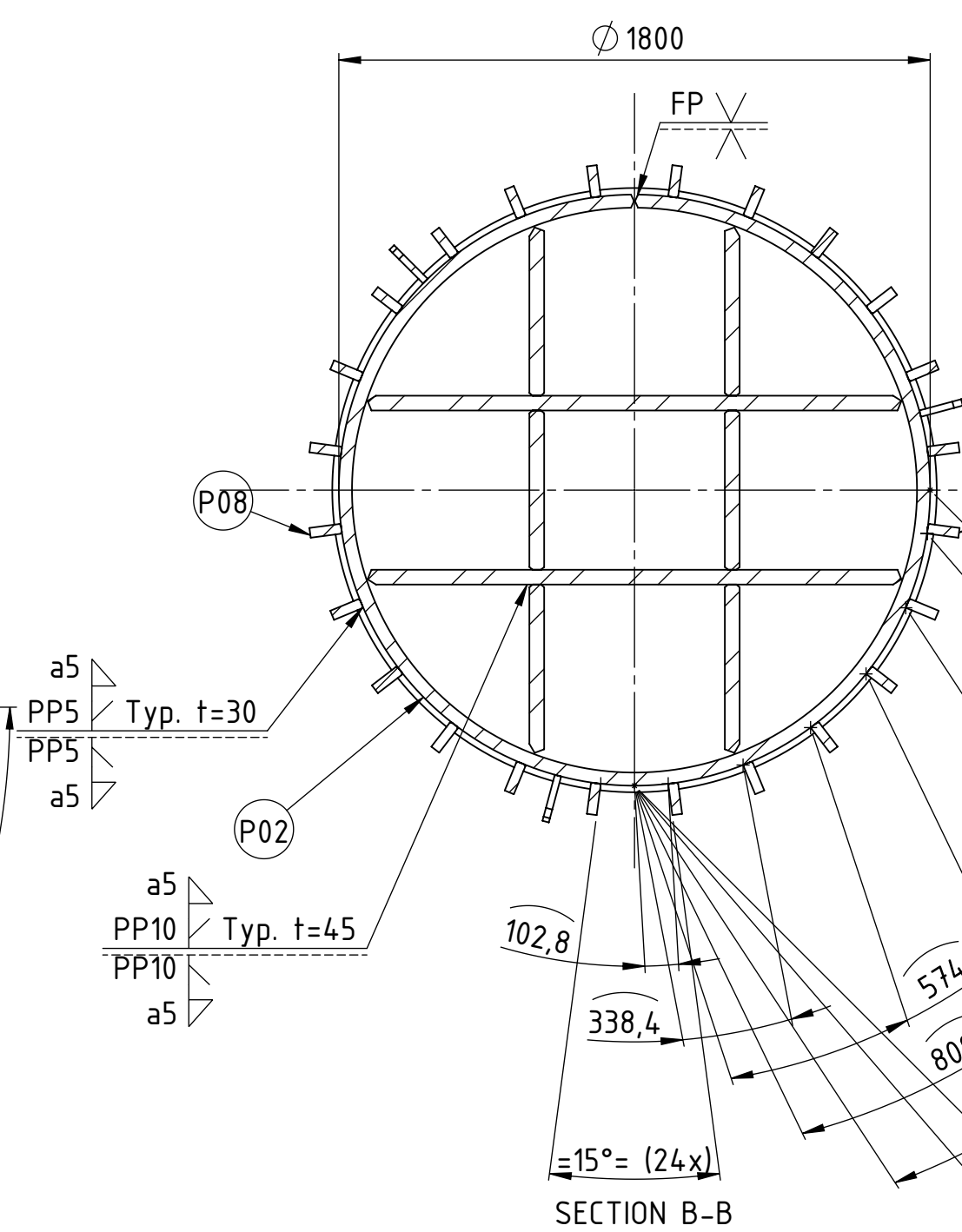
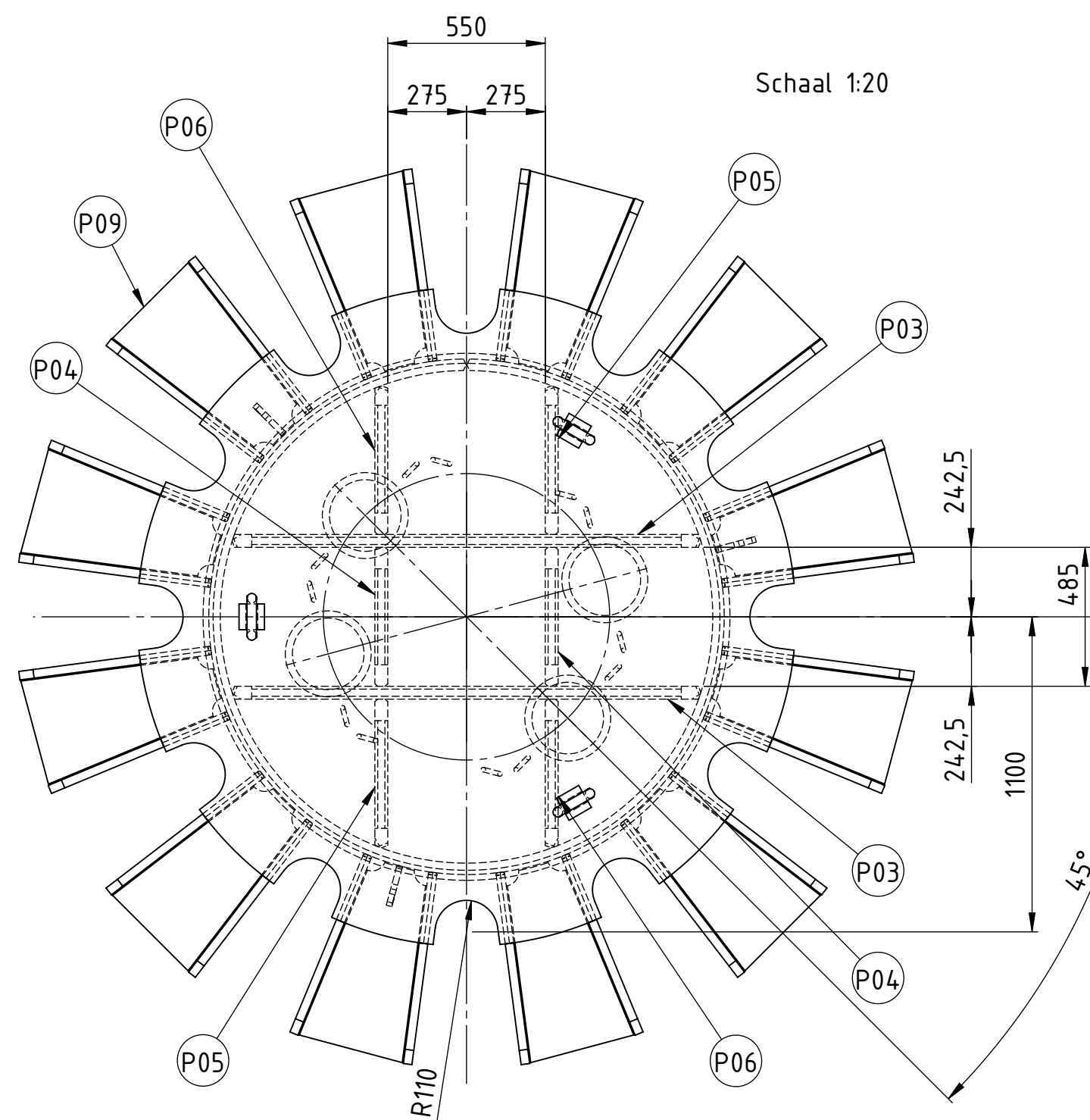


Postbus 21, 4250 DA Werkendam

T 0183 508666
F 0183 502402

E info@deklerkbv.nl
I www.deklerkbv.nl

E.4 Reaction Frame



Opmerkingen:

- 1x Uitvoeren
- Lassen t.a.v. a=0,5t of PP
- Gewicht: 12384,22 kg

Conservering:

- Stralen Sa 2,5
- 1e laag: Primer, droge laagdikte 75mu, RAL n.t.b.
- 2e laag: Polyurethaan, droge laagdikte 75mu, RAL n.t.b.

P18	3	Plaat t=20 (1)	250x145x20		S355 J2	3,62	0
P17	4	Plaat t=6 (1)	Ø250x6		S355 J2	2,31	0
P10	4	Plaat t=45 (5)	Ø300x45		S355 J2	24,97	0
P09	12	Plaat t=30 (2)	667x381x30		S355 J2	44,70	A
P08	24	Plaat t=30 (1)	1600x675x30		S355 J2	140,94	A
P07	1	Plaat t=40 (2)	Ø2300x40		S355 J2	1191,65	0
P06	2	Plaat t=45 (4)	1200x526x45		S355 J2	212,37	B
P05	2	Plaat t=45 (3)	1200x526x45		S355 J2	212,37	B
P04	2	Plaat t=45 (2)	1200x485x45		S355 J2	200,77	A
P03	2	Plaat t=45 (1)	1650x1250x45		S355 J2	711,76	B
P02	1	Plaat t=40 (1) - gewalst	5526x1500x40		S355 J2	2590,17	A
P01	1	Plaat t=90 (1)	Ø1840x90		S355 J2	1878,61	B
06	12	Kettingschalm Ø16mm			S355	0,26	0
05	3	Aantas hijsoog 15 ton			S355	2,35	0

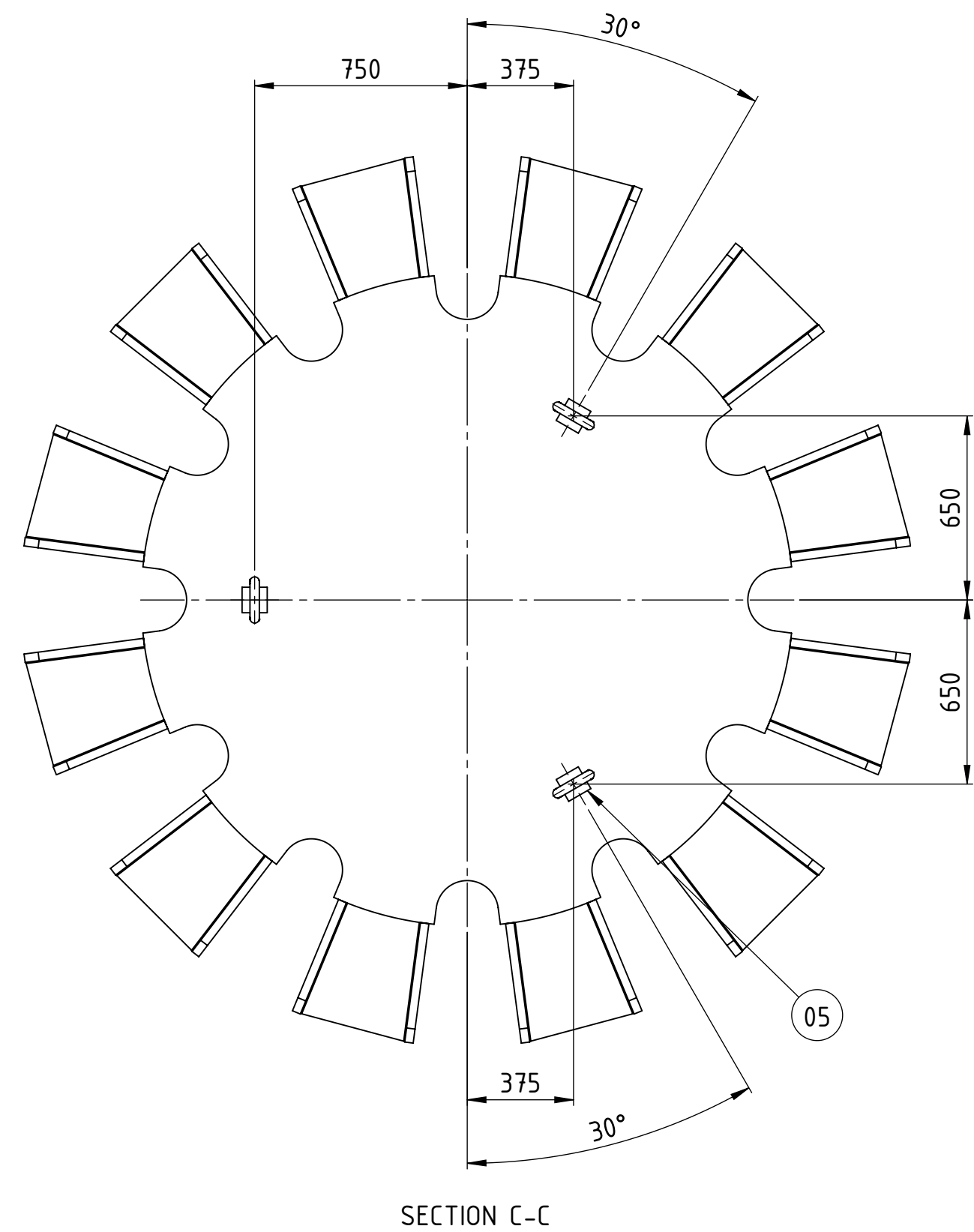
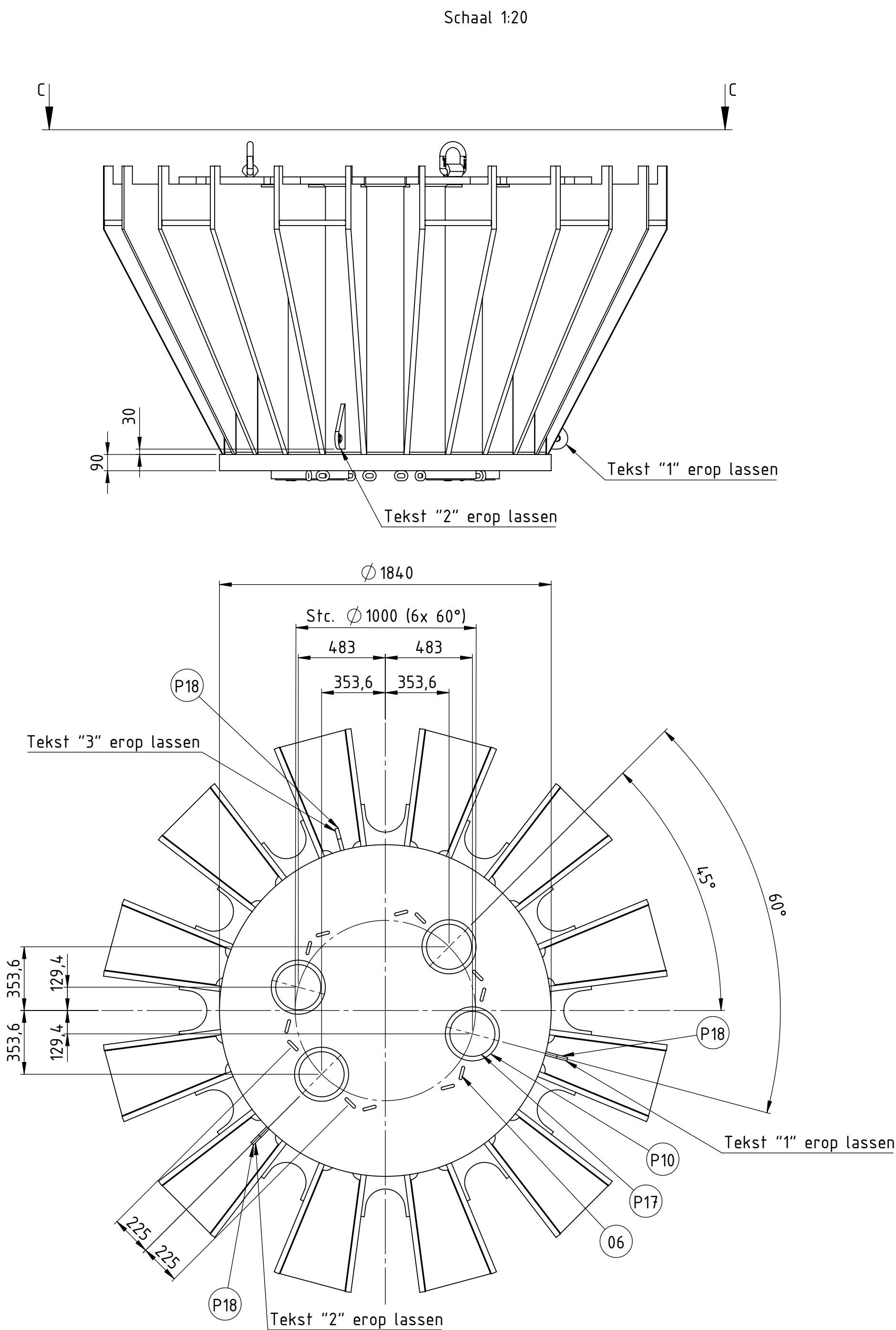
Posnr.	Aantal	Omschrijving	Afmeting	Lengte	Materiaal	Gewicht (kg)	Rev.
B		Diverse opmerkingen verwerkt		S. Maas	A. Versluis	10-10-2019	
A		Laskant P03, P05 en P06 aan buis gewijzigd en dikte P01 gewijzigd		S. Maas	A. Versluis	10-9-2019	
REV.		Omschrijving		Gefekend	Akkoord	Datum	
Gefekend door		Gecontroleerd door		Blad		Documentstatus	
S. Maas		A. Versluis		SHEET 1 OF 2			
Bestek- / Contractnummer		Schaal	Formaat	Documenttype	Exc.	Datum uitgifte	Documentnummer
		Zie tekening	A2	Tekening	2	9-9-2019	A01

Project		19S33 - Spinnenkop MV2					
Opdrachtgever		B.V. Aannemingsbedrijf de Klerk					
Onderdeel		Lassam. spinnenkop MV2					



Postbus 21, 4250 DA Werkendam

T 0183 508666 E info@deklerkbv.nl
F 0183 502402 I www.deklerkbv.nl



- Opmerkingen:
- 1x Uitvoeren
 - Lassen t.a.v. a=0,5t of PP
 - Gewicht: 12384,22 kg
- Conservering:
- Stralen Sa 2,5
 - 1e laag: Primer, droge laagdikte 75mu, RAL n.t.b.
 - 2e laag: Polyurethaan, droge laagdikte 75mu, RAL n.t.b.

Getekend door S. Maas		Gecontroleerd door A. Versluis		Blad SHEET 2 OF 2	Documentstatus
Bestek- / Contractnummer	Schaal Zie tekening	Formaat A2	Documenttype Tekening	Exc. 2	Documentnummer A01
Project 19S33 - Spinnenkop MV2					
Opdrachtgever B.V. Aannemingsbedrijf de Klerk					
Onderdeel Lassam. spinnenkop MV2					
		Postbus 21, 4250 DA Werkendam			
T 0183 508666		E info@deklerkbv.nl			
F 0183 502402		I www.deklerkbv.nl			

Appendix F General Specifications

F.1 Injection Grout – Grout Anchors

Productinformatieblad



webertec GM 42 is een kant en klaar fabrieksmatig vervaardigde cementgebonden droge mortel.

- Kant-en-klaar
- CEM III
- Sterkteklasse >25 N/mm²

Toepassing

De mortel wordt verwerkt op een klantspecifieke wijze als:

Groutmortel in de funderingsindustrie

Leveringsvorm

Silo (afhankelijk van silocapaciteit en de wettelijk toegestane gewichten)

Bulk (afhankelijk van silocapaciteit en de wettelijk toegestane gewichten)

Verkrijgbaarheid

Op aanvraag

Product eigenschappen

Kant-en-klaar groutmortel voor de funderingsindustrie, sterkteklasse >25 N/mm², CEM III.

Classificatie

Sterkteklasse: >25 N/mm²

Kleuren

Grijs

Verbruik

Afhankelijk van de in het werk toegepaste consistentie.

Dosering

Bulk:

Stel de waterdosering in zodat de juist consistentie wordt verkregen. Eigenschappen zijn bepaald op basis van een water-drogemortelfactor van 0,50.

De waterdosering is te controleren doormiddel van het indampen van de groutspecie.

Gebruiksaanwijzing

Productinformatieblad



Vorbereiding

webertec GM 42 wordt op geheel klantspecifieke wijze toegepast.

Aanmaken

Waterhoeveelheid: Klantspecifiek. Gebruik voor het aanmaken van de betonspecie bij voorkeur drinkwater of leidingwater (NEN-EN 1008), bij twijfel is nader onderzoek nodig naar de geschiktheid van het te gebruiken water. Mengen (Weber Beamix equipment): meng overeenkomstig de handleiding behorende bij het desbetreffende mengsysteem.

Verwerken

Verwerk de aangemaakte mortelspecie boven 5°C. Werk niet tegen, op of in een bevroren ondergrond. Een bevroren ondergrond heeft een negatieve reactie op de hydratatiesnelheid van cement.

Nabehandelen

Bescherm het afgewerkte morteloppervlak tegen tocht en uitdroging door langdurig afdekken met vochtig jute of plastic folie. Bescherm het morteloppervlak tegen bevriezing.

Reinigen

Het gebruikte gereedschap kan met water worden gereinigd. Verhard materiaal kan alleen mechanisch worden verwijderd.

Verwerkingssystemen

Afhankelijk van de klantspecifieke toepassing wordt webertec GM 42 aangeleverd in een Silo mengpomp unit, of in een silo met opvoerschroef.

Technische informatie

Grondstoffen

Bindmiddel: hoogovencement CEM III/ B (EN 197-1)
Toeslagmateriaal: geen
Grootste korrelafmeting: 0,125 mm
Toevoegingen: kalksteenmeel (EN 13139)
Hulpstoffen: geen

Eigenschappen mortelspecie

Eigenschappen zijn bepaald op basis van een water-drogemortelfactor 0.50
Uitlevering: 855 l/ton*

Eigenschappen verharde mortel

Eigenschappen zijn bepaald op basis van een water-drogemortelfactor 0.50
Volumieke massa: 1750 kg/m³ (28 dagen)
Druksterkte: >25 N/mm² (28 dagen)*
Proefstukken 150 x 150 x 150 mm, bewaaromstandigheid 20 °C/onder water.
* Productspecificaties met betrekking tot certificering.

Houdbaarheid

12 maanden houdbaar na productiedatum indien droog en vorstvrij opgeslagen in de originele en gesloten verpakking.

Certificeringen

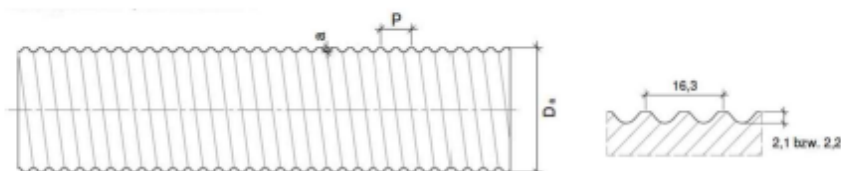
F.2 Grout Anchors

Note that the anchor type is H2800-108 for the vibro piles.



SPECIFICATIE ZELFBOREND ANKERTYPE RR108

Geometrie



Materiaal: 36Mn5 volgens EN-10210 / EN-10297

Item	Eenheid	RR 108					
		H2400-108	H2800-108	H3200-108	H4000-108	H4500-108	
Buitendiameter schroefdraad	D _a	mm	108,1				
Rekenkundige buitendiameter	D _{a;d}	mm	106,0				
Binnendiameter	D _i	mm	82,0	78,3	74,4	62,5	56,5
Rekenkundige doorsnede ^{a)}	A	mm ²	3.550	4.007	4.483	5.757	6.311
Gewicht	m	kg/m ¹	27,9	31,5	35,2	45,2	49,5
Vloeikracht ^{b)}	R _e	kN	1.880	2.125	2.375	3.050	3.345
Vloeispanning ^{c)}	f _{0,2}	N/mm ²	530			530	
Breukkracht ^{b)}	R _m	kN	2.400	2.800	3.200	4.000	4.500
Treksterkte ^{c)}	f _{u,2}	N/mm ²	730			715	
Ductiliteit (R _m /R _e)	k	-	≥1,15				
Minimale rek bij breuk	A _{gt}	%	≥5,0				
Elasticiteitsmodulus	E	N/mm ²	205.000				
Schroefdraadvorm	-	-	RR108				
Norm	-	-	ANP Interne Fabrieksnorm				
Oriëntatie schroefdraad	-	-	Rechts				
Spoed	p	mm	8,15				
Schroefdraadhoogte	a	mm	2,2				
Relatieve rib oppervlak	f _R	-	0,27				

a) berekend middels weging ($50 = 10^5 \times m / 7.850 \text{ [kg/m}^3\text{]}$)

b) karakteristieke waarde volgens EN 1990

c) berekend vanuit de karakteristieke kracht en de rekenkundige doorsnede, afgerond

Rev 1906

Wij behouden ons het recht voor om de gegevens in deze specificatie zonder voorafgaande kennisgeving te wijzigen of te corrigeren

F.3 Calibration Sheet – Load Cells



Uit : WTCB Databank Meetapparatuur (Limapp) :

DYNAMOMETRE		5000	kN						
Etalonnage le :	17/10/2019	T° (°C) :	20.1	ebro - EBI20	Presse 4000 kN + controleur MFL2				
par :	BA	H _{rel} :	61		mesure au TDS602 + robust + 50m cable				
					Ch. Robust	année fabrication	Etat	Remarque	
GM 50-1	Y (kN) = -0.95693 μ e + 72.144				30	2012	OK	Néant	
GM 50-2	Y (kN) = -0.95107 μ e - 40.37				31	2012	OK	Néant	
GM 50-3	Y (kN) = -0.95101 μ e - 43.733				32	2012	OK	Néant	
GM 50-4	Y (kN) = -0.95821 μ e - 118.008				33	2012	OK	Néant	
GM 50-5	Y (kN) = -0.95326 μ e - 1171.132				34	2019	OK	Néant	
GM 50-6	Y (kN) = -0.93888 μ e - 886.656				35	2019	OK	Néant	

Monika De Vos, Labo GM, 21.09.2020

M. De Vos

F.4 Calibration Sheet – LVDTs



Extrait de la banque de données des appareils de mesure du CSTC (Limapp) :

Ametek Sola			capacité	200	pied à coul	Mitutoyo	SC51	num certif: 1907-0030	validité	02/07/2020	
					Voltmètre	Keysight	34401A	num certif: 1-1105691	validité	04/04/2020	
Date etal.			25/06/2019		T°:	26°C					
				hum		56					
N°	M (coef)	B	R²	(k=2)							
1	20.18204	0.0510	0.999998	0.26	$Y(\text{mm}) = 20.1820 * X(\text{volt}) + 0.0510$						
2	20.21321	-17.4623	0.999999	0.27	$Y(\text{mm}) = 20.2132 * X(\text{volt}) - 17.4623$						
3	20.06605	0.0431	0.999996	0.49	$Y(\text{mm}) = 20.0660 * X(\text{volt}) + 0.0431$						
4	20.07985	-0.1744	0.999993	0.56	$Y(\text{mm}) = 20.0798 * X(\text{volt}) + -0.1744$						
5	20.11219	0.1855	0.999997	0.22	$Y(\text{mm}) = 20.1122 * X(\text{volt}) + 0.1855$						
6	20.04977	-0.1158	0.999995	0.33	$Y(\text{mm}) = 20.0498 * X(\text{volt}) + -0.1158$						
7	20.12709	-0.0919	0.999996	0.39	$Y(\text{mm}) = 20.1271 * X(\text{volt}) + -0.0919$						
8	20.0355	0.0343	0.999999	0.27	$Y(\text{mm}) = 20.0355 * X(\text{volt}) + 0.0343$						
9	19.99289	0.1484	0.999999	0.20	$Y(\text{mm}) = 19.9929 * X(\text{volt}) + 0.1484$						

Monika De Vos, Chef de Laboratoire GM, 10.06.2020

M De Vos